T.R.
SAKARYA UNIVERSITY
GRADUATE SCHOOL OF NATURAL AND APPLIED SCIENCES

INVESTIGATION OF LATERAL EARTH PRESSURE ACTING ON RIGID RETAINING WALL WITH COHESIVE BACKFILL UNDER DYNAMIC CONDITIONS

MSc THESIS

Ahmed Amjad Ahmed ALMASSRI

Civil Engineering Department

JUNE 2024

T.R.
SAKARYA UNIVERSITY
GRADUATE SCHOOL OF NATURAL AND APPLIED SCIENCES

INVESTIGATION OF LATERAL EARTH PRESSURE ACTING ON RIGID RETAINING WALL WITH COHESIVE BACKFILL UNDER DYNAMIC CONDITIONS

MSc THESIS

Ahmed Amjad Ahmed ALMASSRI

Civil Engineering Department

Thesis Advisor: Prof. Dr. Sedat SERT

JUNE 2024

The thesis work titled “Investigation of Lateral Earth Pressure Acting on Rigid Retaining Wall with Cohesive Backfill under Dynamic Conditions” prepared by Ahmed Amjad Ahmed ALMASSRI was accepted by the following jury on 28/06/2024 by unanimously of votes as a MSc THESIS in Sakarya University Graduate School of Natural and Applied Sciences, Civil Engineering department, Civil Engineering program.

Thesis Jury

Jury Member :	**Assist. Prof. Dr. Emre AKMAZ** Sakarya University	.....
Head of Jury :	**Prof. Dr. Sedat SERT (Advisor)** Sakarya University	.....
Jury Member :	**Assist. Prof. Dr. Sedat Semih ÇAĞLAYAN** Sakarya University of Applied Sciences	.....

STATEMENT OF COMPLIANCE WITH THE ETHICAL PRINCIPLES AND RULES

I declare that the thesis work titled "INVESTIGATION OF LATERAL EARTH PRESSURE ACTING ON RIGID RETAINING WALL WITH COHESIVE BACKFILL UNDER DYNAMIC CONDITIONS", which I have prepared in accordance with Sakarya University Graduate School of Natural and Applied Sciences regulations and Higher Education Institutions Scientific Research and Publication Ethics Directive, belongs to me, is an original work, I have acted in accordance with the regulations and directives mentioned above at all stages of my study, I did not get the innovations and results contained in the thesis from anywhere else, I duly cited the references for the works I used in my thesis, I did not submit this thesis to another scientific committee for academic purposes and to obtain a title, in accordance with the articles 9/2 and 22/2 of the Sakarya University Graduate Education and Training Regulation published in the Official Gazette dated 20.04.2016, a report was received in accordance with the criteria determined by the graduate school using the plagiarism software program to which Sakarya University is a subscriber, I accept all kinds of legal responsibility that may arise in case of a situation contrary to this statement.

28/06/2024

Ahmed Amjad Ahmed ALMASSRI

ACKNOWLEDGMENTS

Firstly First and foremost, all praise and thanks be to Allah, who granted me the success to complete this thesis, also I am profoundly grateful to several people whose support and guidance have been invaluable throughout my thesis journey. First and foremost, I would like to express my deepest gratitude to my supervisor, Prof. Dr. Sedat SERT, whose expertise and insightful guidance have been instrumental in shaping this research. Your unwavering support and encouragement have been pivotal to my achievements.

I owe a particular debt of gratitude to my family. To my father and mother, thank you for your endless love, support, and sacrifice, which have been the backbone of my journey. To my sisters and brother, thank you for your constant encouragement and always believing in me. Your collective faith and pride in my efforts have given me the strength to persevere.

I am also immensely thankful to my friends, who have provided moral support and a sense of home and community during this challenging academic endeavor. Your companionship and reassurance have made all the difference.

This thesis stands as a testament to my academic growth and as a monument to the collective effort and spirit of all who have been a part of this journey. Thank you all from the bottom of my heart.

Ahmed Amjad Ahmed ALMASSRI

TABLE OF CONTENTS

Page

ABBREVIATIONS

AASHTO : American Association of State Highway and Transportation Officials

TBDY : Turkish Building Earthquake Regulation

OCR : Over Consolidation Ratio

AFAD : Disaster and Emergency Management Presidency

SYMBOLS

σ_h	: Horizontal Stress
σ_v	: Vertical Stress
k_o	: Earth Pressure Coefficient
ϕ	: Soil's Friction Angle
γ	: Soil's Unit Weight
S	: Soil's Shear Strength
C	: Soil Cohesion
P_a	: Active Earth Pressure
k_a	: Active Earth Pressure Coefficient
P_p	: Passive Earth Pressure
k_p	: Passive Earth Pressure Coefficient
z_c	: Depth of Tensile Crackes
β	: Angle of Inclination of Soil Surface from the Horizontal
α	: Angle of Inclination of Retaining Wall from the Vertical
W	: Soil Wedge's Weight
F	: Shear Force on the Failure Plane
θ	: Angle of Inclination of Failure Plane
δ	: Friction Angle Between the Wall and Backfill Soil
$FoS_{Overturning}$	: Factor of Safety Against Overturning
$FoS_{Sliding}$	: Factor of Safety Against Sliding
$\sum MR$	: Moment of Forces Resisting Overturning
$\sum M_o$	: Moment of Forces Tending the Wall to Overturn
q_u	: Ultimate Bearing Capacity of the Foundation Soil
S_e	: Elastic Settlement
P_{ae}	: Seismic Active Earth Pressure
k_h	: Horizontal Seismic Coefficient
K_v	: Vertical Seismic Coefficient
V_s	: Shear Wave Velocity
G	: Shear Modulus

K_{ae} : Seismic Active Eath Pressure Coefficient

K_{pe} : Seismic Passive Eath Pressure Coefficient

SDS : Spectral Response Acceleration Parameter for Short Period

S_s : Mapped Response Acceleration Parameter for Short Period

F_s : Site Coefficient

PGA : Peak Ground Acceleration

A_s : Earth Ground Acceleration Coefficient

B : Foundation Width

H : Retaining Wall's Height

D_f : Foundation Depth

u_x : Horizontal Wall Displacement

u_y : Vertical Wall Displacement

LIST OF TABLE

Page

LIST OF FIGURES

Page

INVESTIGATION OF LATERAL EARTH PRESSURE ACTING ON RIGID RETAINING WALL WITH COHESIVE BACKFILL UNDER DYNAMIC CONDITIONS

SUMMARY

Within the scope of this research, four models of rigid retaining walls, specifically gravity walls with 8 m height and horizontal surface, were designed using clay soil as backfill with cohesion = 20 kN/m^2, unit weight = 17 kN/m^3 and friction angle = 25^o. The foundation soil was sand with cohesion = 0 kN/m^2, unit weight = 18 kN/m^3, and friction angle = 30^o, assuming the presence of an effective and suitable drainage system behind the wall to prevent additional lateral water pressure. The lateral earth pressures for these walls were calculated in both static and dynamic conditions. Based on these pressures, the dimensions of the walls were designed. For the static condition, Rankine's method for cohesive soil was used. Regarding the dynamic condition, Nakajima et al. (2023) method, a newly published approach, was employed. This method incorporates soil cohesion into the calculation of seismic active earth pressures, and it has been combined with the modified Mononobe-Okabe method, which can be applied in cases of high seismic loading. For the four models of retaining walls, the first two were designed under dynamic conditions using the horizontal seismic coefficient k_h defined by the Turkish Building Earthquake Regulation (TBDY 2018). In the first model, the surcharge load on the backfill soil was included, whereas it was not included in the second model. The remaining two models were designed using the horizontal seismic coefficient k_h from American Association of State Highway and Transportation Officials (AASHTO), including the surcharge load on the soil behind the wall in the third model and omitting it in the fourth. This was done to assess the impact of the surcharge load on the wall's dimensions and lateral displacements, as well as to examine the differences in design based on whether the seismic coefficients were taken from the Turkish or AASHTO standards. Additionally, stability analyses were performed for all four designs in both static and dynamic states, and these were compared with safety factors related to overturning, sliding, and bearing capacity as specified by the Turkish standard for the first two designs and the AASHTO standard for the last two, the equation used for these checks were obtained from Das and Sivakugan (2018). Furthermore, Plaxis 2D software version 2024 was utilized to calculate both static and dynamic displacements, which were then evaluated against the permissible limits according to the design standards followed. The results confirmed the unsuitability of this soil for use behind retaining walls, where the dimensions of the designs were relatively large given that the lateral water pressure

was not considered based on the assumption of a suitable drainage system is available. Also, comparisons between the Turkish standards and AASHTO showed a difference concerning horizontal seismic coefficient k_h, where k_h resulting from the Turkish standard was 40% larger, affecting the dynamic lateral pressure, which was greater in the first two designs comparing with the last two. Consequently, the dimensions (base width) of the first two designs were approximately 20% larger than the last two designs. Therefore, it can be said that the Turkish standard is conservative in calculating k_h. The research also highlighted the importance of including dynamic calculations in the design of these walls due to the significant impact of seismic forces on the retaining walls and on the lateral active earth pressures. Furthermore, the displacement results from the Plaxis 2D software indicated the necessity of improving the soil used if construction is required or additional load is to be added on it.

KOHEZYONLU GERİ DOLGULU RİJİT İSTİNAT DUVARINA ETKİYEN YANAL TOPRAK BASINCININ DİNAMİK KOŞULLAR ALTINDA İNCELENMESİ

ÖZET

Bu araştırma kapsamında, özellikle 8 m yüksekliğinde ve yatay yüzeyli ağırlık duvarları olarak dört model rijit istinat duvarı tasarlandı. Geri dolgu malzemesi olarak kohezyonu = 20 kN/m^2, birim ağırlığı = 17 kN/m^3 ve sürtünme açısı = 25^o olan kil zemin kullanıldı. Temel zemini, kohezyonu = 0 kN/m^2, birim ağırlığı = 18 kN/m^3 ve sürtünme açısı = 30^o olan kum alındı. Duvarın arkasında ek yanal su basıncını önlemek için etkili ve uygun bir drenaj sisteminin varlığı kabul edildi. Bu duvarlar için yanal toprak basınçları hem statik hem de dinamik koşullarda hesaplandı. Bu basınçlara dayanarak, duvarların boyutları tasarlandı. Statik koşul için, kohezyonlu zeminler için Rankine yöntemi kullanıldı. Dinamik koşul ile ilgili olarak, Nakajima ve diğerleri (2023) tarafından yayımlanan yeni bir yaklaşım olan yöntem kullanıldı. Bu yöntem, sismik aktif toprak basınçlarının hesaplanmasına zemin kohezyonunu dahil etmekte olup yüksek sismik yüklemelerin söz konusu olduğu durumlar için uygulanabilen modifiye Mononobe-Okabe yöntemi ile birleştirilmiştir. Dört istinat duvarı modelinden ilki, Türkiye Bina Deprem Yönetmeliği (TBDY 2018) tarafından tanımlanan yatay sismik katsayı kh kullanılarak dinamik koşullar altında tasarlandı. İlk modelde, geri dolgu toprağında ek yük dikkate alındı, ikinci modelde ise alınmadı. Kalan iki model, Amerikan Karayolları ve Ulaştırma Devlet Daireleri Birliği (AASHTO) tarafından verilen yatay sismik katsayı kh kullanılarak tasarlandı; üçüncü modelde duvarın arkasındaki toprağa ek yük dahil edilirken, dördüncüde bu yapılmadı. Bu, duvarın boyutlarına ve yanal yer değiştirmelere ek yükün etkisini değerlendirmek ve sismik katsayıların Türk veya AASHTO standartlarından alınıp alınmamasına göre tasarımdaki farklılıkları incelemek için yapıldı. Ayrıca, hem statik hem de dinamik durumlar için dört tasarımın tümü için stabilite analizleri yapıldı ve bunlar, ilk iki tasarım için Türk standardına, son iki tasarım için ise AASHTO standardına göre belirlenen devrilme, kayma ve taşıma kapasitesi ile ilgili güvenlik faktörleri ile karşılaştırıldı, bu kontroller için kullanılan denklemler Das ve Sivakugan (2018)'den alındı. Ayrıca, statik ve dinamik yer değiştirmeleri hesaplamak için Plaxis 2D yazılımı 2024 sürümü kullanıldı ve bu sonuçlar, takip edilen tasarım standartlarına göre izin verilen sınırlarla karşılaştırıldı. Sonuçlar, bu killi zeminin istinat duvarlarının arkasında kullanım için uygun olmadığını doğruladı, tasarımların boyutları nispeten büyük olduğu için, uygun bir drenaj sistemi olduğu varsayımına dayanarak yanal su basıncı dikkate alınmadı. Ayrıca, Türk standartları ile AASHTO arasındaki karşılaştırmalar, yatay sismik katsayı kh açısından bir fark gösterdi; Türk standardından elde edilen kh, %40 daha büyük olup, dinamik yanal basıncı etkiledi ve bu, ilk iki tasarımda son iki tasarıma göre daha büyüktü. Sonuç olarak, ilk iki tasarımın boyutları (taban genişliği) son iki tasarımdan yaklaşık %20 daha büyüktü. Dolayısıyla, Türk standardının kh hesaplamasında muhafazakar olduğu söylenebilir. Araştırma, bu

duvarların tasarımında dinamik hesaplamaların dahil edilmesinin önemini de vurguladı, çünkü sismik kuvvetlerin istinat duvarlarına ve yanal aktif toprak basınçlarına önemli etkisi bulunmaktadır. Ayrıca, Plaxis 2D yazılımından elde edilen yer değiştirme sonuçları, duvar gerekiyorsa veya üzerine ek yük eklenecekse kullanılan doğal zeminin iyileştirilmesi gerekliliğini gösterdi.

1. INTRODUCTION

Retaining walls are crucial structural elements for supporting slopes and excavations, as they help stabilize soil when the earth becomes unusually steep. These walls come in various types, including gravity, semi-gravity, and cantilever walls, which will be detailed in upcoming chapters. Historically, these walls were built to support the soil behind them and prevent it from collapsing under static conditions. However, in seismic zones, it is insufficient for these walls only to withstand static pressures. They must also consider the dynamic impacts of earthquakes, which can significantly increase pressure on the walls. Additionally, the choice of backfill soil type plays a critical role in the success of these walls' designs. Most international standards recommend using granular soil due to its high friction angle and permeability, which prevents water accumulation and reduces pressure on the wall. However, in this study, clay soil, which is characterized by its high cohesion and low friction angle, was chosen as backfill to explore its potential use behind retaining walls, not only in static but also in dynamic conditions, assuming a high-quality drainage system that allows for water permeability. The future chapters of this research will discuss the types of retaining walls and their applications, and present examples of retaining walls that failed under soil pressure, examining the reasons for their failure. It will also cover the methods used for calculating static and dynamic lateral earth pressures. Stability tests and safety factors used in the design of these walls will also be explored. In this study, four gravity retaining walls with a constant height of 8 meters were designed, using clay soil as backfill with cohesion = 20 kN/m^2, unit weight = 17 kN/m^3 and friction angle = 25^o. The foundation soil was sand with cohesion = 0 kN/m^2, unit weight = 18 kN/m^3, and friction angle = 30^o. The walls were designed in a static condition using Rankine's method for calculating active static earth pressure. For dynamic conditions, Nakajima et al. (2023) method was used to calculate seismic active earth pressure The dimensions of the walls were designed and compared with the necessary safety factors according to TBDY 2018 and AAHSTO 2014. Additionally, these walls were analyzed using the Plaxis 2D software

version 2024, and their displacements were calculated and compared with allowable displacements.

2. RETAINING WALLS

2.1. Introduction

Long ago, an unidentified person placed a row of rocks on each other to prevent the soil behind them from falling to where they were camping. This action laid the foundation for what we now call retaining walls. Retaining walls could be defined as any wall built to keep what is behind it, whether soil or any matter, in place without any displacement or sliding in areas with a significant elevation difference (Brooks and Nielsen, 2013).

Since that time, we have been using retaining walls, with modifications to their shapes and types, for various purposes and objectives of civil engineering applications, including supporting the soil behind those walls and resisting any external forces in multiple applications, such as roads, embankments, excavation projects, and others.

Retaining walls must be engineered to withstand the wall's weight and the lateral pressures from the water and soil behind it; the wall design should further consider any surcharge loads applied to the soil while also accounting for weather conditions such as temperature fluctuations leading to thermal expansion and shrinkage, as well as the dynamic forces associated with seismic events (AASHTO, 2002).

Retaining walls come in various types and shapes depending on the purpose of their use, and they can consist of several materials, such as reinforced concrete or lining up some rocks regularly and bonding them using concrete. In this section, details about the classifications of retaining walls and their applications, in addition to their places of use, will be presented.

2.2. Types of Retaining Walls

An appropriate wall type could be chosen based on an accurate evaluation of several factors. These factors include the purpose of building the wall, the wall's planned height, the characteristics and topography of the land, the space available for building, and its

nearness to groundwater sources. Furthermore, the accessibility of required construction materials and financial considerations are crucial when selecting the suitable type of wall to be constructed (BS 8002, 1994).

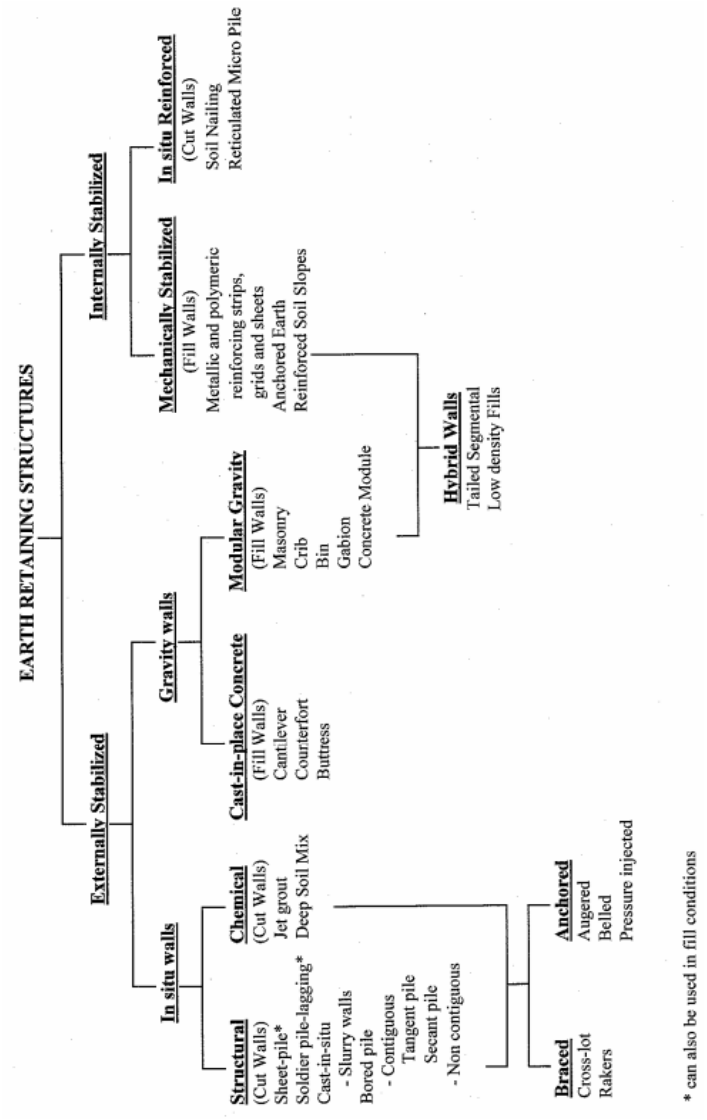

Figure 2.1. Retaining wall classifications (Taha and Prust, 2001).

The classifications of retaining walls could differ from one researcher to another based on their point of view; for example, according to Das and Sivakugan (2018), retaining walls could be categorized mainly into mechanically stabilized walls and conventional retaining walls. On the other hand, other researchers like Taha and Prust (2001) and Khan and Sikder (2004) classified them into externally and internally stabilized walls Figure (2.1).

The following subtitles will present classifications of retaining walls, explaining some of the types used to support the soil.

2.2.1. Externally Stabilized Walls

The stability of such walls, along with their capacity to withstand lateral earth pressure and surcharge loads, depends mainly on the wall's weight. Therefore, this type of wall requires a considerable amount of concrete or reinforced concrete for construction. These retaining walls are also described as rigid walls and can be built using locally available materials, reducing the costs needed for constructing that type of wall (Xie and Yang, 2009; Khan and Sikder, 2004).

2.2.1.1. Gravity Retaining Walls

In this type of wall, masonry stone or concrete is used for the construction. Stability and balance are achieved through the wall's weight, and the resistance to wall lateral sliding primarily comes from the friction at the interface between the foundation soil and the wall's base. It's worth mentioning that gravity walls are typically employed in locations where there is no need for substantial height to resist lateral pressure; otherwise, it would not be economically feasible. They also require a strong foundation soil due to their relatively large mass (Clayton et al., 2014; Das and Sivakugan, 2018). Furthermore, gravity walls are usually built on a horizontal surface before starting the backfilling process in order to make the elevation difference for the wall to support. In terms of places of use, this type of wall could be applied to hold up the excavations as well as the embankments either for railways or highways (Brown et al., 2023).

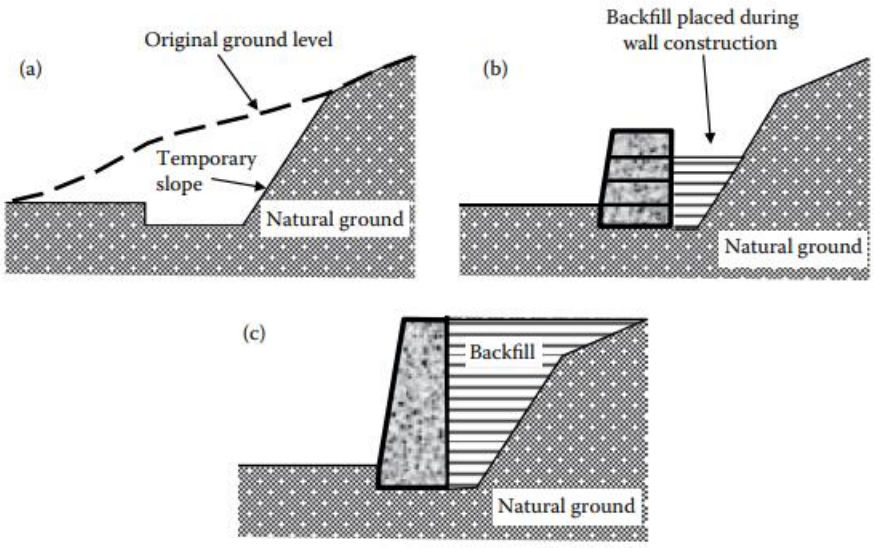

Figure 2.2. Stages illustrating the process of constructing a gravity retaining wall (Clayton et al., 2014).

2.2.1.2. Semi-Gravity Retaining Walls

Semi-gravity walls differ from gravity walls in the amount of steel they contain since the semi-gravity type of walls has less reinforcement steel; as Figure 2.3 illustrates, the reinforcement aims to link the wall's stem to the base. Placing the steel bars reduces the overall concrete mass, resulting in a lighter weight for the wall. Moreover, this wall design depends more on internal resistance to withstand bending and shearing forces (Clayton et al., 2014).

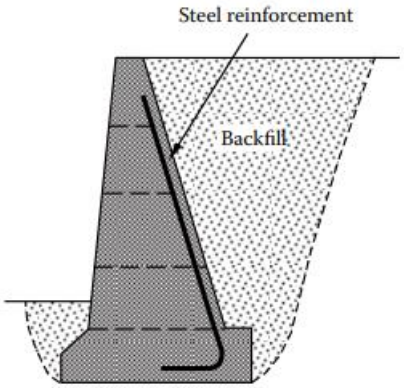

Figure 2.3. Semi-gravity retaining wall (Clayton et al., 2014).Cantilever Retaining Walls

This type of wall is constructed using reinforced concrete, composed of a thin vertical stem fixed at the bottom by a concrete base. It could be considered an economical choice for walls up to a height of 8 meters (Das and Sivakugan, 2018). This wall is usually designed in an 'L' shape or an inverted 'T' configuration. The vertical section extending from the base acts as a cantilever, supporting the backfill. Furthermore, it is recommended that these walls be provided with a good drainage system as they are less dependable than water-supporting structures. Also, shear keys could be added to enhance the resistance to sliding, as seen in Figure (2.4) (Clayton et al., 2014).

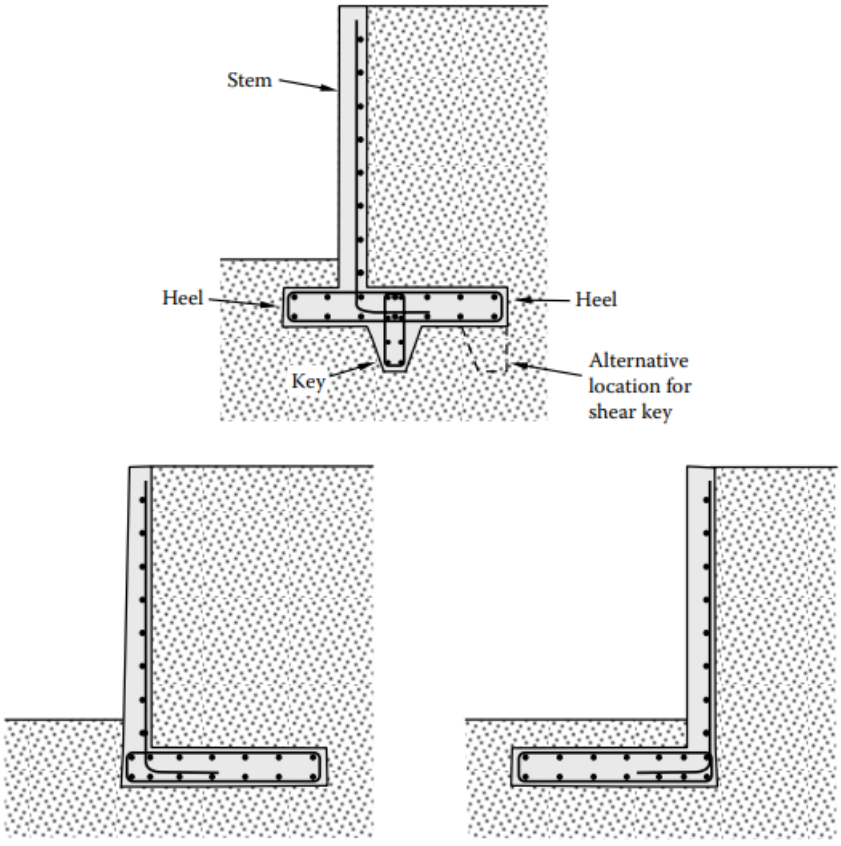

Figure 2.4. Cantilever retaining wall (Clayton et al., 2014).

2.2.1.3. Counterfort and Buttressed Retaining Walls

These two types of walls are similar to the earlier type, except that they have counterforts, which are slim slabs made of concrete on the wall's backside or front side to connect it with its base, as presented in Figure 2.5. The presence of these supports helps to resist the forces of shearing and bending moment forces when the wall is exposed to the tension,

unlike the buttressed type, which contains the same counterforts, but from the front, this helps withstand the forces when the wall is exposed to compression. These types are used when high retaining walls up to 12 m are needed. They were widely used in earlier times, but because of the complexity of their construction compared with the other types of retaining walls, their usage has declined recently, except in cases of enormous pressure or very high walls (Clayton et al., 2014).

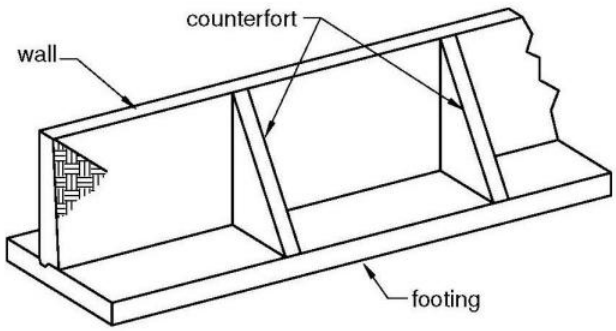

Figure 2.5. Counterfort retaining wall (Clayton et al., 2014).

2.2.2. Internally Stabilized Walls

This type of wall, known as mechanically stable walls, could be made up of placing reinforcement layers horizontally, which in turn resist the majority of the lateral pressure coming from the backfill soil, which contributes to significantly decreasing the quantity of the reinforcement and concrete needed. These walls could also be described as flexible, and what makes these walls differ from the rigid ones is that they require less foundation-bearing capacity. Moreover, they have lower costs and less time needed to be constructed due to the reduced quantity of concrete and reinforcement steel necessary for the construction process. Furthermore, considering the fact that wall panels, reinforcement layers with the compacted backfill could be made simultaneously. Examples of these walls are walls reinforced with geosynthetics, and anchored earth walls, (see Figure 2.6). (Xie and Yang, 2009; Khan and Sikder, 2004).

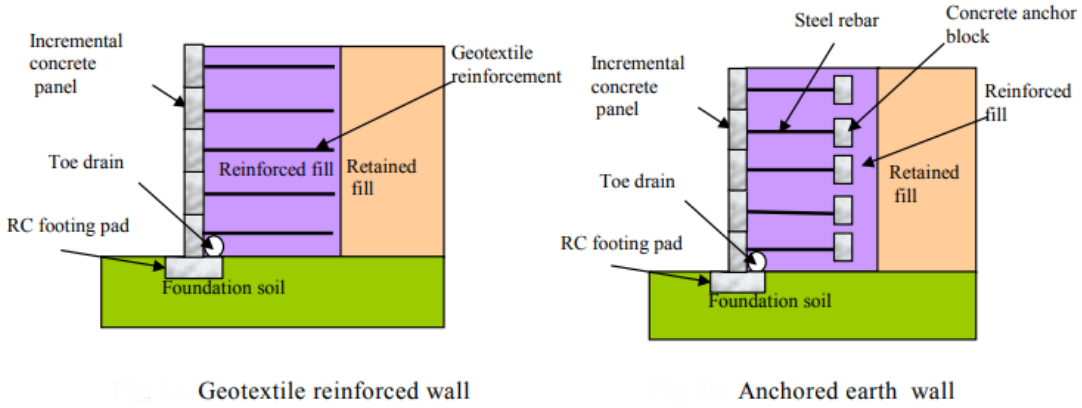

Figure 2.6. Mechanically stabilized walls (Khan and Sikder, 2004).

2.3. Backfill Material for Retaining Structures

The choice of appropriate backfill soil behind the wall is important and closely related to the safety of the wall. When selecting backfill soil, whenever feasible, it is better to use non-cohesive or granular soil to prevent water accumulation and the resultant additional lateral pressure that could adversely impact the wall's stability. In some projects, using another type of soil, such as cohesive soil like clay or silt, may be more suitable and cost-effective. However, the high value of cohesion, low friction angle, and low permeability, in addition to its swelling when it absorbs water, make this type of soil undesirable to be used behind walls unless the necessary measures and care are taken while designing, in addition, to create a suitable drainage system to prevent water from accumulating behind the wall.

2.4. Retaining Walls Drainage System

The water drainage system is considered as one of the essential elements that must be given attention when designing retaining walls; such a system contributes to disposing of additional pressure resulting from the presence of water due to rain, proximity to the groundwater level, or other factors, and its accumulation in the soil filled behind the wall, which leads to significant damage regarding long term condition. However, to implement a suitable drainage system, it's essential to consider the type and properties of the soil, and the drainage system should be designed accordingly. According to Das and Sivakugan (2018), a suitable drainage system can be made by drilling weep holes through the wall at

1.5 m centers for horizontal and vertical directions as shown in Figure 2.7(a), when applying weep holes, for example, their minimum diameter should be about 0.1 m, while taking care to Adding filter materials with suitable size to prevent parts of the backfill soil from leaking with the water into the drainage weep hole or pipe, which may lead to clog them, as well as the accumulation of water inside the soil and thus additional lateral pressure and ultimately collapse of the wall. Another drainage system that is considered more effective, this system is constructed by placing a drainage blanket that separates the backfill and the wall; the blanket carries the water leaking from the backfill to perforated pipes, as illustrated in Figure 2.7(b) (Das and Sivakugan, 2018).

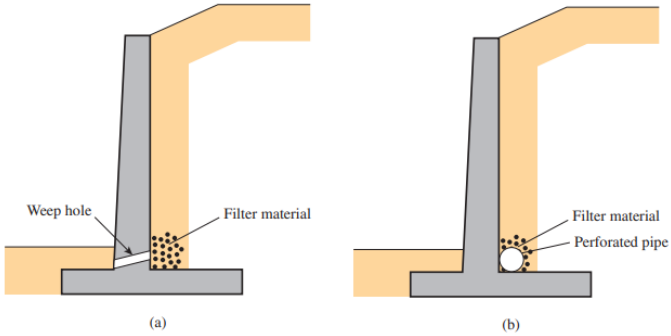

Figure 2.7. Drainage systems of retaining walls (Das and Sivakugan, 2018).

2.5. Retaining Wall Failure

Anticipating the causes of future failure and addressing them in advance is a critical factor in guaranteeing the practical design of retaining walls. To achieve this, understanding the factors that can lead to the collapse or failure of the retaining structure and applying the necessary precautions to avoid these risks on the construction site is crucial. The reasons that could lead to the failure of retaining walls are the improper selection of backfill soil, the absence of a suitable drainage system, and ignoring the force of rainwater and its accumulation behind the wall, which can lead to additional lateral pressure that leads to the collapse of the facility, in addition to some construction errors resulting from a lack of correct implementation for the wall and others (Binici et al., 2010).

Examples of retaining walls in Türkiye that experienced collapse between the years 2018 and 2022 due to the impact of static pressures are presented below:

On July 31, 2018, in the Istanbul Sancaktepe district, the retaining wall of the Mevlana School collapsed. After examining the causes of the collapse, as demonstrated by Figure 2.8, the ground was damp. Subsequent observations revealed that the drainage system was not made properly and that unsuitable backfill soil was used.

Figure 2.8. Collapsed example of retaining wall in Sancaktepe (url1, 2018; Sönmez, 2023)

Another example of a retaining wall collapse in Turkey On December 2, 2021, a wall collapsed in Kayseri during landscaping. This wall, which was built from crushed stones without the incorporation of blocks and mortar, could barely withstand its weight and subsequently failed under the construction machine's additional loads, as presented in Figure 2.9. It later became clear that the soil of the backfill was not suitable, in addition to the absence of a good drainage system.

Figure 2.9. Collapsed example of retaining wall in Kayseri (url2, 2021; Sönmez, 2023).

On February 9, 2022, Figure 2.10 shows another collapse of a 12-meter-high wall that occurred near one of the residual buildings under construction in the city of Trabzon due to the explosion of the water pipe inside the backfill behind the wall. After some investigations, which indicated that the soil type had not been chosen well, the lack of quality of the drainage system further worsened the situation.

Figure 2.10. Collapsed example of retaining wall in Trabzon (url3, 2022; Sönmez, 2023).

3. LATERAL EARTH PRESSURE

The stresses resulting from the soil mass itself and any other load applied to the soil, which leads to pressure on the wall, are called lateral earth pressure. Regarding the context of earth pressure, two varieties of stresses are present in that situation: vertical stresses, which can be determined at any depth by multiplying that depth with the unit weight of used soil, and horizontal stresses, which could arise from the vertical stresses themselves and affect the wall's stability. We can calculate the lateral earth pressure with the help of the vertical stresses already known to us.

To properly design retaining walls, lateral earth pressure calculations should be included, which depend on several components:

a) The supported soil's unit weight.
b) Backfill permeability and its drainage considerations.
c) The magnitude of the wall movement and its type.
d) Soil shear strength variables.

Depending on whether the wall moves or not, along with that motion's direction, there are three categories for the lateral earth pressures that the wall might face or be exposed to from the supported soil:

- At-rest earth pressure (the lateral pressure the wall will be exposed to at any depth when the wall is restricted or secured from changing its state of moving in any direction) (Figure 3.1a).
- Active earth pressure (the lateral pressure the wall will be exposed to while it is allowed to bend outward, the opposite side of the backfill) (Figure 3.1b).
- Passive Earth pressure (the lateral pressure the wall will be exposed to while it is allowed to bend inward, towards the supported soil) (Figure 3.1c).

Additionally, it must be known that for the last two conditions, with enough bending for the wall, the wedge of the supported soil will fail (Das and Sivakugan, 2018). In the coming sections, each situation related to lateral earth pressure will be covered.

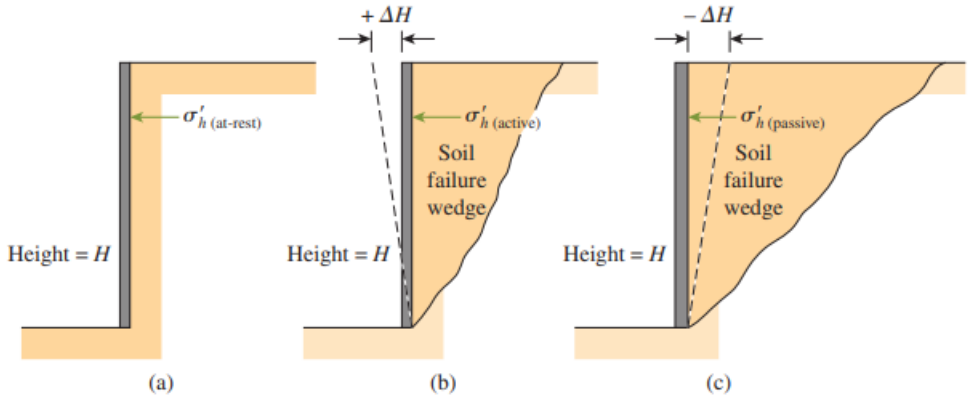

Figure 3.1. The variation of the magnitude of wall movements in the cases of at rest, active and passive situations (Das and Sivakugan, 2018).

3.1. Lateral Earth Pressure at Rest

Assuming that we have a rigid wall with a vertical face and behind the wall, we have a homogeneous soil having a horizontal or level surface. Suppose the wall's movement was restricted and didn't experience a horizontal displacement in any direction after the backfilling process. In that case, the pressure acting on it is the pressure for the at-rest case.

If we consider element X behind the wall illustrated in Figure 3.2, then it will be exposed to these pressures:

Vertical pressure $\sigma'_v = \gamma z$

and horizontal pressure σ'_h

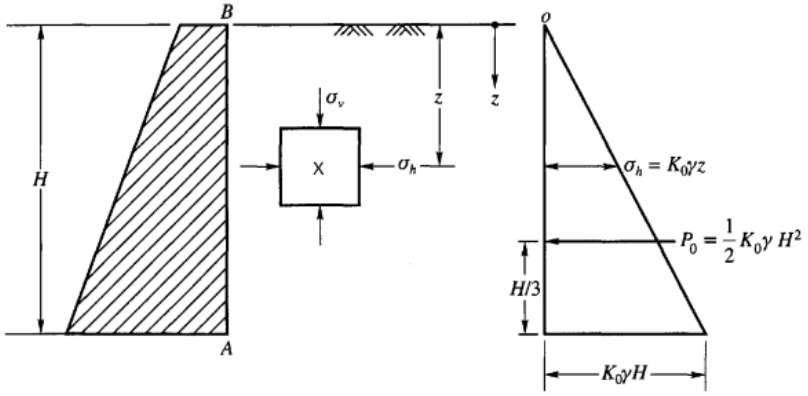

Figure 3.2. At rest earth pressure (Murthy, 2002).

Where ɣ is the soil effective unit weight. Moreover, the vertical effective stress σ'_v and the horizontal effective stress σ'_h in that case would increase linearly with increasing depth. Therefore, the vertical stress to the horizontal stress ratio will remain constant by depth as:

$$\frac{\sigma'_h}{\sigma'_v} = \text{constant} = K_0 \tag{3.1}$$

Where K_0 is the coefficient of earth pressure at rest,

So σ'_h could be found by

$$\sigma'_h = K_0 \, \gamma \, z \tag{3.2}$$

According to Mesri and Hayat (1993), K_0 is not easy to be determined directly through laboratory or site tests, but it is often estimated through some empirical equations, as Jacky (1944) created a mathematical equation for normally consolidated clays and granular soil:

$$K_0 = 1 - sin\phi' \tag{3.3}$$

Following Jackie's lead Mayne and Kulhawy (1982), K_0 for over consolidated soil could be estimated by:

$$K_0 = (1 - sin\phi')(OCR)^{sin\phi'} \tag{3.4}$$

Where OCR is the over consolidation ratio, an important criteria that describes the history stress of the soil (Szymanski et al, 2006). Could be calculated using:

$$OCR = \frac{\sigma'_p}{\sigma'_{vo}} \tag{3.5}$$

Where σ'_p : pre-consolidation pressure.

And σ'_{vo}: the vertical effective stress.

For the soil loaded with a surcharge load q with dry unit weight behind a wall with height H, the total lateral pressure P_o at the rest condition will equal to the total area of the pressure diagrams shown in Figure 3.3 using this equation:

$$P_o = K_0 \mathrm{qH} + \frac{1}{2} K_0 \, \gamma \, H^2 \tag{3.6}$$

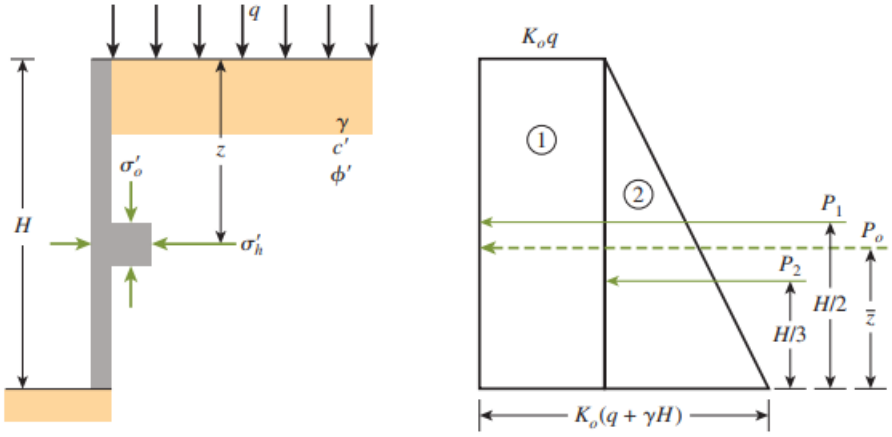

Figure 3.3. Lateral earth pressure diagram (Das and Sivakugan, 2018).

3.2. Active and Passive Earth Pressures

In the previous state (at rest state), the wall was restricted from movement, whether away from or towards the soil, and the soil was applying pressure on the wall, which we defined as the earth pressure at rest; however, if the movement of the wall was allowed so the wall could bend or yield away from the soil as shown in Figure 3.4, the horizontal soil pressure will gradually decrease, and thus the earth pressure coefficient K, because ($K_0 = \frac{\sigma_h}{\sigma_v}$) at the same time the pressure in the vertical direction remains constant, this decrease will continue until we reach the lowest value of the ground pressure coefficient so that if the pressure decreases after that, the value of that coefficient would not be affected. At that moment, the lowest value of the earth pressure coefficient (K) when the wall bends away

from the soil is called the Active earth pressure coefficient, and the minimum value of lateral pressure from the soil that pushes the wall outward in that case, called Active earth pressure (Clayton et al., 2014).

Conversely, suppose the wall bend was towards the soil Figure 3.4. In that case, the lateral pressure will increase, as will the earth pressure coefficient, continuing until the coefficient reaches its peak value before the failure occurs, which is known as the Passive earth pressure coefficient, and the maximum lateral pressure that pushes the wall inward in that case called Passive earth pressure.

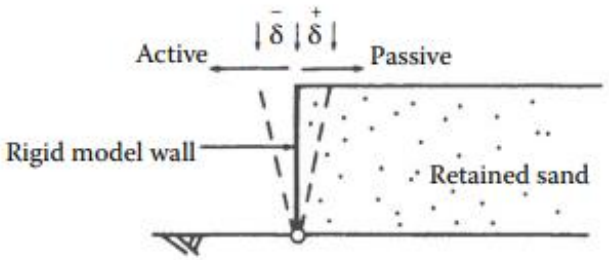

Figure 3.4. Displacement modes of retaining wall (Clayton et al., 2014).

3.3. Rankine Earth Pressures Theory

In 1857, Rankine established a method for estimating the static lateral earth pressures for cohesionless soil, which was later modified to apply to cohesive soils. The foundational principles of this method rely on various assumptions, one of which is that the backfill soil should be homogeneous, isotropic, and cohesionless so that soil properties such as friction angle, unit weight, and cohesion should be consistent throughout the soil. Another assumption is that the soil surface needs to be planar, and in the coming two sections, the case where the soil has a horizontal surface will be discussed. Also, the vertical and horizontal boundaries should not be exposed to shear loads. Moreover, the retaining wall should be rigid and form a 90° angle with the ground, meaning the wall should be vertical and have no friction between its surface and the soil behind it (Budhu, 2010).

3.3.1. Rankine Active Earth Pressure

As was mentioned previously, in the active case, when the mass of soil behind the wall pushes it outward a certain distance, this force, in this case, is called active earth pressure

Figure 3.5. When the wall displaces by a certain amount, this will cause a reduction of the lateral pressure and, thus, the lateral pressure coefficient. Figure 3.6 shows Mohr's circles, and the conversion from the state of rest to the state of failure is marked. When the wall is permitted to bend a certain distance, the lateral pressure will decrease, and this will make the Mohr circle spread until it touches the Mohr-Coulomb line of failure given by the equation (Coduto et al., 2016):

$$S = c' + \sigma' \tan \phi' \tag{3.7}$$

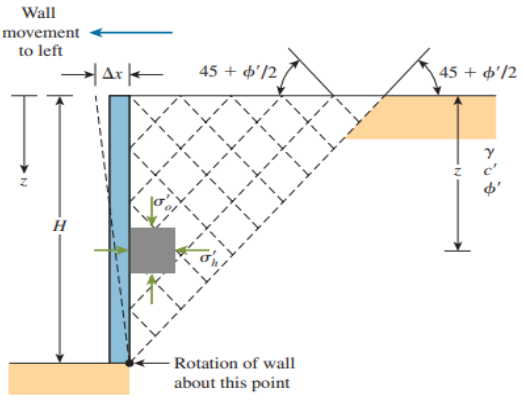

Figure 3.5. Wall movement due to Rankine active earth pressure (Das and Sivakugan, 2018).

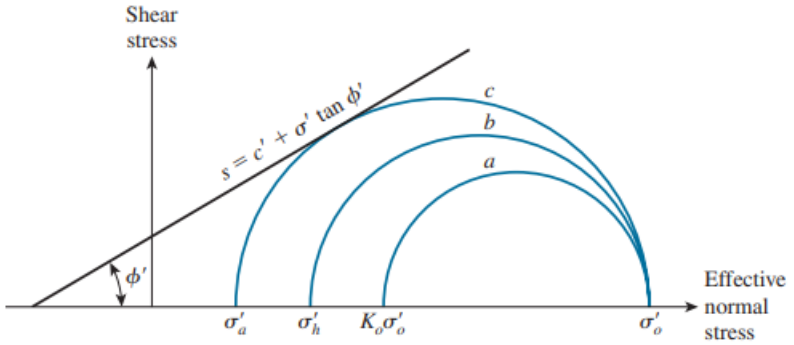

Figure 3.6. Mohr's circles related to the wall displacements of active earth pressure (Das and Sivakugan, 2018).

When failure occurs, the lateral pressure, in this case, will equal to σ'_a , which is the Rankine active pressure, so that inclination angle of the failure surface from the horizontal would be $(45 + \frac{\phi'}{2})$.

Rankine (1857) provided an equation to find K_a as follows:

$$K_a = \frac{1-sin\phi'}{1+sin\phi'} = tan^2(45 - \frac{\phi'}{2}) \quad (3.8)$$

Where, K_a: Rankine active pressure coefficient.

For the cohesionless soil the Rankine active earth pressure could be found by:

$$\sigma'_a = \gamma z \, tan^2\left(45 - \frac{\phi'}{2}\right) \quad (3.9)$$

Where: σ'_a: Rankine active pressure.

If a graph is made for the active earth pressure and the depth, the lateral pressure's distribution would take triangular shape. So, the resultant force in the active case per unit length (P_a) acting on the wall from the cohesionless soil:

$$P_a = \frac{1}{2} K_a \gamma H^2 \quad (3.10)$$

3.3.2. Rankine passive earth pressure

When a rigid frictionless wall is allowed to move a certain distance, the lateral pressure that could push that wall towards the soil direction is called passive earth pressure. Unlike the active case, the lateral pressure will increase, with the vertical pressure not changing. The lateral pressure will continue to increase, and thus the ground pressure coefficient until it reaches its highest value, so that if the pressure increases, the coefficient value would not be affected (Clayton et al., 2014). Moreover, for the passive case, when the failure occurs, the inclination angle of the failure surface from the horizontal is $(45 - \frac{\phi'}{2})$, as shown in Figure 3.7. Also the Mohr's circles when failure happens due to the increase in the earth pressure are shown in Figure 3.8.

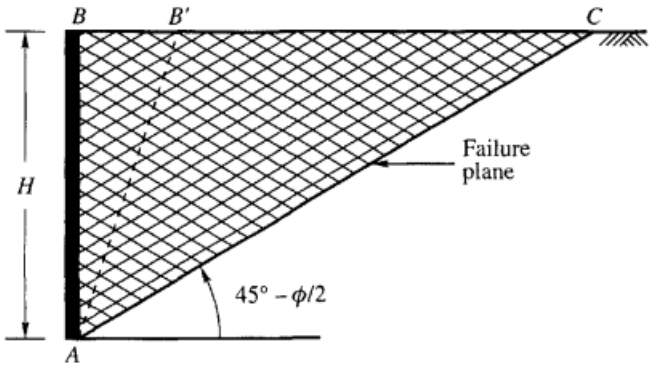

Figure 3.7. Rankine's passive earth pressure (Murthy, 2002).

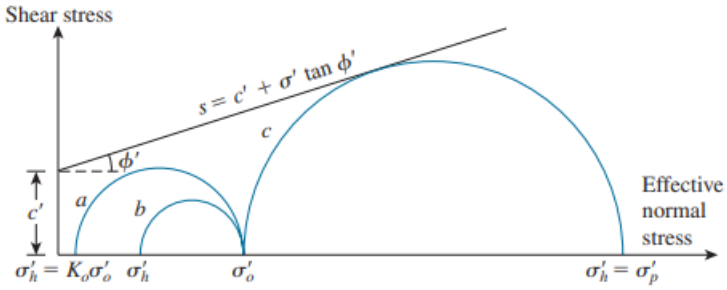

Figure 3.8. Mohr's circles related to the wall displacements from passive earth pressure (Das and Sivakugan, 2018).

Considering the assumptions utilized in section 3.3, Rankine provided some equations to calculate that passive pressure along with the coefficient of passive earth pressure for cohesionless soil as follows:

$$K_p = \frac{1}{K_a} = \frac{1+sin\phi'}{1-sin\phi'} = tan^2(45 + \frac{\phi'}{2}) \quad (3.11)$$

Where, K_p: Rankine Passive pressure coefficient.

Rankine Passive earth pressure could be found by:

$$\sigma'_p = \gamma z\, tan^2\left(45 + \frac{\phi'}{2}\right) \quad (3.12)$$

Where, σ'_p: Rankine Passive pressure

If a graph is made for the soil depth and passive earth pressure, the lateral pressure's distribution will take a triangular shape. So, the total force in the active case (P_p) acting on the wall from the cohesionless soil:

$$P_p = \frac{1}{2} K_p \, \gamma \, H^2 \tag{3.13}$$

3.4. Lateral Earth Pressure for Cohesive Backfill

When Rankine calculated the active and passive lateral pressures based on various assumptions, soil cohesion wasn't considered a parameter in his equations. Therefore, equations (3-9) and (3-12) from Rankine theory are designed for non-cohesive soils and do not apply to cohesive soils. It wasn't until Bell (1915) addressed this issue by modifying the last two equations and incorporating the cohesion parameter of the soil with them. Bell directly used Mohr's circle to formulate his equations, ultimately providing a solution for calculating active earth pressure and passive pressure using cohesive soil. This solution allows for the inclusion of Rankine or Coulomb's earth pressure coefficients (Bowles and Guo, 1996).

3.4.1. Active Earth Pressure Status

The active earth pressure, considering the cohesion of the backfill behind a retaining wall with no friction, could be calculated by:

$$\sigma'_a = \sigma'_o K_a - 2\, c' \sqrt{K_a} \tag{3.14}$$

Where: σ'_a: Active earth pressure

$\sigma'_o = \gamma\, z$

K_a: Active pressure coefficient

And by substituting the value of Rankine coefficient of active earth pressure the equation will be:

$$\sigma'_a = \gamma\, z\, tan^2\left(45 - \frac{\phi'}{2}\right) - 2\, c' tan(45 - \frac{\phi'}{2}) \tag{3.15}$$

Figure 3.9a shows the variation or the relation between the active earth pressure and depth. However, it shows that at ground surface the vertical stress equals to zero and at bottom

of the wall equals to γH, also, the active pressure at the ground surface starts from the value of $-2\,c'\sqrt{K_a}$. The reason behind this value being negative is considering the soil to be under tension, and it keeps decreasing due to the impact of the tensile stresses until it reaches zero at the depth z = z_c. So that:

$$\gamma\, z_c\, K_a \; - 2\, c'\sqrt{K_a} = 0$$

or,

$$z_c = \frac{2\, c'}{\gamma\sqrt{K_a}} \tag{3.16}$$

Where, z_c: Depth of tensile crack.

Figure 3.9b shows the term $-2\,c'\sqrt{K_a}$ distribution takes a rectangular shape, which is an expression of cohesion resistance for the shear stress that develops after permitting the wall to bend a certain distance (McCarthy, 2013). Also, the total pressure diagram after the tensile crack occurs due to the tensile stress is illustrated in Figure 3.9c.

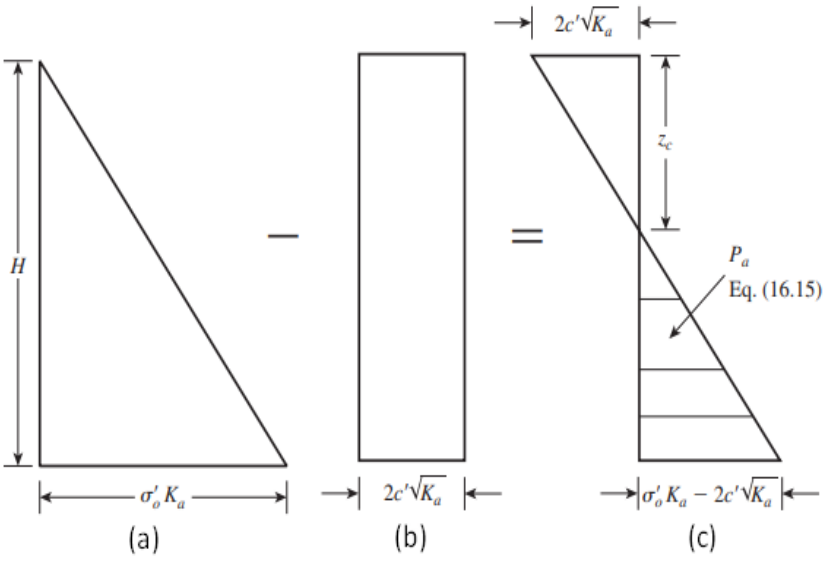

Figure 3.9. Distribution of the active pressure for cohesive soil (Das and Sivakugan, 2018).

The total force for the active case by unit length for Rankine before the tension cracks happened could be expressed by:

$$P_a = \frac{1}{2} K_a \, \gamma \, H^2 - 2 \, c' \sqrt{K_a} \, H$$

(3.17)

And if we have clay soil with $\phi' = 0$, then the total pressure before the tension cracks happened would be:

$$P_a = \frac{1}{2} \gamma \, H^2 - 2 \, H \, c' \tag{3.18}$$

The force for the active case by unit length after the cracks occur would be generated due to the soil pressure from z = z_c to until the total depth z = H as Figure 3.9c shows, and could be found by:

$$P_a = \frac{1}{2} \, (H - z_c)(K_a \, \gamma \, H - 2 \, c' \sqrt{K_a})$$

$$= \frac{1}{2} \, (H - \frac{2 \, c'}{\gamma \sqrt{K_a}})(\gamma \, H \, K_a - 2 \, c' \sqrt{K_a} \tag{3.19}$$

Note that the active pressure case would be accomplished if the wall was permitted to bend sufficient distance outward. This distance could be about 0.001H-0.004H for granular backfills and 0.01H-0.04H for cohesive backfills (Das and Sivakugan, 2018).

3.4.2. Passive Earth Pressure Status

Passive earth pressure for cohesive backfill behind a retaining wall with no friction could be calculated by:

$$\sigma'_p = \sigma'_o K_p + 2 \, c' \sqrt{K_p} \tag{3.20}$$

Where: σ'_p: Rankine passive pressure

$\sigma'_o = \gamma \, z$

K_p: Rankine passive pressure coefficient

Figure 3.10, shows the distribution of passive earth pressure from soil surface where depth $z = 0$ to the depth $z = H$,

At z = 0 , $\sigma'_o = 0$ and $\sigma'_p = 2 \, c' \sqrt{K_p}$

And for z = H , $\sigma'_o = \gamma \, H$ and $\sigma'_p = \sigma'_o K_p + 2 \, c' \sqrt{K_p}$

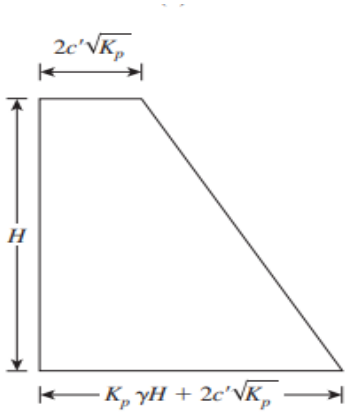

Figure 3.10. Distribution of the passive pressure for cohesive soil (Das and Sivakugan, 2018).

Using the coefficient of Rankine passive earth pressure, the equation will be:

$$\sigma'_p = \gamma z\, tan^2\left(45 + \frac{\phi'}{2}\right) + 2\, c' tan(45 + \frac{\phi'}{2}) \qquad (3.21)$$

The total force for the passive case by unit length using the Rankine coefficient could be expressed by:

$$P_p = \frac{1}{2}\gamma H^2 K_p + 2H\, c'\sqrt{K_p} \qquad (3.22)$$

And if we have clay soil with $\phi' = 0$, then the total force by unit length would be acting on the wall would be:

$$P_p = \frac{1}{2}\gamma\, H^2 + 2\, c'\, H \qquad (3.23)$$

Note that the passive pressure case would be accomplished if the wall was permitted to bend sufficient distance inwards towards the soil. This distance could be as illustrated in Table 3.1.

Table 3.1. Required wall movement for passive case (Das and Sivakugan, 2018).

Soil type	Wall movement
Dense sand	0.005H
Loose sand	0.01H
Stiff clay	0.01H
Soft clay	0.05H

3.5. Coulomb's Theory of Earth Pressure

In 1776, Coulomb gave a theory, also known as the Wedge theory, related to the computation of the lateral earth pressure affecting retaining structures based on the limit equilibrium state. Relying on that, the backfill mass of the vertical wall will slide by the side of a plane, which in turn forms an angle θ with the horizontal surface, and then he determines the maximum thrust that would act on that slip plane (Budhu, 2010). Unlike Rankine's theory, Coulomb considered the friction or the interaction resistance between the wall and the backfill. Also, he made his theory relying on some assumptions, including that the backfill should be cohesionless, homogeneous, and isotropic soil. Also, the wedge in which the failure will happen is a rigid body, and the failure surface is accepted to be a plane surface (Murthy, 2002).

Figure 3.11 shows the failure condition in the active case regarding Coulomb's theory in which AB is the wall side facing the active and passive pressures, BE is the soil mass surface plane inclined at β^o with horizontal, α^o is the inclination angle that the pressure face makes with the horizon, the wall height H, the surface of rupture plane AC and θ the angle that AC making with the horizontal.

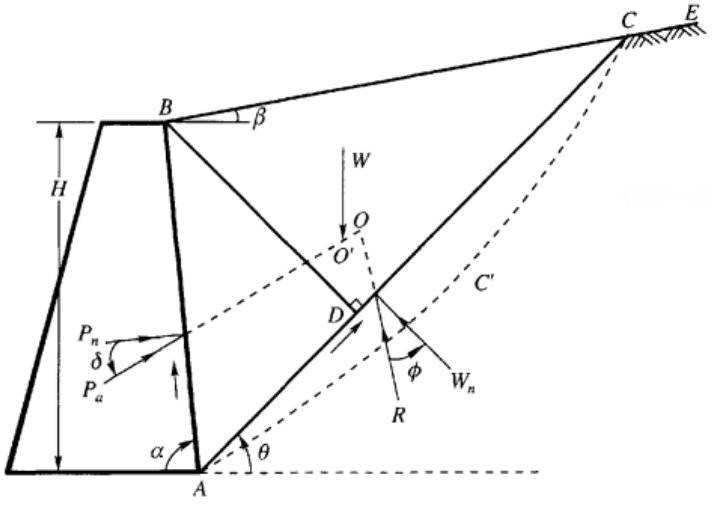

Figure 3.11. Coulomb's active earth pressure (Murthy, 2002).

3.5.1. Coulomb Active Earth Pressure

As Rankine's theory, Coulomb's method supposed a movement in the wall outwards for the active case. In this theory that depends on the sliding wedge concept, the wall

movement would make the sliding wedge shift outwards in the opposite side of the backfill and downwards on the slip surface for the active case (Punmia and Jain, 2005). There are three forces included in this theory when considering the stability of the wedge at which failure could take place regarding the active condition. They are the soil wedge's weight (W), the resultant force from the perpendicular force on the failure surface and the shear force (F) and the third force is the active force (P_a) which is the resultant of W and F like Figure 3.12 illustrates:

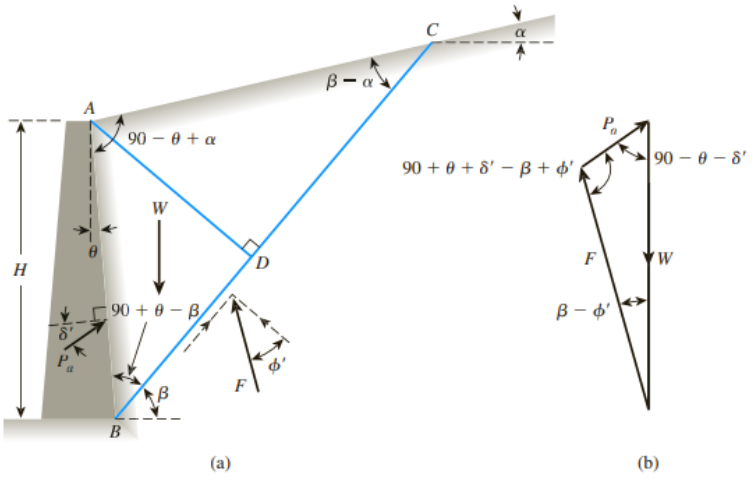

Figure 3.12. Forces included in Coulomb's active earth pressure (Das and Sobhan, 2018).

The Coulomb's active earth pressure coefficient could be found using :

$$K_a = \frac{cos^2\,(\phi' - \theta)}{\cos(\delta' + \theta)\,cos^2(\theta)\left[1 + \sqrt{\frac{\sin(\phi' - \alpha)\ \sin(\delta' + \phi')}{\cos(\theta - \alpha)\ \cos(\delta' + \theta)}}\right]^2} \tag{3.24}$$

nd the Coulomb active force can be expressed by:

$$P_a = \frac{1}{2} K_a\, \gamma\, H^2 \tag{3.25}$$

3.5.2. Coulomb Passive Earth Pressure

For the passive pressure case, the movement of the sliding wedge would be inwards and upwards. As in the active case, Coulomb considered that the soil's failure surface would be a plane and pass through the B point, as Figure 3.13 shows. Regarding the forces impacting the wedge in the passive case, these forces are the soil wedge's weight (W), the

resultant force from the perpendicular force on the failure surface and the shear force (F), and the third force is the passive force which is the consequent of W and F (Das and Sivakugan, 2018).

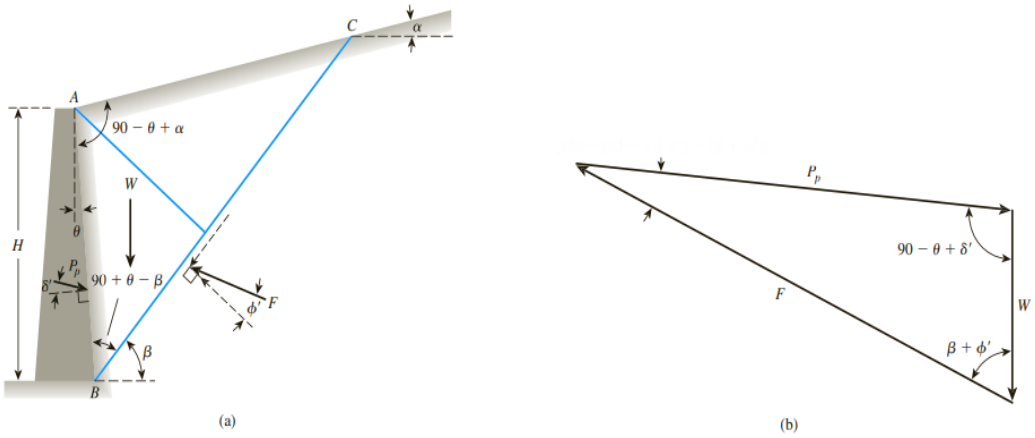

Figure 3.13. Forces included in Coulomb's passive earth pressure (Das and Sobhan, 2018).

The Coulomb's passive earth pressure coefficient could be found using :

$$K_p = \frac{cos^2(\phi' + \theta)}{\cos(\delta' - \theta)cos^2(\theta)\left[1 - \sqrt{\frac{\sin(\delta' + \phi')\ \sin(\phi' + \alpha)}{\cos(\delta' - \theta)\ \cos(\alpha - \theta)}}\right]^2} \quad (3.26)$$

And the Coulomb passive force can be expressed by:

$$P_p = \frac{1}{2} K_p\ \gamma\ H^2 \quad (3.27)$$

3.6. Comments on Rankine and Coulomb Theories

- Rankine's theory is considered easier and more widely used because Rankine relied on the absence of friction between the backfill and the wall, while Coulomb took friction into account in his theory. (Yavan et al., 2022).
- In his theory of calculating the lateral earth pressure, Coulomb relied on the resultant force, while Rankine showed the distribution of lateral pressure in his theory.
- Both Rankine and Coulomb did not consider the cohesive property of soil in their equations. However, Rankine's theory is considered more suitable for application

to cohesive soils than Coulomb's theory. Furthermore, Bell modified an equation to suit cohesive soils, and it is applicable for both Rankine and Coulomb's earth pressure coefficients (Leblebici, 2021).

3.7. Culmann's Earth Pressure Theory

Neither Rankine nor Coulomb included soil cohesion in their theories, in addition to not considering the irregular state of the soil, as they based their methods on the fact that the soil was homogeneous. In 1886, Culmann found a graphical solution to determine the lateral pressure forces for irregularly shaped soils, cohesive soils, and various cases of surcharge loads. In his method, which is considered a graphical implementation of Coulomb's theory, Culmann plotted several trial wedges and considered the largest thrusts on these sliding wedges to be the active or passive earth pressure. Moreover, Culmann's method could be used for estimating the static earth pressures as well as the dynamic ones. (Bowles and Guo, 1996; ds, 20).

The active earth pressure using Culmann's method could be determined according to these steps, which explain Figure 3.14 a:

- First, draw the slope line or Φ-line making angle Φ with the horizontal.
- From point B, draw earth pressure line or ψ-line making ψ angle with Φ-line, note that ψ is the angle of inclination that the resultant earth pressure P_A makes with the vertical and it depends on the backfill inclination angle and the wall friction angle δ (Terzaghi et al, 1996).
- To locate E_1, find the wedge's weight of ABC_1 and lay it off along Φ-line at a suitable scale to have BE_1.
- From point E_1 draw a line parallel to ψ-line until it intersects the slip plane BC_1, the point of intersection is called F_1.
- For the other wedges, repeat the previous two steps and locate E_2, E_3 and E_4 and from them plot lines parallel to ψ-line until they intersect with their slip planes to have F_2, F_3 and F_4.
- From point B, draw Culmann's line, which is a curve that passes through points B, F_1, F_2, F_3, etc.

- For Culmann's line, draw a tangent parallel to Φ-line, then to have point E, draw a parallel line to ψ-line from the tangency point F. Figure 3.14 b, shows the force polygon which is similar to the triangle BFE, so that EF is considered as the maximum earth pressure P_A and the critical sliding surface would be BFC.

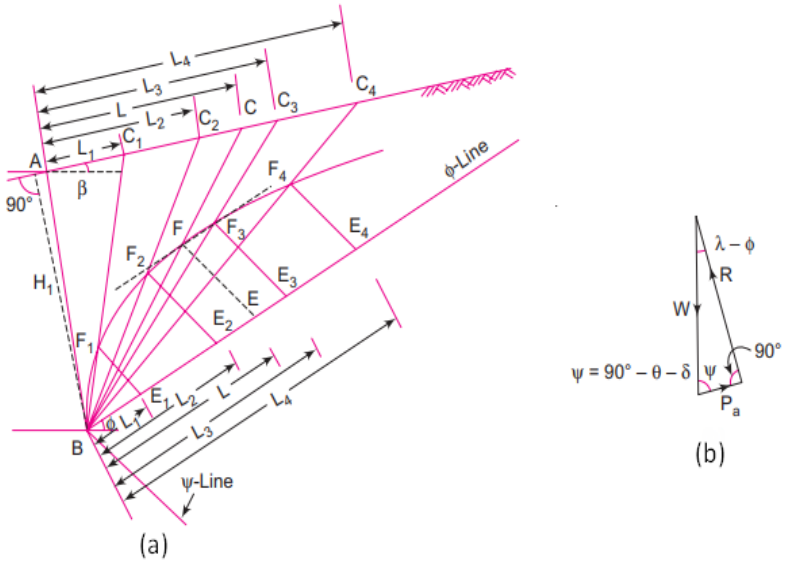

Figure 3.14. Culmann's theory of active pressure (Punmia and Jain, 2005).

Where:

λ: The angle between the rupture plane and the horizontal.

θ: Wall inclined angle from the vertical.

The procedure in the active case is also used, as illustrated in Figure 3.15a, to estimate the passive earth pressure using the Culmann method. The difference is only for the angles of Φ-line and ψ-line. The reason for that comes from the angle difference for the force polygon of the passive case, as illustrated in Figure 3.15b. Moreover, when we have such a surcharge load, the weight of wedges should include the load's weight while locating E points, and then a modified Culmann line will appear. If the new line is more significant than the first one, the difference should be added to have the maximum earth pressure.

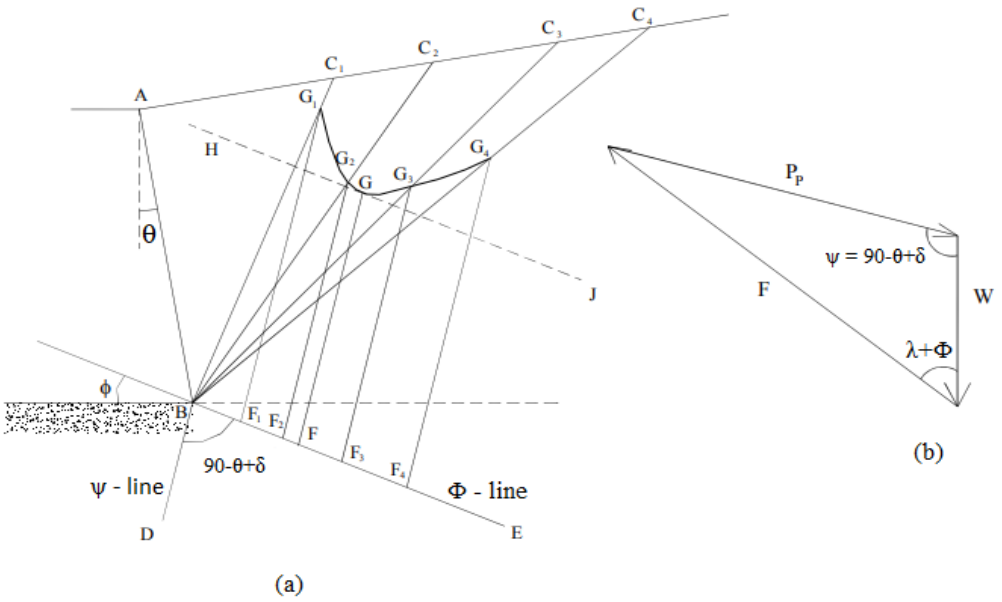

Figure 3.15. Culmann's theory of passive pressure (Özcan , 2007).

Moreover, the point of the resultant pressure could be determined by locating the center of gravity for the sliding wedge ABC and drawing a line parallel to the critical plane BC passing through the center O, as shown in Figure 3.16. The intersection of the parallel line with AB is the location of the resultant force.

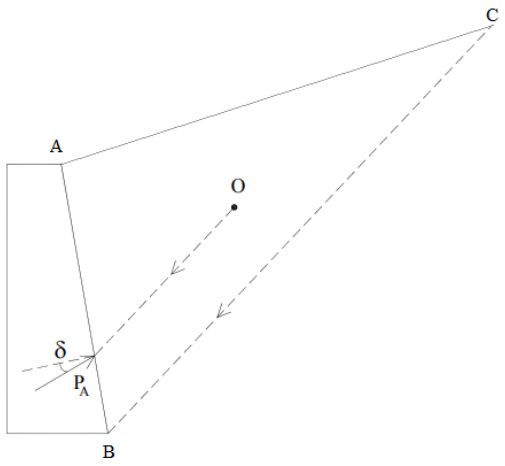

Figure 3.16. Point of action for the resultant force (Özcan , 2007).

3.8. Stability of Retaining Walls

In addition to estimating the active and passive thrusts affecting retaining structures, it is also necessary to ensure the safety and stability of the retaining walls against many failure modes to which they may be exposed. As illustrated in Figure 3.17 and according to Das and Sivakugan (2018), the retaining wall could fail in several ways, including:

- Overturning failure.
- Sliding failure.
- Bearing capacity failure.
- Deep-seated shear failure.
- Failure due to excessive settlement.

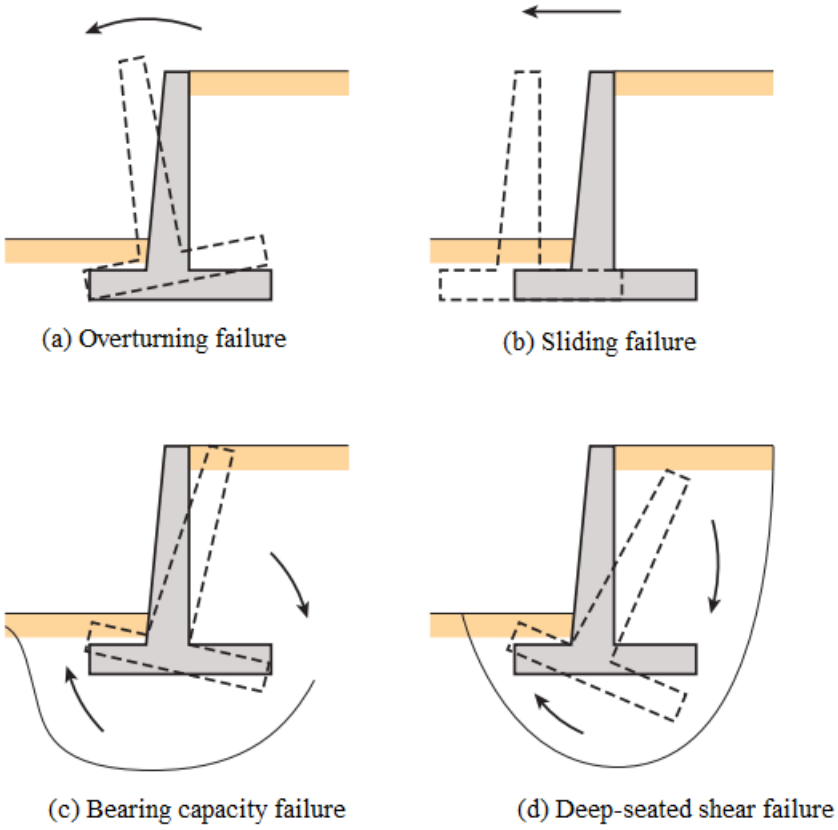

Figure 3.17. Failure modes of retaining structures (Das and Sivakugan, 2018).

3.8.1. Check for Overturning

To ensure the stability of the retaining wall against overturning, the summation of moment of forces supporting the wall and resisting overturning (ΣM_R) must be greater than the summation of that working to push it towards failure (ΣM_o). This can be expressed using a safety factor expressed as in the following equation:

$$\mathrm{FS}_{(\text{overturning})} = \frac{\Sigma M_R}{\Sigma M_o}$$

(3.28)

To find the moments correctly, let's consider Figure 3.18, which shows the forces that impact a gravity retaining wall for overturning check. For these calculations, the Rankine method assumed to be valid to estimate the active and passive thrusts due to the high values for the lateral earth pressures that could be gained from this method. Still, other methods could be used, especially when there is a seismic thrust is faced, in that cases other theories which will be explained in the next chapter, could be more practical.

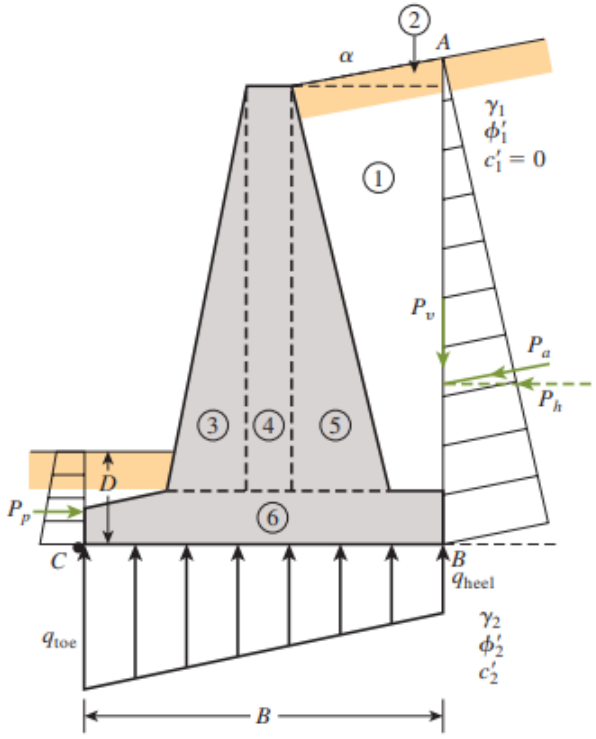

Figure 3.18. Check retaining wall against overturning (Das and Sivakugan, 2018).

The resisting moment (ΣM_R) could be calculated about the wall's toe (point C) firstly by determining the passive earth pressure using equation (3.13) expressed as:

$$P_p = \frac{1}{2} K_p \, \gamma \, H^2$$

Where, K_p is the passive earth pressure coefficient could be found by using equation (3.11):

$$K_p = tan^2(45 + \frac{\Phi'}{2})$$

For the other resisting forces that are coming from the soil's weight located above the heel and the weight of the concrete, Table 3.2 could be used to evaluate the moment about the toe by calculating the weight per unit length for the soil and the concrete expressed in Figure 3.18 by the numbers (1-6) and multiply it by the moment arm as:

Table 3.2. Process of evaluating ΣM_R.

Section	Area	Weight per unit length	Moment Arm (X)	Resisting Moment (ΣM_R)
1	A_1	$W_1 = \gamma_1 * A_1$	X_1	M_1
2	A_2	$W_2 = \gamma_1 * A_2$	X_2	M_2
3	A_3	$W_3 = \gamma_c * A_3$	X_3	M_3
4	A_4	$W_4 = \gamma_c * A_4$	X_4	M_4
5	A_5	$W_5 = \gamma_c * A_5$	X_5	M_5
6	A_6	$W_6 = \gamma_c * A_6$	X_6	M_6

Where,

γ_1 is the unit weight of the backfill.

γ_c is the unit weight of the concrete.

X_i is the horizontal distance between the point C and the centroid of the section.

Furthermore, the vertical component of the active earth pressure (P_v) is also considered as a resisting force for the overturning, which could be calculated by multiplying the active earth pressure calculated from the Rankine method using equation (3.10) with sinα which is the inclination angle of the backfill:

$$P_a = \frac{1}{2} K_a \, \gamma \, H^2$$

Where, K_a is the active earth pressure coefficient could be found by using equation (3.8):

$K_a = \ tan^2(45 - \frac{\phi'}{2})$

So that , $$P_v = P_a \ sin\alpha \tag{3.29}$$

And the moment of the force P_v is:

$$M_v = P_v B = \ P_a \ sin\alpha \ B \tag{3.30}$$

B is the slab's base width.

Moreover, to find the moment of the forces that makes the wall overturns (ΣM_o), the following equation could be used:

$$\sum M_o = \ P_h(\frac{H'}{3}) \tag{3.31}$$

Where $$P_h = \ P_a \ cos\alpha \tag{3.32}$$

Finally, and by neglecting the effect of the passive earth pressure for safety reasons, the factor of safety for overturning can be estimated using equation (3.33), however, the recommendable minimum value for $FS_{(overturning)}$ is 2-3:

$$FS_{(overturning)} = \frac{M_1+M_2+M_3+M_4+M_5+M_6+M_v}{P_a \cos\ \alpha\left(\frac{H'}{3}\right)} \tag{3.33}$$

3.8.2. Check for Sliding

Another check has to be made to ensure the design stability of retaining structures against sliding. The safety factor for this check consists of the forces resisting sliding ($\Sigma F_{R'}$) and the forces causing it ($\Sigma F_{R'}$), both in the horizontal direction. The value of the safety factor must not be less than 1.5:

$$FS_{(sliding)} = \frac{\Sigma F_{R'}}{\Sigma F_d} \quad (3.34)$$

Considering Figure 3.19, the sliding resistance force would be generated from two parts: the passive lateral earth pressure, which can be calculated using equation (3.13), and another force that is generated between the soil and the bottom base of the wall and can be expressed by the following equation:

$$R' = s\,(cross\ section\ area) = (\sigma' \tan\delta' + c'_a) * (B * 1) \quad (3.35)$$

$$R' = B\sigma' \tan\delta' + Bc'_a \quad (3.36)$$

Where,

S is the soil shear strength located at the bottom of the concrete slab.

c'_a is the adhesion between the concrete slab and the soil.

δ' is the friction angle between the concrete slab and the soil.

B is the width of the concrete slab.

But $B\sigma'$ is the summation of all the vertical forces = $\sum$V

So, the total sliding resistance force including the passive pressure could be written as:

$$\Sigma F_{R'} = (\sum V) \tan\delta' + Bc'_a + P_p \quad (3.37)$$

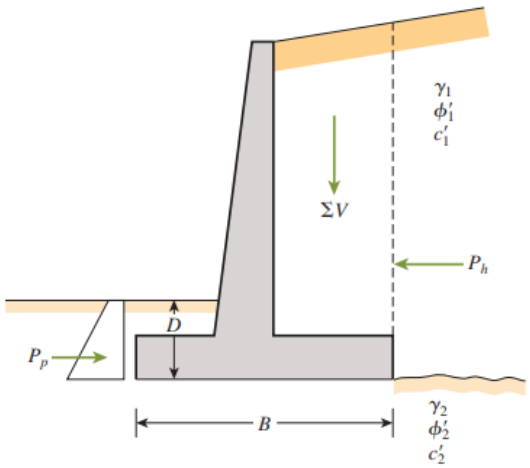

Figure 3.19. Check retaining wall against sliding (Das and Sivakugan, 2018).

The only force that causes the sliding of the wall, is the horizontal component of the active earth pressure (P_h) expressed in equation (3.32). So, the factor of safety regarding to sliding ($FS_{(sliding)}$) for the retaining structures would be:

$$FS_{(sliding)} = \frac{(\sum V)\tan\delta' + Bc'_a + P_p}{P_a\, cose\ \alpha} \geq 1.5 \qquad (3.38)$$

3.8.3. Check for Bearing Capacity Failure

Another possible failure of retaining walls, for which it is necessary to be checked, is the failure regarding bearing capacity of the foundation soil ($FS_{bearing\ capacity}$); the factor of safety for this check depends on the ultimate bearing capacity of the foundation soil (q_u) which should be greater than the pressure applied to the ground by the foundation of the retaining wall (q_{max}). However, the value of the safety factor for the bearing capacity of the wall foundation shouldn't be less than 3 (Sönmez, 2023; Das and Sivakugan, 2018).

Figure 3.20 below shows a retaining wall and the forces acting on it at point E, and those forces are ($\sum V$), (P_h), and their resultant force R. Point E is not located at the center of the foundation, but has a distance away from the wall's toe therefore we have an eccentric load case that gives a soil pressure distribution that has a variation on its value from q_{min} to q_{max}.

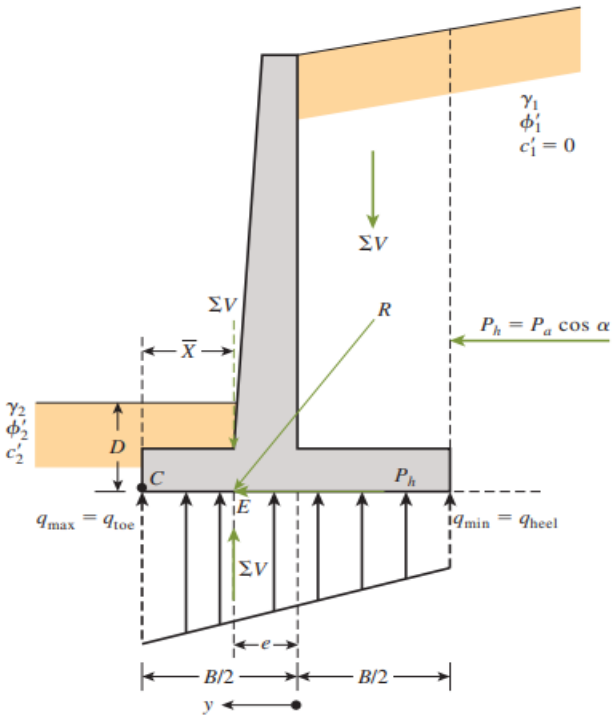

Figure 3.20. Check retaining wall for bearing capacity (Das and Sivakugan, 2018).

Therefore, the eccentricity (e) could be expressed by :

$$e = \frac{B}{2} - \bar{X} \tag{3.39}$$

note that e should be less than B/6, otherwise the design should redone to minimize this value, and the distance from point E and the wall's toe is:

$$\bar{X} = \frac{\sum M_R - \sum M_o}{\sum V} \tag{3.40}$$

Where $(\sum M_R)$ and $(\sum M_o)$ are the same as the check for the overturning.

$$q_{min} = \frac{\sum V}{B}\left(1 - \frac{6e}{B}\right) \tag{3.41}$$

$$q_{max} = \frac{\sum V}{B}\left(1 + \frac{6e}{B}\right) \tag{3.42}$$

Note that when the eccentricity value is greater than $\frac{B}{6}$, the value of q_{min} will be negative giving an indication that the soil is under tension. Because the soil has low tension strength, it is recommended that the wall be modified to reduce the value of the eccentricity. Moreover, for the estimation of the ultimate bearing capacity of the foundation soil, the Meyerhof equation could be used as follows:

$$q_u = c_2' N_c F_{cd} F_{ci} + q N_q F_{qd} F_{qi} + \frac{1}{2}\gamma_2 B' N_\gamma F_{\gamma d} F_{\gamma i} \tag{3.43}$$

Where,

$$q = \gamma_2 D \tag{3.44}$$

$$B' = B - 2e \tag{3.45}$$

And,

$$F_{cd} = F_{qd} - \frac{1 - F_{qd}}{N_c \tan \phi_2'} \tag{3.46}$$

$$F_{qd} = 1 + 2\tan \phi_2' (1 - \sin \phi_2')^2 \frac{D}{B'} \tag{3.47}$$

$$F_{\gamma d} = 1 \tag{3.48}$$

$$F_{ci} = F_{qi} = \left(1 - \frac{\psi^\circ}{90^\circ}\right)^2 \tag{3.49}$$

$$F_{\gamma i} = \left(1 - \frac{\psi^\circ}{\phi_2'^\circ}\right)^2 \tag{3.50}$$

$$\psi^\circ = \tan^{-1}\left(\frac{P_a \cos \alpha}{\Sigma V}\right) \tag{3.51}$$

Finally, the factor of safety regarding to bearing capacity failure is given by :

$$\mathrm{FS}_{(\text{bearing capacity})} = \frac{q_u}{q_{\max}} \tag{3.52}$$

3.8.4. Check for Settlement

Settlement is considered one of the critical problems that must be taken into consideration in the design of structural projects in general and retaining structures in particular because it is critical and followed by a tilt of the wall if it occurs, mainly when differential settlement occurs. The settlement is divided into two parts: the elastic settlement, which appears for the foundations immediately after the construction is completed, and the consolidation settlement, which depends on the permeability of the soil itself and the time required for water molecules to gradually dissipation from the soil voids, and thus takes time to occur. Figure 3.21 shows a footing and the loading acting on it, in addition to the deformation shapes for the case of rigid foundation, which has a uniform settlement, and the flexible one, which has a nonuniform settlement.

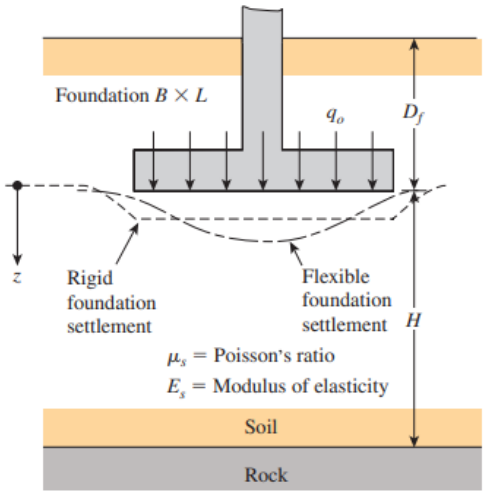

Figure 3.21. Elastic settlement for rigid and footing (Das and Sivakugan, 2018).

The elastic settlement could be calculated by:

$$S_e = \frac{q_o B}{E_s}(1-\mu_s^2)I \text{ (under the center of flexible foundation)} \qquad (3.53)$$

$$S_e = \frac{q_o B}{E_s}(1-\mu_s^2)\frac{I}{2} \text{ (under the corner of flexible foundation)} \qquad (3.54)$$

Where, q_o is the pressure applied by the foundation to the soil under it.

B is the foundation width.

E_s is the soil's modulus of elasticity.

μ is the Poisson's ratio of the soil.

I is the influence factor that can be estimated using:

$$I = \frac{1}{\pi}\left[m'\ln\left(\frac{1+\sqrt{m'^2+1}}{m'}\right) + \ln\left(m' + \sqrt{m'^2+1}\right)\right] \quad (3.55)$$

And for the case where the foundation is underlying with saturated clay, Janbu and Kjaernsli (1956) gave an equation to estimate the average settlement for a flexible foundation as:

$$S_e = A_1 A_2 \frac{q_o B}{E_s} \quad (3.56)$$

Where, A_1 and A_2 factors could be found using Figure 3.22.

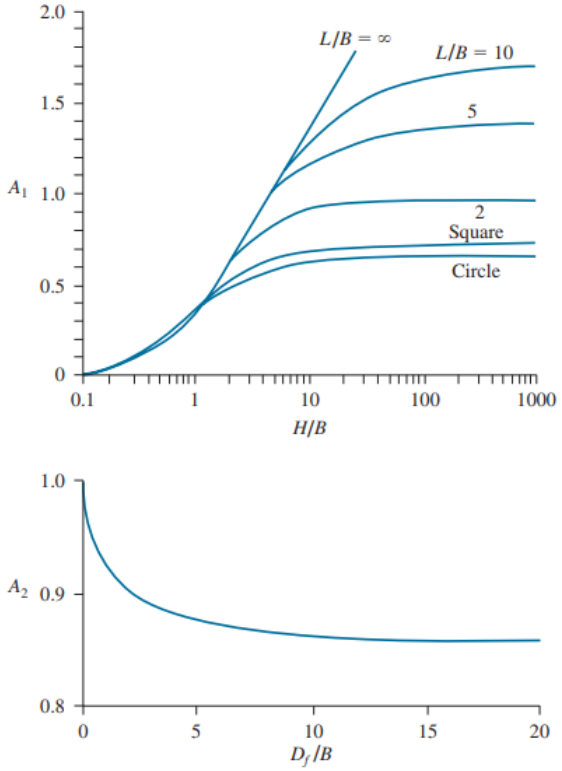

Figure 3.22. Evaluating of A_1 and A_2 (Das and Sivakugan, 2018).

For the walls settled on clayey soil, consolidation settlements can calculated by using Terzaghi theory (Das and Sivakugan, 2018).

3.8.5. Deep Shear Failure

In the previous sections, some checks that could help in ensuring the design quality of the retaining walls were covered. The checks were related to the stability of these walls from failure resulting from a close distance to the wall. Still, in the case of deep shear failure, the failure occurs within a greater and more comprehensive distance than the rest of the previous types of failure, as shown in Figure 3.23 a, which illustrates a wall built near a slope. Another case that causes the deep shear failure to occur is building the wall on weak soil with a depth that can reach one and a half times the width of the base of the wall, as shown in Figure 3.23 b (Clayton et al., 2014; Das and Sivakugan, 2018).

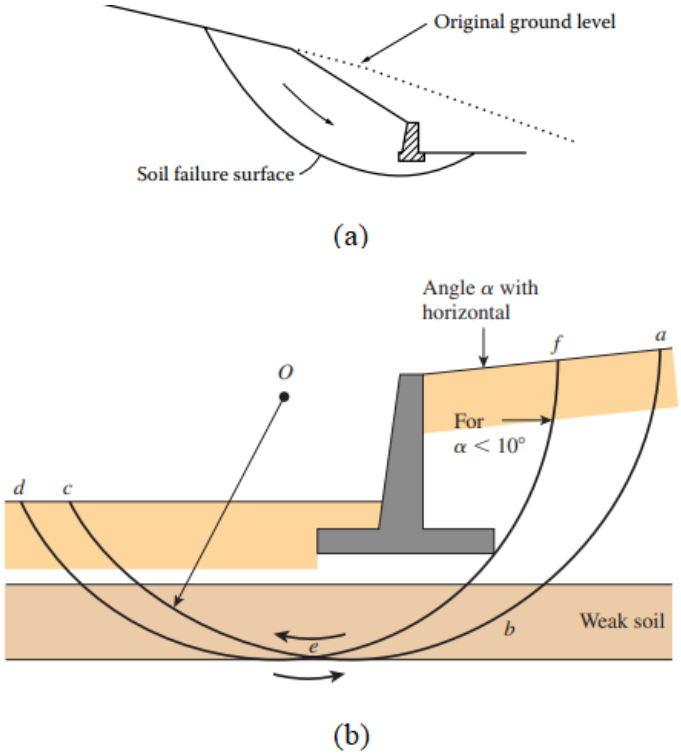

Figure 3.23. Deep shear failure (Clayton et al., 2014; Das and Sivakugan, 2018).

This type of failure can cause critical damage due to its large size compared to other kinds of failure, and therefore, necessary measures must be taken to avoid it. However, a check against this collapse can be done using the Swedish Slice method, which is a standard method used to make calculations for the stability of slopes, in addition to some software that relies on the finite element method, such as Plaxis 2D (Sönmez, 2023).

4. DYNAMIC EARTH PRESSURE

When designing retaining walls in earthquake zones, the dynamic forces resulting from earthquakes have to be considered in the calculations along with the static forces, as the seismic behavior of the wall depends on these forces combined. Methods for calculating static forces according to the Rankine and Coulomb method were covered in the previous chapter, but when talking about dynamic forces, given the wall movement relies on the response or the interaction of the backfill soil and also the foundation soil under the wall, in addition to its dependence on the response of the wall itself to the flexural and inertial forces, knowing that the soil layers in their nature are not Homogeneous, determining the seismic behavior of the retaining structures is somewhat complex, and to facilitate this, the forces resulting from seismic activities have been represented by an equivalent static force. In this chapter, some of the methods used to calculate dynamic lateral forces will be discussed in detail (Kramer, 1996).

4.1. Mononobe-Okabe

Okabe (1926) and Mononobe (1929) are the first to present a theory for calculating ground lateral pressures for the dynamic conditions where the seismic influence is playing a role. Their theory, Mononobe-Okabe (M-O), is considered an extension of Coulomb's method and is applied to dry cohesionless soil. Mononobe and Okabe built their theory based on the state of perfect plastic, or what is known as pseudo-static, by adding a horizontal and vertical component that expresses the seismic acceleration to the Coulomb wedge and, thus, the dynamic lateral pressure of the pseudo-static case is calculated through the force equilibrium for Coulomb's wedge (Das and Puri, 1996; Woodward and Griffiths, 1970).

Based on Nazarian and Hadjian (1979), the basic assumptions of Mononobe-Okabe's theory can be summarized in the following points:

- The lateral forces' influence point is located at ($\frac{H}{3}$) from the base of the wall.

- It was assumed that there is an appropriate distance for the wall to displace to generate a state of static equilibrium at the minimum value of the active earth pressure and mobilize the maximum value for the shear strength of the soil along the sliding surface.
- To make the acceleration in the horizontal and vertical directions uniform for the wedge of the soil, meaning that the value of the acceleration behind the wall is the same at any depth, it was assumed that the wall and the soil behind it act like a rigid body.

Figure 4.1 shows the expressed forces in the theory of Mononobe-Okabe in addition to the force polygon of the failure wedge:

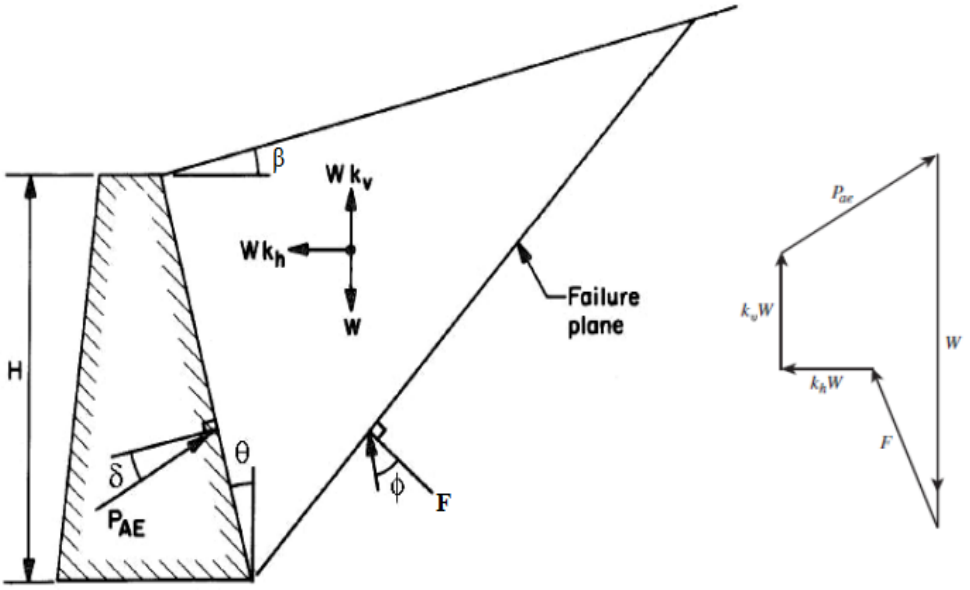

Figure 4.1. Forces regarding seismic active earth pressure (Das and Sobhan, 2018).

Where:

- W is the weight of the soil wedge.
- F is the resultant force from the normal of the failure surface and the shear.
- P_{ae} is the active lateral earth pressure.
- k_h is the inertial force in the horizontal direction.
- k_v is the inertial force in the vertical direction.

Also, k_h and k_v are the pseudo-static accelerations in the horizontal and the vertical directions respectively and could be expressed as:

$$k_h = \frac{earthquake\ acceleration\ in\ the\ horizontal\ direction\ (a_h)}{g}$$

$$k_v = \frac{earthquake\ acceleration\ in\ the\ vertical\ direction\ (a_v)}{g}$$

And g is the gravity acceleration.

The total active lateral pressure in the dynamic condition according to M-O theory could be expressed by the equation:

$$P_p = \frac{1}{2} K_{AE}\ \gamma\ H^2(1 - K_v) \tag{4.1}$$

And the dynamic earth pressure for the active case (K_{AE}) is given by:

$$K_{AE} = \frac{cos^2(\phi' - \theta - \psi)}{cos\psi cos^2\theta \cos(\delta' + \theta + \psi)\left[1 + \sqrt{\frac{\sin(\delta' + \phi')\ \sin(\phi' - \beta - \psi)}{\cos(\delta' + \theta + \psi)\ \cos(\theta - \beta)}}\right]^2} \tag{4.2}$$

And:

$$\psi = tan^{-1}\left(\frac{K_h}{1 - k_v}\right) \tag{4.3}$$

For the passive case, where the force acting to push the wall inwards as illustrated in Figure 4.2, (M-O) equation to calculate the total passive lateral pressure in the dynamic condition could be given by:

$$P_p = \frac{1}{2} K_{PE}\ \gamma\ H^2(1 - K_v) \tag{4.4}$$

And the dynamic earth pressure for the passive case (K_{pE}) is given by:

$$K_{PE} = \frac{cos^2(\phi' + \theta - \psi)}{cos\psi cos^2\theta \cos(\delta' - \theta + \psi)\left[1 + \sqrt{\frac{\sin(\delta' + \phi')\ \sin(\phi' + \beta - \psi)}{\cos(\delta' - \theta + \psi)\ \cos(\beta - \theta)}}\right]^2} \tag{4.5}$$

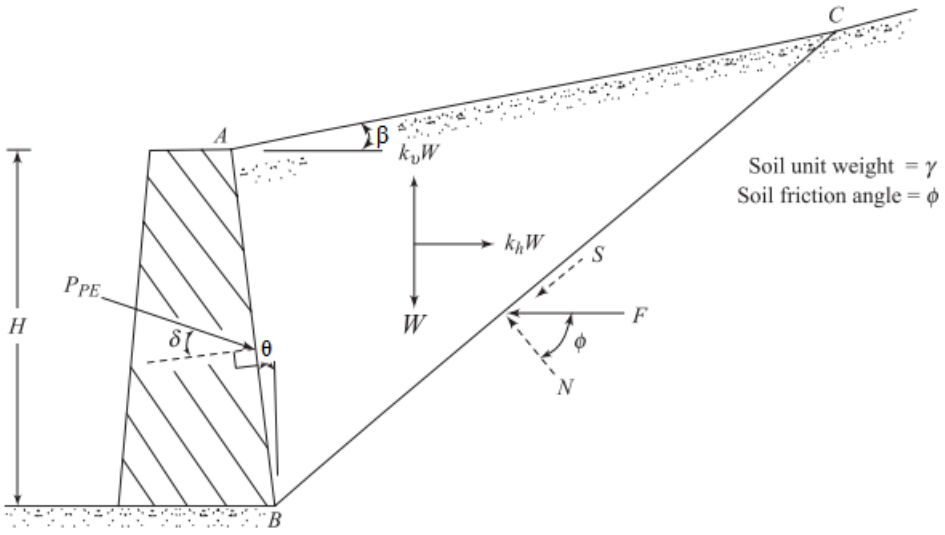

Figure 4.2. Seismic passive earth pressure regarding Mononobe-Okabe (Özcan , 2007).

4.1.1. Limitations for Mononobe- Okabe (M-O) Theory

Mononobe-Okabe theory couldn't be applicable in some engineering problems due to some limitations and inability to answer some questions such as:

- In the M-O method, soil cohesion was not taken into account, as it can only be applied to cohesionless soils.
- The equation that Mononobe and Okabe provided did not include the effect of the water table in the backfill soil behind the wall.
- For the case where $(\phi' - \beta - \psi) < 0$, the value of the total dynamic thrust remains unknown, the M-O method doesn't have an answer for this case.

4.2. Seed and Whitman Theory

As an alternative to the Mononobe-Okabe method for calculating dynamic earth pressure, which is considered as a complex formulated dynamic behavior, Seed and Whiteman (1970) presented a parametric study to estimate the effects on the value of the dynamic earth pressure by changing the slope of the backfill soil, the angle of friction of the soil, and the angle of friction of the wall. Seed and Whitman (1970) divided the total thrust for the dynamic condition (P_{AE}) into two components, a component for the static state (P_A) and a component for the dynamic state (ΔP_{AE}) so that:

$$P_{AE} = P_A + \Delta P_{AE} \quad (4.6)$$

Also,

$$K_{AE} = K_A + \Delta K_{AE} \quad (4.7)$$

Based on the analysis carried out by Seed and Whitman (1970) and for practical objective, they proposed that:

$$\Delta K_{AE} \approx \frac{3}{4} K_h \quad (4.8)$$

$$\Delta P_{AE} = \frac{1}{2} \gamma H^2 \left(\frac{3}{4}\right) K_h = \left(\frac{3}{8}\right) K_h \ \gamma H^2 \quad (4.9)$$

Where ɣ is the soil's unit weight, H is the wall's height and K_h is the horizontal acceleration of the ground. Furthermore, Seed and Whitman (1970) provided recommendations when designing retaining walls to resist seismic thrusts; they suggest using a value for ground acceleration of about 85% of its peak value, as they noticed that the highest value of the acceleration occurs instantaneously, so that there is not enough period to make a large displacement for the wall to collapse. Thus, it is possible to use a lower value for the ground acceleration. (Mikola and Sitar, 2013). M-O theory presented an assumption that the effect of the total thrust in the active state acts at a height $(\frac{H}{3})$ from the wall's base, but experiments and practical research results have suggested that the point of influence of these forces as a result of the effect of the dynamic state, is at a point higher than that. Thus, Seed and Whitman (1970) pointed out that the action point of the dynamic component could be approximately at a height (0.6H) from the wall's base, as shown in Figure 4.3 (Kramer, 1996).

Therefore, the point of impact of the total thrust in the active case (P_{AE}) can be determined using the following equation:

$$h = \frac{P_A H/3 + \Delta P_{AE}\,(0.6H)}{P_{AE}} \quad (4.10)$$

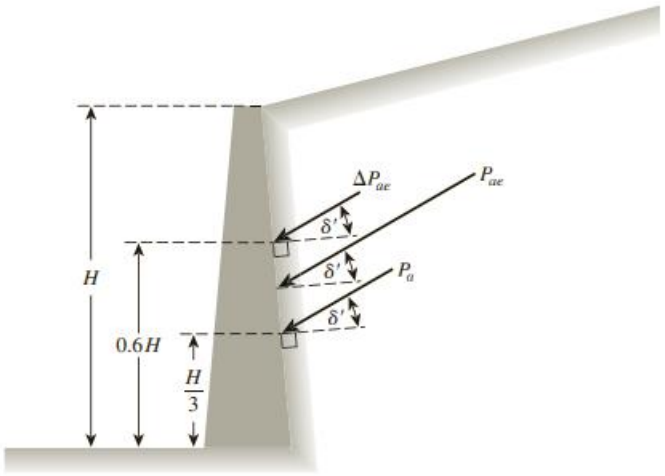

Figure 4.3. Seismic active pressure's point of action (Das and Sobhan, 2018).

4.3. Steedman and Zeng Theory

In Mononobe-Okabe's theory, it was assumed that the acceleration in the backfill soil behind the retaining wall is uniform, not only in the value but also in the phase of the acceleration. Steedman and Zeng (1990) presented that the situation is different. In practice, the shear modulus within the soil behind the wall is reducing as it approaches the ground surface for cohesionless soil. This leads to a phase change and amplification in the motion between the ground surface and the wall base. Steadman and Zeng (1990) presented a solution to calculate dynamic earth pressure by considering the amplification and phase changes in the backfill soil.

Dynamic analysis was made based on the assumption that only the phase of the acceleration will vary, not the magnitude, to show the effect of the change in phase between the ground surface and the base of the wall. Figure 4.4 shows a vertical cantilever wall with horizontal backfill and for harmonic motion, the acceleration for time t and at the depth z would be:

$$A(z,t) = k_h\, g \sin\, \omega\left(t - \frac{H-z}{V_s}\right) \tag{4.11}$$

Where, the shear wave velocity $V_s = \sqrt{\frac{G}{\rho}}$, G is the shear modulus and ρ is the soil density.

And the period of the shaking $T = \frac{2\pi}{\omega}$, ω is the angular frequency.

The wedge's weight

$$W = \frac{1}{2}\frac{\gamma H^2}{\tan\alpha} \tag{4.12}$$

ɣ is the soil's unit weight and α is the inclination angle of the failure plane.

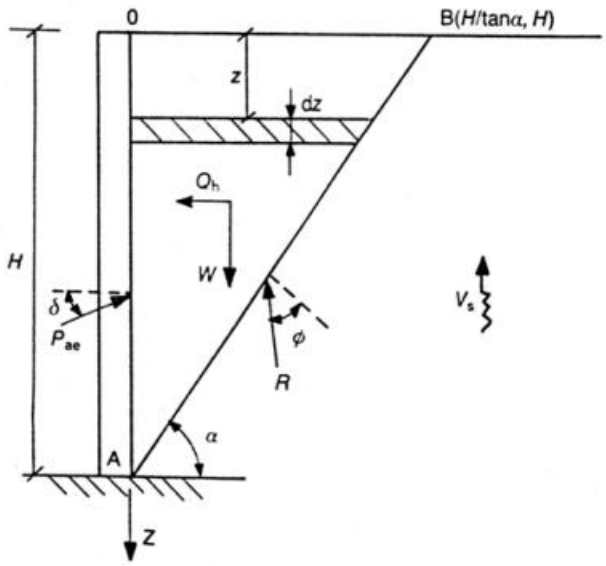

Figure 4.4. Forces for estimation of seismic earth pressure (Steedman and Zeng, 1990).

By taking a horizontal element from the failure wedge and considering its mass, the inertial horizontal force Q_h could be expressed by:

$$Q_h = \int_0^H \rho\left(\frac{H-z}{\tan\alpha}\right) A(z,t)dz \tag{4.13}$$

and the total lateral earth pressure acting on the wall (P_{AE}) in addition to the lateral pressure coefficient (K_{ae}) could be found using the following:

$$P_{AE} = \frac{Q_h\cos(\alpha-\phi)+W\sin(\alpha-\phi)}{\cos(\delta-\alpha+\phi)} \tag{4.14}$$

$$K_{AE} = \frac{2P_{AE}}{\gamma H^2} \tag{4.15}$$

Note that K_{ae} depends on the expression $(\frac{H}{T V_s})$, which is the ratio of the time needed for a wave to travel the total height to the period of the lateral vibrating. This conclusion is shown in Figure 4.5.

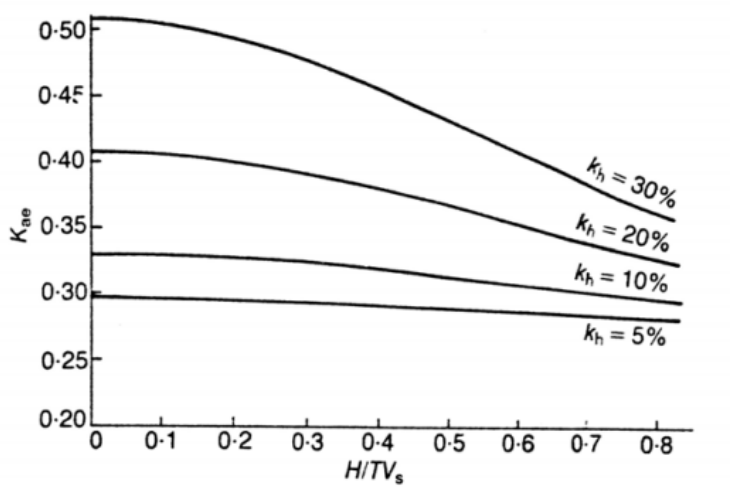

Figure 4.5. Effect of changing the phase on earth pressure coefficient (Steedman and Zeng, 1990).

An assumption was made to recognize the influence of the amplification on K_{ae}, on which the lateral acceleration value varies from the layer's base to the ground surface, where the factor of constant amplification f_a is constant. At depth z and for time t, the acceleration could be calculated by:

$$A(z,t) = \left[1 + \frac{H-z}{H}(f_a - 1)\right] k_h \, g \sin \, \omega \left(t - \frac{H-z}{V_s}\right) \qquad (4.16)$$

In a similar way, Q_h can be calculated through the equation (4.13), and the variation of K_{AE} with f_a is shown in Figure 4.6.

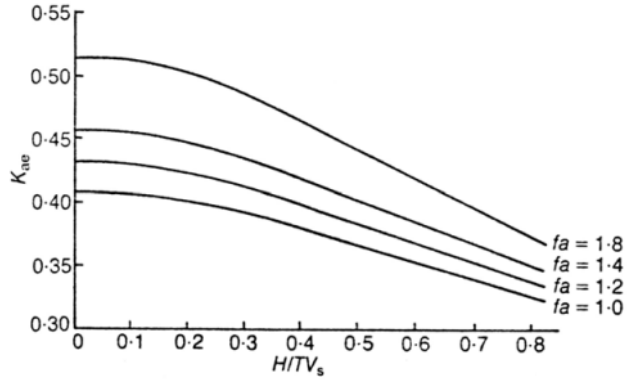

Figure 4.6. Effect of amplification factor on earth pressure coefficient (Steedman and Zeng, 1990).

4.4. Wood's Theory

All the solutions and the methods that were presented previously were based on the theory that the walls are allowed to move a sufficient distance to reach the active state, which reduces the lateral loads on the retaining walls and helps in mobilizing the shear strength of the soil located behind the wall. But when using the type of gravity walls, for example, in retaining projects, such walls do not move sufficiently to develop either the active or the passive states.

Wood (1973) presented a solution related to calculating dynamic thrusts, based his analysis on two rigid walls. Between them, is an elastic linear homogeneous soil, as shown in Figure 4.7, and below the soil is a rigid base. According to Wood, if the input motions have a low frequency ($f_o = \frac{V_s}{4H}$), then the amplification resulting from the dynamic state can be neglected. Accordingly, Wood proposed equations to calculate the dynamic thrust and the bending moment for the dynamic case turning about the wall's base (Kramer, 1996; Yıldız, 2007).

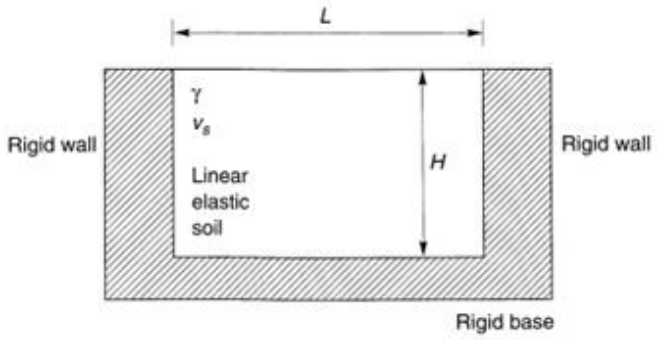

Figure 4.7. Wood's model for analysing nonyielding walls (Wood, 1973).

$$\Delta P_{eq} = \gamma H^2 \frac{a_h}{g} F_p \tag{4.17}$$

$$\Delta M_{eq} = \gamma H^3 \frac{a_h}{g} F_m \tag{4.18}$$

Where;

ΔP_{eq}: The dynamic thrust

a_h : The horizontal acceleration

F_p , F_m : Dimensionless factors for the dynamic thrust and bending moment could be found using Figure 4.8.

Moreover, the dynamic thrust's influence point could be located from the walls' base using:

$$h_{eq} = \frac{\Delta M_{eq}}{\Delta P_{eq}} \tag{4.19}$$

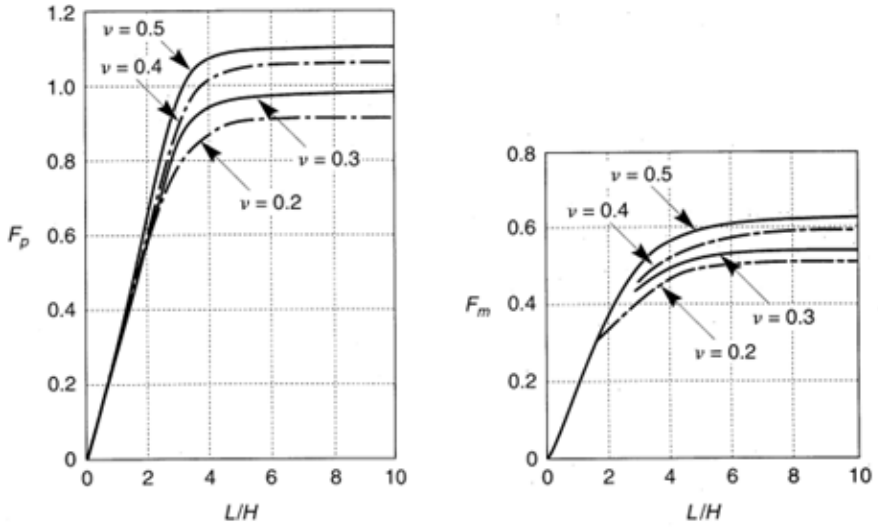

Figure 4.8. F_p and F_m for different geometries (Wood, 1973).

4.5. Culmann Method

In the third chapter, Cullmann's method, which is considered a graphical solution for calculating the static earth pressures that could be developed behind the retaining walls, was covered. However, Kapila (1962) modified for this method to be used in estimating the dynamic earth pressures for the active case (P_{AE}) and for the passive case (P_{PE}) by adding some additional forces resulting from the impact of earthquakes to the force polygon.

Looking at Figure 4.9a, the value (W - K_v W) represents the resultant of the vertical forces by subtracting (K_vW) from (W), and to limit the force triangle to only three forces which are F, P_{AE} and $W\sqrt{(1-K_v)^2+{K_v}^2}$as shown in Figure 4.9b and by applying the Pythagorean law, the value $W\sqrt{(1-K_v)^2+{K_v}^2}$ can be obtained. By considering

multiple trial wedges, this process aims to obtain the maximum active lateral pressure P_{AE}. Knowing that θ is the wall angle of inclination from the vertical, β is the backfill inclination angle from the horizontal, Φ is the friction angle of the soil, δ is the friction angle between the wall and the soil, α is the angle of inclination for the failure plane from the horizontal and $\psi = tan^{-1}\left(\frac{K_h}{1-k_v}\right)$.

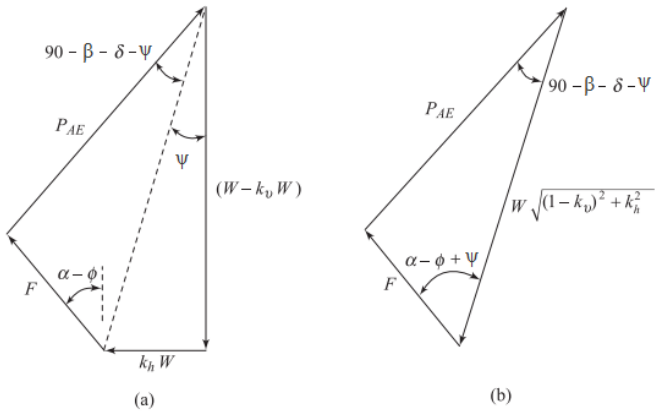

Figure 4.9. Force polygon regarding Culmann's method for seismic active earth pressure (Das and Ramana, 2010).

Taking Figure 4.10 as a reference, the following steps could be used to determine the maximum active earth pressure using the modified Culmann method:

- Draw a line making angle (Φ-ψ) with the horizontal (BE).
- Draw another line (BD) making angle (90-θ-δ-ψ) under the first line.
- To make trial failure surfaces, draw BC_1, BC_2, and so on.
- Calculate the value $\sqrt{(1-k_v)^2 + {k_v}^2}$ by determining k_h and k_v.
- By multiplying the area of every wedge by the unit weight of the soil ɣ, determine the weights W_1, W_2, …. of the failure wedges ABC_1, ABC_2, … per unit length.
- Determine the value of W_1', W_2', W_3', … where:

  $W_1' = W_1\sqrt{(1-k_v)^2 + {k_v}^2}$

  $W_2' = W_2\sqrt{(1-k_v)^2 + {k_v}^2}$, and so on.

- On the line BE and using a proper scale draw BF_1 on which $BF_1 = W_1'$, and do the same for BF_2, BF_3
- Make the force triangles for the trial wedges by drawing F_1G_1, F_2G_2, F_3G_3, …., parallel to the line BD.
- Draw a smooth curve passing through G_1, G_2, G_3, …
- Draw HJ a tangent line parallel to BE and locate the tangency point G.
- From point G, draw a line parallel to BD until it intersects BE at point F.
- The active pressure (P_{AE}) could be determined by multiplying GF with the adopted scale.

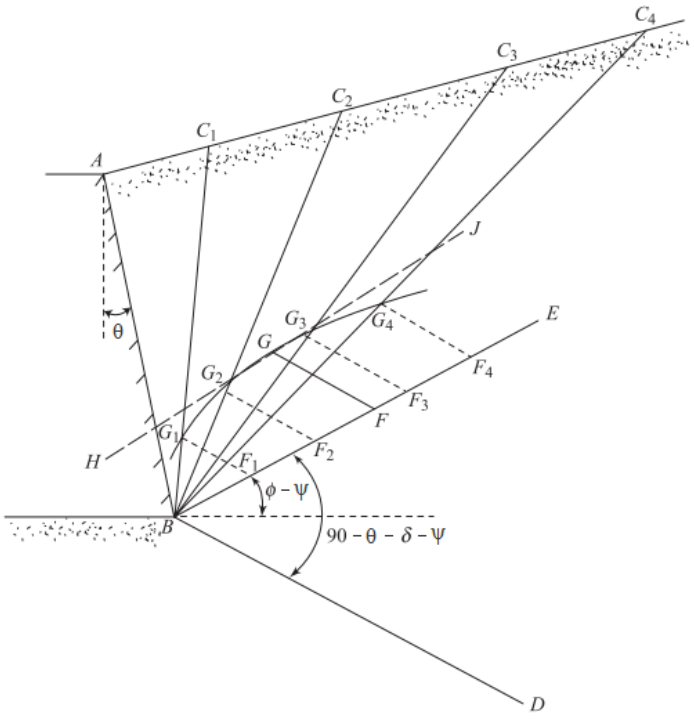

Figure 4.10. Modified Culmann method for estimation of seismic active pressure (Das and Ramana, 2010).

For the Passive case, the same procedure is followed as the active case to find the Passive dynamic earth pressure (P_{PE}); the difference would be in the angles for the lines BE and BD because the angles of the force polygon for the passive case is changed as shown in Figure 4.11. Moreover, Figure 4.12 shows the modified Culmann method to calculate the

total passive thrust for the dynamic condition, which would equal to FG the smallest force found multiplied by the chosen scale.

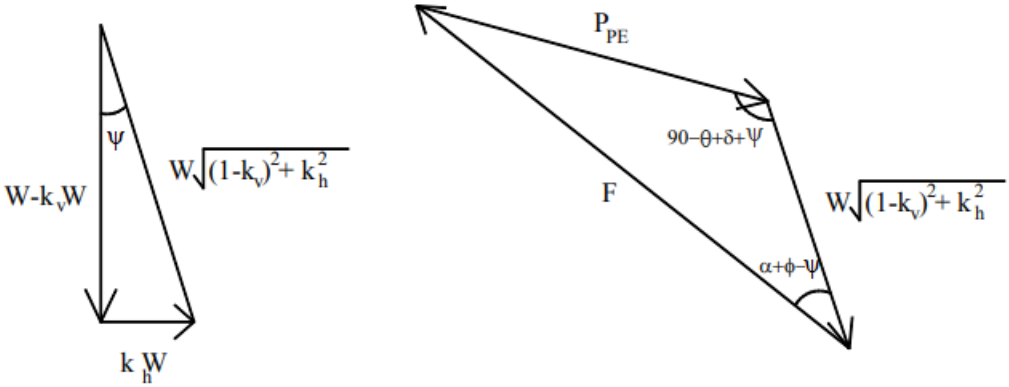

Figure 4.11. Force polygon regarding Culmann's method for seismic passive earth pressure (Özcan , 2007).

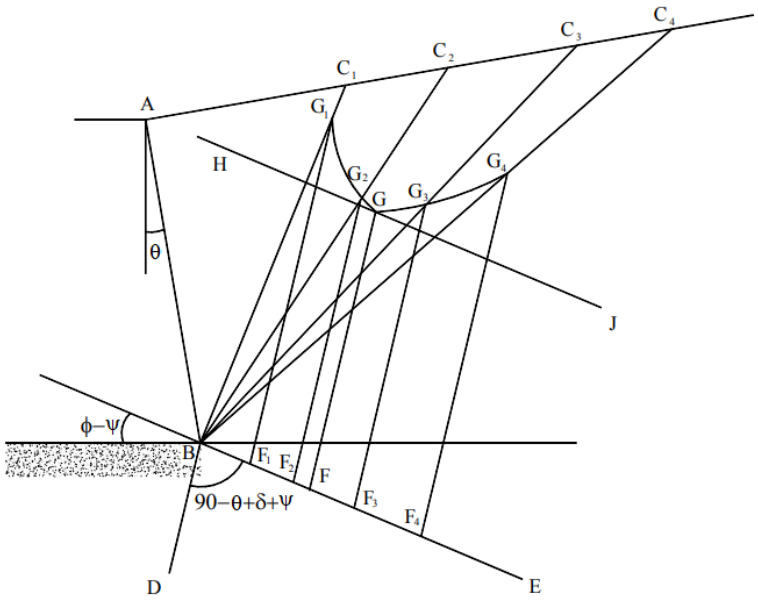

Figure 4.12. Modified Culmann method for estimation of seismic passive pressure (Özcan , 2007).

4.6. Prakash and Saran Method

The past methods discussed in this chapter were solutions for estimating the dynamic earth pressures affecting retaining walls. The similarity between these methods is that they are

based on the assumption that the soil behind the wall is cohesionless. Prakash and Saran (1968) developed a general way of calculating these dynamic and static earth pressures, taking into account the cohesion of the soil. They based their method on several basics, including that the soil surface is horizontal and subjected to a surcharge load. In addition to that, they neglected the effect of the vertical component of the internal force (K_vW) and they considered the value of the adhesion between the interface of the wall and the soil to be equal to the value of the cohesion of the backfill soil (Das and Ramana, 2010; Saran, 2021). Considering Figure 4.13, showing a retaining system with wall face AB, α the wall's inclination angle with the vertical, $\theta_1$the trial surface inclination angle and the area of cracks in clayey soil being A D_1C_1E, which extends to depth h_o at the bottom of AD_1. The depth of the cracked zone h_o is given by:

$$h_o = \frac{2c}{\gamma\sqrt{K_a}} \tag{4.20}$$

Where,

$$K_a = tan^2(45 - \frac{\Phi}{2}) \tag{4.21}$$

and

$$n = \frac{h_o}{H_1 - h_o} \tag{4.22}$$

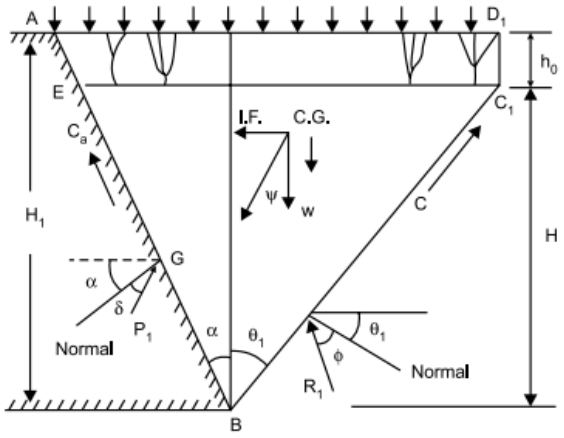

Figure 4.13. Forces for calculating seismic earth pressure (Saran, 2021).

Where,

H: is the height of the retaining wall where is no cracks and

H_1: is the wall's total height.

The forces considered in this method that is acting on the wedge D_1C_1BEA and their components is summarized in Table 4.1 below:

Table 4.1. Calculating seismic earth pressure using Prakash and Saran method.

Designation	Vertical components	Horizontal components
The wedge's weight, W	$\frac{1}{2}\,\gamma H^2(\tan\alpha+\tan\theta_1)$ $+\gamma n H^2(\tan\alpha+\tan\theta_1)$ $+\frac{1}{2}\gamma n^2 H^2(tan\,\alpha)$	-
Cohesion, C= c H sec θ_1	cH	c H tan θ_1
Adhesion, C_a=c'H sec α	c'H	c'H tan α
Surcharge, Q	q [H (tan α + tan θ_1)+ n H tan α]	-
Soil reaction, R_1	R_1 sin (θ_1+ Φ)	R_1 cos (θ_1+ Φ)
Inertia force	-	(W + Q) α_h
Earth pressure, P_1	P_1 sin (α + δ)	P_1 cos (α + δ)

Let $\beta = \Phi + \theta_1 + \alpha$

Cohesion coefficient,

$$(N_{ac})_{dyn} = \frac{\cos\beta\sec\alpha+\cos\phi\sec\theta_1}{\sin(\beta+\delta)} \tag{4.23}$$

Surcharge load coefficient,

$$(N_{aq})_{dyn} = \frac{[(n+1)\tan\alpha+\tan\theta_1][\cos(\theta_1+\phi)+\alpha_h\sin(\theta_1+\phi)]}{\sin(\beta+\delta)} \tag{4.24}$$

Coefficient respective to the ground,

$$(N_{a\gamma})_{dyn} = \frac{[(n+1/2)(\tan\alpha+\tan\theta_1)+n^2\tan\alpha][\cos(\theta_1+\phi)+\alpha_h\sin(\theta_1+\phi)]}{\sin(\beta+\delta)} \tag{4.25}$$

The dynamic active earth pressure could be calculated using:

$$(P_A)_{dyn} = \gamma H^2(N_{a\gamma})_{dyn} + qH(N_{aq})_{dyn} - cH(N_{ac})_{dyn} \tag{4.26}$$

Where the coefficients $(N_{ac})_{dyn}, \left(N_{aq}\right)_{dyn}, \left(N_{a\gamma}\right)_{dyn}$ are dimensionless parameters and they depend on n, α, δ, ϕ, and θ_1. Moreover, they should be calculated for different angles of wedge $\theta_1, \theta_2, \theta_3$ etc and the maximum of $\left(N_{aq}\right)_{dyn}$ and $\left(N_{a\gamma}\right)_{dyn}$ in addition to the minimum of $(N_{ac})_{dyn}$ values are found.

Prakash and Saran method has some limitations, which can be summarized in the following points:

- They assumed that the soil's surface is horizontal, which may not be the case in many retaining projects.
- The adhesion between the wall's face and the backfill soil may not be equals to the soil's cohesion in practice, however the assumed theses values to be equal.
- They neglected the effect of the seismic coefficient in the vertical direction ($K_v w$), which in some situations may be significant.

5. METHODOLOGY

The design of a gravity retaining wall must be made in a way that ensures its stability against overturning, sliding, and bearing capacity; the equation for these checks is presented in section (3.8). Regarding the methodology used in this study and the subsequent chapters, the minimum values for the safety factors of the stability checks from two codes for the static and the dynamic cases will be presented to compare the difference between the two designs, in addition to that, a new solution to evaluate the seismic active earth pressure for the rigid type of retaining wall having cohesive backfill with its equations along with all the steps that will be followed to calculate that earth pressure in the dynamic state and the required calculation of related parameters will also be presented. A brief overview of the Plaxis 2D software will also be presented, and the outputs from the software, such as the deformations and the slope stability regarding the retaining wall, will be commented on and compared with the suitable criteria. Finally, recommendations will be given that will help design retaining walls that contain cohesive backfill.

5.1. Safety Factors Criteria Regarding to Different Codes

The values of safety factors to be accomplished according to different regulations for static and dynamic loading are provided in Tables 5.1, 5.2, and 5.3 below:

Table 5.1. Safety factors for different failure modes (AASHTO, 2014).

Failure Mode	Static	Dynamic
Overturning	2	75% of the static value
Sliding	1.5	75% of the static value
Bearing Capacity	3	1.5

Table 5.2. Safety factors for different failure modes (Council, 2009).

Failure Mode	Static	Dynamic
Overturning	1.5	1.1
Sliding	1.5	1.1
Bearing Capacity	3	1.5

Table 5.3. Safety factors for different failure modes (TBDY, 2018).

Failure Mode	Static	Dynamic
Overturning	1.5	1.3
Sliding	1.5	1.3
Bearing Capacity	3	1.4

5.2. New Generalized Method for Calculating Seismic Active Earth Pressure

Nakajima et al. (2023) presented a solution to calculate the active earth pressure for rigid walls based on the pseudo-static approach of Mononobe-Okabe. In addition to Coulomb's theory of earth pressure, considering the cohesion effect of the backfill soil, several studies have been conducted to explore the extent of soil cohesion's impact on the seismic active earth pressure calculations of retaining walls. Wilson and Elgamal (2015) studied retaining walls, considering backfill cohesion. The results clarified that the Mononobe-Okabe method is conservative in calculating seismic active earth pressures due to its exclusion of soil cohesion from its calculations. Furthermore, Ozaki and Nakajima (2021) presented research that investigated the influence of soil cohesion on the behavior of retaining walls during earthquakes. They highlighted that the dynamic or seismic behavior of retaining walls is influenced by soil cohesion.

They found that the presence of soil cohesion can lead to an increase in the shear resistance generated between the soil and the wall's back face, and it also increases the soil's shear strength on the backfill failure plane. Moreover, they also observed a stable zone in the upper part of the soil. These three effects of soil cohesion on the dynamic behavior of retaining walls are illustrated in Figure 5.4.

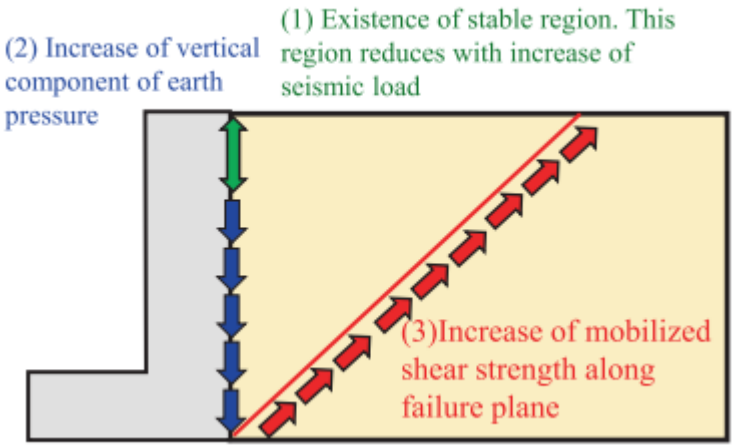

Figure 5.1. Backfill cohesion's impact on seismic stability of retaining walls (Nakajima et al., 2023).

Additionally, studies have been conducted on calculating seismic active earth pressure, considering soil cohesion. Among these, Lin et al. (2015) proposed an equation to calculate this lateral pressure based on the slice method, taking into account the influence of the cohesion of backfill at the failure plane and its effect on the shear resistance between the soil and the wall back face, as well as the presence of tension cracks. The results were compared with model tests under light seismic loads. Also, Kim et al. (2010) introduced an equation for calculating seismic lateral pressure, considering the wall adhesion and the presence of line load along with soil cohesion. The proposed solution was based on the trial-and-error theory, which resembles the trial wedge method. However, most of these studies only presented results concerning the active seismic pressure coefficient.

In their approach, Nakajima et al. effectively combined their method with the modified Mononobe-Okabe method, which can be applied in cases of significant seismic loading and considers the impact of the post-peak reduction in soil shear strength in addition to

the strain localization of that backfill along with the soil's cohesion. Moreover, they conducted displacement analyses regarding retaining walls. They demonstrated that soil cohesion reduces the horizontal displacement of the wall, highlighting its importance in calculating lateral earth pressure under seismic conditions (Nakajima et al., 2023).

Nakajima et al. method depends on several assumptions, including:

1. The pressure from the backfill and acting on the wall is distributed hydrostatically.
2. It was assumed that the characteristics of backfill soil, such as the unit weight, cohesion, and friction angle, are constant and uniform.
3. The failure surface is straight and starts from the wall's heel. It has also been assumed that the wedge of the soil is uniformly affected by inertial forces.

Figure 5.5 a shows a rigid wall along with the forces acting on it, which are used in deriving the equations that will be presented later in this chapter, in addition to the polygon forces as in Figure 5.5b.

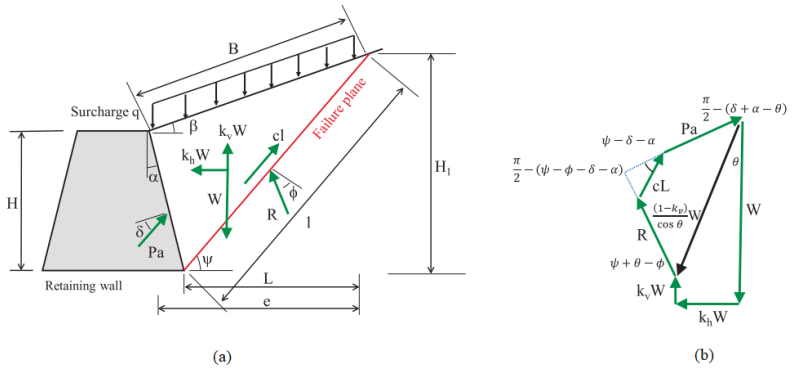

Figure 5.2. Rigid retaining wall with the forces acting on it (Nakajima et al., 2023).

The dynamic earth pressure for the active case expressed by this method could be calculated using:

$$P_{ae} = \frac{1}{2}\gamma H^2(1-k_v)\left[K_{a_\gamma} + n_q K_{aq} - n_c K_{ac}\right] \qquad (5.1)$$

Where n_q and n_c are coefficient for surcharge load and cohesion respectively expressed by:

$$n_q = \frac{2q}{\gamma H} \qquad (5.2)$$

$$n_c = \frac{2c}{(1-k_v)\gamma H} \tag{5.3}$$

As expressed in equation (5.1), we have three terms that could be described as:

The term related to the gravity, which can be calculated as:

$$K_{a_\gamma} = \frac{(1+\tan\alpha\tan\psi)(1+\tan\alpha\tan\beta)\sin(\psi+\theta-\phi)}{\cos\theta(\tan\psi-\tan\beta)\cos(\psi-\phi-\delta-\alpha)} \tag{5.4}$$

The term related to the surcharge load, which can be calculated as:

$$K_{aq} = \frac{K_{a\gamma}}{\cos\beta(1+\tan\alpha\tan\beta)} \tag{5.5}$$

The term related to the backfill cohesion, which can be calculated as:

$$K_{ac} = K_{a_\gamma}\frac{\cos\phi\cos\alpha}{\cos(\psi-\alpha)\cos(\psi-\phi)[\tan(\psi-\phi)+\tan\theta]} \tag{5.6}$$

Angle of the failure plane ψ could be found using the following equation:

$$\cot(\psi-\beta) = -\tan(\phi+\alpha+\delta-\beta) + \frac{1}{\cos(\phi+\alpha+\delta-\beta)} \times \sqrt{\frac{m\sin(\phi+\delta)\cos(\alpha+\theta+\delta)-n\cos(\alpha-\beta)}{[m\sin(\phi-\beta-\theta)-n]\cos(\alpha-\beta)}} \tag{5.7}$$

Where:

$$m = -\left(\frac{\cos(\alpha-\beta)}{\cos\alpha} + n_q\right) \tag{5.8}$$

$$n = n_c\cos\phi\cos\theta \tag{5.9}$$

$$\theta = \tan^{-1}\frac{k_h}{1-k_v} \tag{5.10}$$

5.3. Calculating Seismic Acceleration Coefficients

The steps for k_h and k_v estimation differ from one standard to another; in this section, the approach used to calculate these two coefficients according to 4 regulations will be presented, and two criteria will be chosen to be used in the calculations. Also, a comparison will be made of the results that will be obtained.

5.3.1. TBDY 2018 Criteria to Calculate k_h and k_v

Türkiye Building Earthquake Regulation, which was published in 2018 and stat to be applicable in 2019, provided a way to calculate k_h and k_v using the design spectral response acceleration parameter for the short period S_{DS} and r coefficient which depends on the allowable displacement of the retaining wall and its type which could be found using Table 5.5. Coefficients k_h and k_v could be calculated using the following:

$$k_h = \frac{0.4S_{DS}}{r},\ k_v = 0.5k_h \tag{5.11}$$

S_{DS} could be obtained based on the site coefficient F_s that can be found using Table 5.4 and the mapped response acceleration parameter for the short period S_s found from the Türkiye earthquake hazard map.

$$S_{DS} = S_S\, F_S \tag{5.12}$$

Table 5.4. Site coeffiecients for short period regarding different soil classes.

Soil class	Short period site coefficient F_S					
	$S_s \leq 0.25$	$S_s = 0.50$	$S_s = 0.75$	$S_s = 1.00$	$S_s = 1.25$	$S_s \geq 1.5$
ZA	0.8	0.8	0.8	0.8	0.8	0.8
ZB	0.9	0.9	0.9	0.9	0.9	0.9
ZC	1.3	1.3	1.2	1.2	1.2	1.2
ZD	1.6	1.4	1.2	1.1	1.0	1.0
ZE	2.4	1.7	1.3	1.1	0.9	0.8
ZF	Site-specific soil behavior analysis will be performed					

Table 5.5. r coefficient for retaining structures.

Type of Retaining Structure	r
Gravity type walls allowed a maximum displacement of 120 SDS (mm)	2.0
Gravity type walls allowed a maximum displacement of 80 SDS (mm)	1.5
Anchored walls, weight type walls where displacement is not allowed	1.0

Table 5.6. Site classification (TBDY, 2018).

Site class	Soil type	Average in the upper 30 meters		
		$(V_s)_{30}$ [m/s]	$(N_{60})_{30}$ [blow /30 cm]	$(c_u)_{30}$ [kPa]
ZA	Solid, hard rocks	> 1500	–	–
ZB	Slightly weathered, medium-solid rocks	760 – 1500	–	–
ZC	Very dense sand, gravel and hard clay or weathered, weak rocks with many cracks	360 – 760	> 50	> 250
ZD	Medium dense-dense layers of sand, gravel or very solid clay	180 – 360	15 – 50	70 – 250
ZE	Profiles containing loose sand, gravel or soft-solid clay layers or a total thickness of more than 3 meters of soft clay (c_u < 25 kPa) that meet the conditions of PI > 20 and w > 40%	< 180	< 15	< 70
ZF	Soils that require site-specific research and evaluation: 1) Soils at risk of collapse and potential collapse under the influence of earthquake (liquefiable soils, highly sensitive clays, collapsible weakly cemented soils, etc.), 2) Peat and/or clays with high organic content, with a total thickness of more than 3 meters, 3) High plasticity (PI >50) clays with a total thickness of more than 8 meters, 4) Very thick (>35 m) soft or medium solid clays.			

5.3.2. AASHTO Criteria to Calculate k_h and k_v

The horizontal seismic coefficient k_h could be calculated according to the AASHTO standard in several ways, including:

$$k_{h0} = F_{PGA}\, PGA = A_s \tag{5.13}$$

Where,

F_{PGA}: Site factor obtained based on the site class from Table 5.7.

PGA: Mapped peak ground acceleration obtained from earthquake maps.

A_s: Coefficient of earthquake ground acceleration.

This method assumes that the wall's lateral displacement is not allowed. Based on several studies, this is considered a conservative option, and the motion of the ground would be less than that. Other methods that can be used to estimate the value of k_h are to consider the allowance of wall displacement, which reduces the seismic impact, and consider the dispersion of seismic wave scattering, which lowers the k_h and makes it more suitable for use in design.

Among the equations that consider the wall's allowance for yielding or displacing is the equation of Kavazanjian et al. (1997), which can be used for walls with allowed displacement of 25-200 mm, providing a better estimation of the wall displacement's effect on reducing the seismic acceleration coefficient. Other equations presented by Anderson et al. (2008), Bray and Travasarou (2009), and Bray et al. (2010) could be found in AASHTO (2014). However, in this study, the equation provided by Kavazanjian et al. was chosen to be used for the estimation of k_h due to its simplicity.

$$k_h = 1.66 A_s \left(\frac{A_s}{d}\right)^{0.25} \tag{5.13}$$

Where d is the permissible lateral displacement of the wall, according to AASHTO, d equals 250 amax (mm). Another way to estimate d, as Wu and Prakash (1999) presented as A function of the wall height H, is d equals 0.02H, and the horizontal displacement at failure would be 0.1H. Moreover, according to Das and Sivakugan (2018), the allowed for the wall displacement to yield sufficiently for the active case could be 0.001H-0.004H for granular backfill and 0.01H-0.04H for cohesive backfill.

Table 5.7. values for F_{PGA} (AASHTO, 2014).

Soil class	Peak Ground Acceleration Coefficient (PGA)				
	PGA ≤ 0.10	PGA = 0.20	PGA = 0.30	PGA = 0.40	PGA > 0.50
A	0.8	0.8	0.8	0.8	0.8
B	1.00	1.00	1.00	1.00	1.00
C	1.20	1.20	1.10	1.00	1.00
D	1.60	1.40	1.20	1.10	1.00
E	2.50	1.70	1.20	0.90	0.90
F	Specific site investigations and dynamic analysis should be performed				

The site classification according to AASHTO 2014 is provided in Figure 5.3 below:

Site Class	Soil Type and Profile
A	Hard rock with measured shear wave velocity, $\overline{v}_s > 5{,}000$ ft/s
B	Rock with 2,500 ft/sec < $\overline{v}_s$ < 5,000 ft/s
C	Very dense soil and soil rock with 1,200 ft/sec < $\overline{v}_s$ < 2,500 ft/s, or with either $\overline{N} > 50$ blows/ft, or $\overline{s}_u > 2.0$ ksf
D	Stiff soil with 600 ft/s < $\overline{v}_s$ < 1,200 ft/s, or with either 15 < $\overline{N}$ < 50 blows/ft, or 1.0 < $\overline{s}_u$ < 2.0 ksf
E	Soil profile with $\overline{v}_s$ < 600 ft/s or with either $\overline{N}$ < 15 blows/ft or $\overline{s}_u$ < 1.0 ksf, or any profile with more than 10 ft of soft clay defined as soil with $PI > 20$, $w > 40$ percent and $\overline{s}_u$ < 0.5 ksf
F	Soils requiring site-specific evaluations, such as: • Peats or highly organic clays (H > 10 ft of peat or highly organic clay where H = thickness of soil) • Very high plasticity clays (H > 25 ft with PI > 75) • Very thick soft/medium stiff clays (H >120 ft)

Figure 5.3. Soil classification (AASHTO, 2014).

AASHTO (2014) neglected the effect of the vertical seismic acceleration K_v for some reasons, which are:

- The vertical and horizontal components of seismic acceleration at the peak don't happen simultaneously, so it is not logical to overlay the vertical component on the horizontal one, which is related to the peak ground acceleration.

- Vertical seismic acceleration has different characteristics regarding the frequency compared with the horizontal component. Consequently, it could act downwards in a way that enlarges the earth's pressure or upwards, decreasing the earth's pressure.
- As the vertical acceleration acts downward, the earth's pressure increases, and the resistance against overturning and sliding increases (Kavazanjian et al., 2011).

5.3.3. Eurocode Criteria to Calculate k_h and k_v

According to Eurocode 8 and based on Soil factor S and factor r, which depends on the type of the wall and the displacement allowed, in addition to the factor α, which is the ratio of the design acceleration to the gravity acceleration, the provided equations could be used to calculate the seismic acceleration coefficients:

$$k_h = \alpha \frac{S}{r} \tag{5.14}$$

Factor S could be considered as 1 for A and B soil groups and 0.9 for soil group C. For the calculation of the vertical seismic acceleration, it could be estimated based on the ratio of the most significant earthquake acceleration in the vertical (a_{vg}) direction to the most significant earthquake acceleration in the horizontal direction (a_g) using the following:

$$k_v = \pm 0.5 k_h \text{ , if } a_{vg}/a_g \text{ is larger } 0.6 \tag{5.15}$$

Otherwise, $$K_v = \pm 0.33 K_h \tag{5.16}$$

r factor would be determined using Table 5.8 below.

Table 5.8. r coefficient for retaining structures (Eurocode 8, 2005).

Type of Retaining Structure	r
Gravity retaining walls that allowed to displace a distance equals to 300 α S (mm)	2.0
Gravity retaining walls that allowed to displace a distance equals to 200 α S (mm)	1.5
Anchored walls, gravity walls where displacement is not allowed	1.0

5.3.4. Japan Criteria to Calculate k_h and k_v

In this regulation, as in AASHTO regulations, the vertical component of the seismic acceleration will be neglected for the same reasons mentioned in section 5.3.2. However, the horizontal component of the seismic acceleration, according to the Japanese code, is found using the following equation (Yıldırım, 2004):

$$k_h = C_I C_G C_Z C_T K_o \tag{5.17}$$

Where, $K_o = 0.2$

C_I: Importance structure coefficient.

C_T: Behavior coefficient of the structure.

C_G: Type of soil coefficient.

C_Z: Coefficient for the earthquake zone.

The first two regulations (AASHTO and TBDY) were chosen to be used for the calculation of the seismic horizontal acceleration k_h, knowing that there is a method to calculate the active dynamic thrust for each of them. Still, in this thesis, only the way to evaluate k_h will be taken from these standards. However, the method mentioned in section 5.2 will be used to calculate the active dynamic earth pressure.

6. WALL DESIGN AND STABILITY CHECKS

6.1. Determination of Soil Parameters Used in the Wall Design

In this chapter, a rigid gravity retaining wall with 8 m height with horizontal backfill having surcharge load q (10 kN/m^2) was designed, and the checks were made to ensure the stability of that wall against the overturning, sliding, and bearing capacity under the effect of the static and the dynamic conditions. In the design, it was assumed that a good drainage system was applied and the groundwater level was away down the wall zone so that the effect of the water pressure could be neglected.

The soil behind the wall was assumed to be clay soil. For simplicity, the soil surface is set to be horizontal. Table 6.1 shows the accepted values for the characteristics of the backfill soil, including the cohesion, friction angle, and unit weight. For the foundation soil beneath the retaining wall, it was assumed that it is dense sand, and its properties values, along with the surcharge load and other parameters, are also provided in the same table.

Table 6.1. Properties of backfill and sub-soil.

Parameter	Notation	Backfill (clay)	Sub-soil (sand)
γ (kN/m^3)	Unit weight	17	18
c (kN/m^2)	Cohesion	20	0
ϕ (^{o})	Friction angle	25	30

6.2. Determination of The Wall Dimensions

Referring to Das and Sivakugan (2018), to start designing a gravity retaining wall, the first assumption could be made to estimate the suitable dimensions, and then stability checks should be applied against overturning, sliding, and bearing capacity for the static and dynamic thrusts. If the design doesn't meet the desired safety factors, the dimensions may

be changed until we have a safe design. Figure 6.1 shows the related parameters, such as the first assumption for a, which is (0.12-0.17) H, (0.5-0.7) H for B, and a minimum value of 0.6 m and 0.3 m for D and c, respectively.

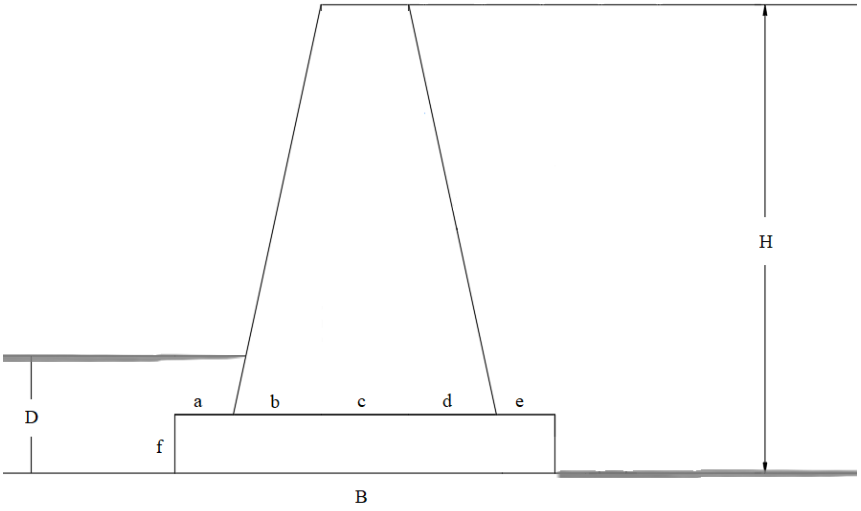

Figure 6.1. Design parameters of the wall model.

The values that have been chosen for the wall that will be used to make the stability checks for the static and dynamic earth pressure according to TBDY (2018) and AASHTO (2014) safety factors are presented in Table 6.2.

Table 6.2. Designed dimensions of the models.

Parameter	First wall design according to k_h from TBDY 2018	Second wall design according to k_h from AASHTO
Wall height H (m)	8	8
Base width B (m)	6.8	5.7
Foundation depth D (m)	2	2
a (m)	1	1
b (m)	1.8	2
c (m)	1.5	1.1
d (m)	1.5	1.1
e (m)	1	0.5
f (m)	1	1

6.3. Determination of Active Earth Pressure with Surcharge Load Existence

6.3.1. Static Active Earth Pressure for the First Wall Design

In this study, since we have a cohesive backfill, the static active earth was found using Rankine theory for the cohesive soil after the tension cracks happened because it is the maximum. The soil properties used for the design and the related wall dimensions according to the calculated active pressure are provided in Table 6.1 and 6.2, respectively. So, the total active static earth pressure that will affect the 8 m gravity wall could be calculated using Rankine equation (3.17) as follows:

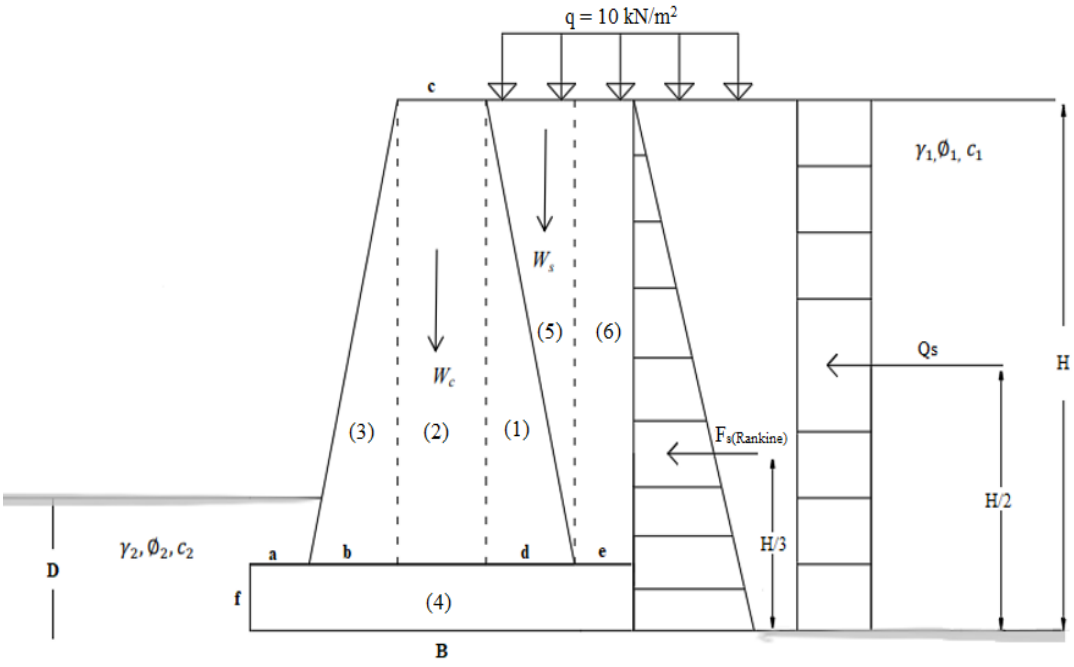

Figure 6.2. Static forces affecting gravity wall using Rankine method.

Active earth pressure coefficient: $K_a = tan^2\left(45 - \frac{25}{2}\right) = 0.41$

$$\sqrt{K_a} = 0.64$$

Static active pressure before tensile crack and considering the effect of the surcharge load :

$$P_{as} = \frac{1}{2} K_a \, \gamma \, H^2 - 2\, c\sqrt{K_a}\, H + qHK_a$$

$$= [\tfrac{1}{2}(0.41)\,(17)\,(8)^2] - [(2)(20)(0.64)\,(8) + (10)(8)(0.41)$$

$$= 51.04\ kN/m$$

Static active pressure after tensile crack and considering the effect of the surcharge load:

$$z_c = \frac{2c}{\gamma\sqrt{K_a}} = \frac{(2)(20)}{(17)(0.64)} = 3.68\ m$$

$$P_{as} = \frac{1}{2}\left(H - \frac{2\,c'}{\gamma\sqrt{K_a}}\right)(\gamma\,H\,K_a - 2\,c'\sqrt{K_a}) + qHK_a$$

$$= \frac{1}{2}\,(8 - 3.68)((17)(8)(0.41) - (2)(20)(0.64)) + (10)(8)(0.41)$$

$$= 97.95\ kN/m$$

Since the pressure after the tension cracks happen is more significant than before tension cracks, the design situation that considers the tension cracks will be adopted because it is critical.

$$\text{Fs} = \frac{1}{2}\left(H - \frac{2\,c'}{\gamma\sqrt{K_a}}\right)(\gamma\,H\,K_a - 2\,c'\sqrt{K_a})$$

$$= \frac{1}{2}\,(8 - 3.68)((17)(8)(0.41) - (2)(20)(0.64))$$

$$= 65.15\ kN/m$$

And it affects at distance = $\frac{H - z_c}{3} = 1.44\ m$ from the wall base.

$$Q_s = qHK_a = (10)(8)(0.41) = 32.80\ kN/m$$

And it affects at distance = $\frac{H}{2} = 4\ m$ from the wall base.

6.3.2. Static Active Earth Pressure for The Second Wall Design

By applying the same procedure for the wall design to be checked according to the safety factors from AASHTO, knowing that the static active earth pressure is the same for both designs due to considering a constant height of 8 m and the same soil parameters were used in the calculations, but the difference would be in the dimensions because every design is compared with safety factors from different regulations. The calculated values of the total static active earth pressure P_a along with the earth pressure coefficient K_a, earth

pressure due to the soil F_s, and lateral pressures from the surcharge load Q_s are given in Table 6.3 below:

Table 6.3. Static pressure results for the second design (including q).

Parameter	Value
P_a (kN/m)	97.95
F_s (kN/m)	65.15
Q_s (kN/m)	32.80
K_a (-)	0.41

6.3.3. Dynamic Active Earth Pressure for the First Wall Design

The dynamic calculation for the active earth pressure was applied according to the method mentioned in section 5.2, and that requires determining a coefficient related to the horizontal seismic acceleration k_h. The estimation of k_h can vary based on the specific code or standard used. Different regulations and their methodologies to evaluate that coefficient were presented in section 5; in this study, the Turkish and AASHTO approaches were used, and then the results from dynamic earth pressure were compared according to different values of k_h. To calculate the dynamic active thrust P_{ae} that will affect the retaining wall stability as a result of the earthquake activity, a location was chosen in Turkey (Sakarya) located within the coordinates of latitude (40.865015°) and longitude (30.346562°) in Karaman region. The values of the parameters needed to evaluate k_h, such as SDS and PGA have been taken from the Turkey earthquake hazard map. Figure 6.3 shows the Turkish map for the earthquake, which was first applied in 1966 and then updated in 2018. It considered the recent earthquake parameters such as the peak ground acceleration PGA instead of the earthquake zone concept.

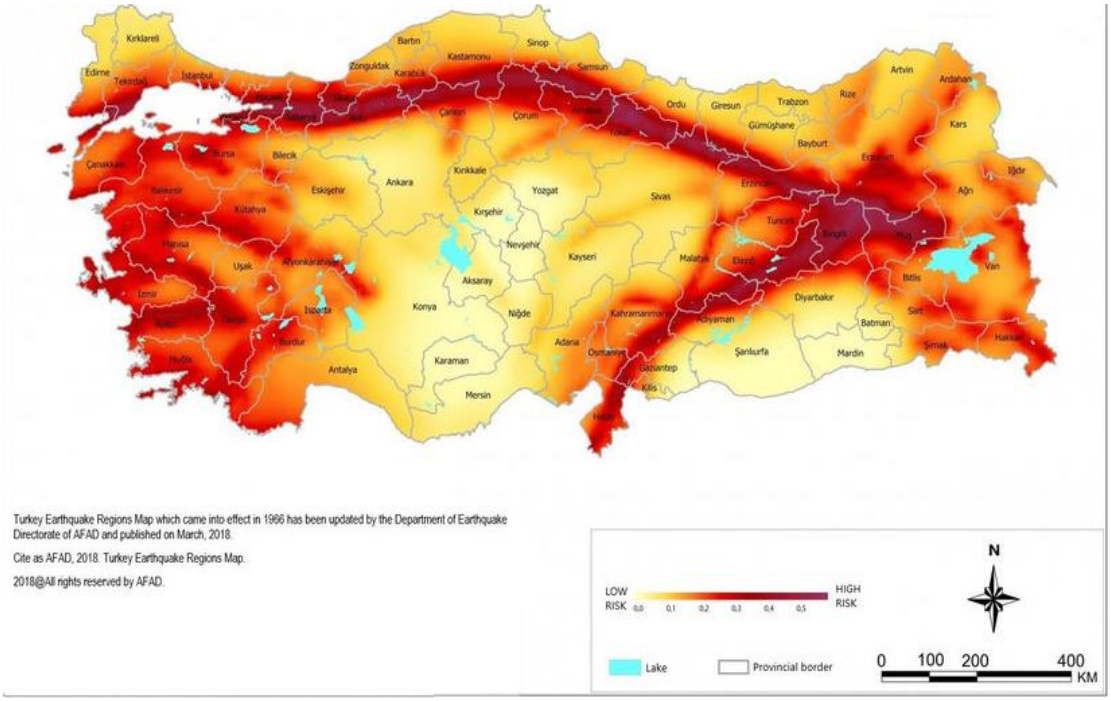

Figure 6.3. Turkish earthquake hazard map.

Soil type ZC was selected as a backfill soil with values ranges such as V_{s30} and N_{60} presented in Table 5.6 for TBDY (2018) and Figure 5.3 for AASHTO (2014), and the earthquake degree is DD-2. The values obtained from the earthquake map are listed in Table 6.4 below:

Table 6.4. Obtained parameters from turkish earthquake map.

Soil classification	SS	FS	SDS	PGA (g)
ZC	1.15	1.20	1.38	0.47

The process of estimation of the horizontal and vertical seismic coefficients k_h and k_v according to TBDY is as follows:

$$k_h = \frac{0.4\, S_{DS}}{r}$$

$$k_h = \frac{(0.4)\ (1.380)}{2} = 0.276$$

$$k_v = 0.5\, k_h$$

$$k_v = (0.5)(0.276) = 0.138$$

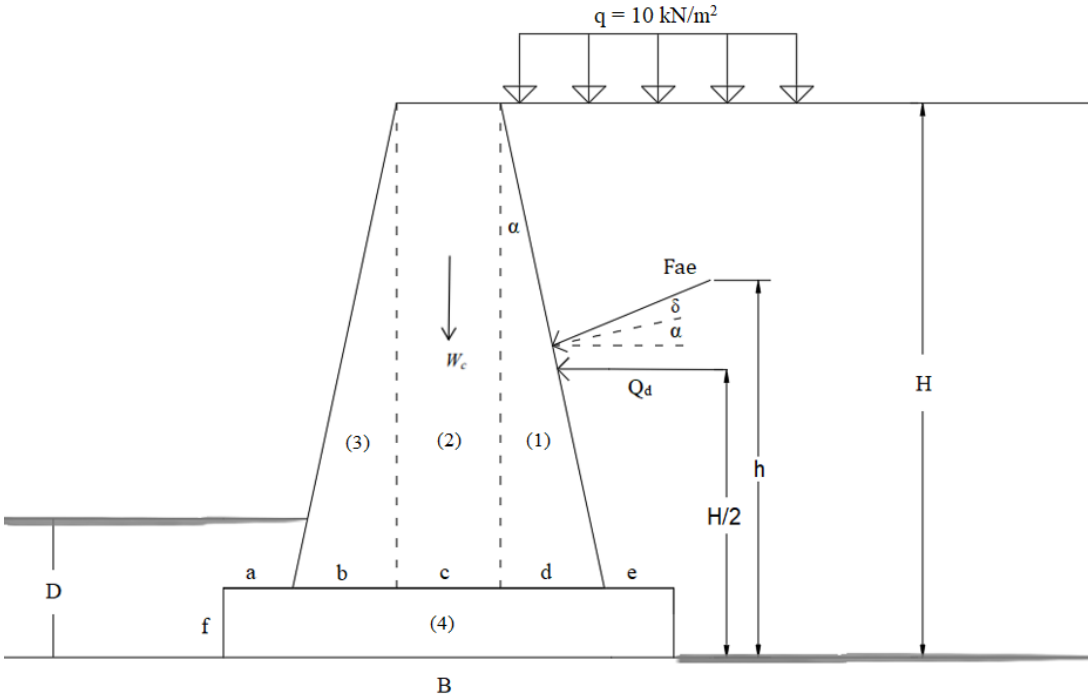

Figure 6.4. Dynamic forces affecting gravity wall.

According to Das and Sivakugan (2018), when Coulomb's theory is applied, the weight of the soil behind the retaining wall is not considered in the calculation of the active earth pressure. And because the method of Susumu et al. is an implementation of Coulomb-type active earth pressure, the only forces considered in the calculations are the seismic active earth pressure F_{ae}, lateral pressure due to surcharge load Q_d, and weight of the wall sections as illustrated in Figure 6.4. Therefore, the procedure for estimation of the seismic active thrusts using the horizontal and vertical acceleration coefficients calculated from TBDY 2018 is as follows:

$$\theta = \tan^{-1}\frac{k_h}{1 - k_v}$$

$$\theta = \tan^{-1}\frac{0.276}{1-0.138} = 17.75^o$$

$$n_q = \frac{(2)(10)}{(17)(8)} = 0.15$$

$$n_c = \frac{(2)(20)}{(1-0.138)(17)(8)} = 0.34$$

$$m = -\left(\frac{\cos(12.09-0)}{\cos 12.09} + 0.15\right) = -1.15$$

$$n = (0.193\ )(\cos 30)(\cos 17.788) = 0.29$$

$$\cot(\psi-\beta) = -\tan(\phi+\alpha+\delta-\beta) + \frac{1}{\cos(\phi+\alpha+\delta-\beta)} \times \sqrt{\frac{m\sin(\phi+\delta)\cos(\alpha+\theta+\delta) - n\cos(\alpha-\beta)}{[m\sin(\phi-\beta-\theta)-n]\cos(\alpha-\beta)}}$$

By simplifying the equation:

$$\psi = tan^{-1}\left(\frac{1}{-\tan(25+12.09+12.5-0)+\frac{1}{\cos(25+12.09+12.5-0)}\times\sqrt{\frac{(-1.15)\sin(25+12.5)\cos(12.09+17.75+12.5)-((0.29)\cos(12.09-0))}{[(-1.15)\sin(25-0-17.75)-0.29]\cos(12.09-0)}}}\right) + 0$$

$$\psi = 46.89^o$$

$$K_{a_\gamma} = \frac{(1+\tan(12.09)\tan(46.31))(1+\tan(12.09)\tan(0))\sin(46.31+18-25)}{\cos 18(\tan(46.31)-\tan(0))\cos(46.31-25-12.5-12.09)} = 0.77$$

$$K_{aq} = \frac{0.78}{\cos(0)(1+\tan(12.09)\tan(0))} = 0.77$$

$$K_{ac} = 0.78\frac{\cos 25\cos 12.09}{\cos(46.31-12.09)\cos(46.31-25)[\tan(46.31-28)+\tan 18]} = 1.24$$

$$P_{ae} = (\tfrac{1}{2})(17)(8)^2(1-0.138)[(0.77\ ) + (0.15)(0.77\ ) - (0.34)(1.24)]$$

$$P_{ae} = 216.15\ kN/m$$

$$\text{Fae} = \frac{1}{2}\gamma H^2(1-k_v)\left[K_{a_\gamma} - n_c K_{ac}\right]$$

$$= \frac{1}{2}(17)(8)^2(1-0.138)[0.77-(0.34)(1.24)]$$

$$= 162.94\ kN/m$$

So that, $$\Delta F_{ae} = F_{ae} - Fs$$

$$= 162.94 - 65.15 = 97.79\ kN/m$$

And it affects at distance = $0.6H = 4.8\ m$ from the wall base.

And F_{ae} affects at distance h = $\frac{F_s\frac{H-z_c}{3}+\Delta F_{ae}\ (0.6H)}{F_{ae}} = \frac{(65.15)(\frac{8-3.68}{3})+97.79\ (0.6)(8)}{162.94} = 3.45\ m$

$$Q_d = \frac{1}{2}\gamma H^2(1-k_v)n_q K_{aq}$$

$$= \frac{1}{2}(17)(8)^2(1-0.138)(0.15)(0.77) = 53.21\ kN/m$$

And it affects at distance = $\frac{H}{2} = 4\ m$ from the wall base.

Horizontal and vertical components of F_{ae}:

$$F_{aeh} = F_{ae} * \cos(\alpha+\delta)$$

$$= 162.94 * cos\ (12.09 + 12.5) = 148.16\ kN/m$$

$$F_{aev} = F_{ae} * (\alpha+\delta)$$

$$= 162.94 * sin\ (12.09 + 12.5) = 67.82\ kN/m$$

6.3.4. Dynamic Active Earth Pressure for the Second Wall Design

The process of estimation the horizontal and vertical seismic coefficients k_h and k_v according to TBDY is as follows:

$$k_h = 1.66A_s\left(\frac{A_s}{d}\right)^{0.25}$$

$$A_s = (1)(0.47) = 0.47$$

$$d = (250)\ (0.47) = 117.5\ mm$$

$$k_h = 1.66(0.47)\left(\frac{0.47}{117.5}\right)^{0.25} = 0.196$$

Following the same steps in section 6.3.2., Table 6.5 summarizes the dynamic values estimated during the design of third wall.

Table 6.5. Dynamic pressure results for the second design (including q).

Parameter	Value
θ^o	11.12^o
ψ^o	52.00^o
K_{a_γ}	0.60
K_{a_q}	0.60
K_{a_c}	1.16
$P_{ae}\ (kN/m)$	185.30
$F_{ae}\ (kN/m)$	137.82
$\Delta F_{ae}\ (kN/m)$	72.67
$Q_d\ (kN/m)$	47.47

The locations at which the pressures F_{ae}, ΔF_{ae} and Q_d affect measured from the bottom of the wall are presented in Table 6.6 below:

Table 6.6. The points of action of dynamic pressures for the second design (including q).

Pressure (kN/m^2)	Point of action (m)
F_{ae}	3.21
Q_d	4.00
ΔF_{ae}	4.80

6.4. Determination of Active Earth Pressure without Surcharge Load Existence

In this section, the same previous approach was followed to calculate the lateral pressure in both the static and dynamic conditions for both designs, but without accounting for the surcharge load. This was done to study the extent of the impact of the presence or absence

of surcharge load on the wall dimensions and stability in both static and dynamic conditions.

6.4.1. Static Active Earth Pressure for the First and Second Wall Designs

As mentioned before, the active earth pressure in the static case is equal for both designs due to considering the same wall height and soil characteristics. The difference would be in the stability when compared with the safety factors. We can see that K_a didn't change while considering and neglecting the surcharge load. The values obtained without considering the surcharge load effect are given in Table 6.7.

Table 6.7. Static pressure results for the first design (without q).

Parameter	Value
$P_a = F_s$ (kN/m)	65.15
Q_s (kN/m)	0
K_a (dim.)	0.41

6.4.2. Dynamic Active Earth Pressure for the First and Second Designs

By neglecting the presence of surcharge loads, the lateral pressure has decreased, allowing for the reduction of the wall dimensions in both the first and second designs. As shown in Table 6.8, the dynamic lateral pressure values are found in Table 6.9.

Table 6.8. Designed dimensions of the models (without q).

Parameter	First wall design according to k_h from TBDY 2018	Second wall design according to k_h from AASHTO
Wall height H (m)	8	8
Base width B (m)	5.8	4.7
Foundation depth D (m)	2	2
a (m)	1	1
b (m)	1.5	1.1
c (m)	1	1
d (m)	1.3	1.1
e (m)	1	0.5
f (m)	1	1

Table 6.9. Dynamic pressure results for the first and second designs (without q).

Parameter	First wall design according to k_h from TBDY 2018	Second wall design according to k_h from AASHTO
θ^o	17.79^o	11.12^o
ψ^o	47.90^o	52.80^o
K_{a_γ}	0.75	0.6
K_{a_q}	0.75	0.6
K_{a_c}	1.22	1.15
$P_{ae}(kN/m)$	154.19	137.94
$F_{ae}(kN/m)$	154.19	137.94
$\Delta F_{ae}(kN/m)$	89.04	72.80

The locations at which the pressures F_{ae} and ΔF_{ae} affect measured from the bottom of the wall for the first and second designs without q, are presented in Table 6.10 below.

Table 6.10. The point of action of dynamic pressures for the first and second designs (without q).

	First Wall design according to k_h from TBDY 2018	Second Wall design according to k_h from AASHTO
Pressure (kN/m^2)	Point of action (m)	Point of action (m)
F_{ae}	3.38	3.21
ΔF_{ae}	4.80	4.80

6.5. Stability Checks for Static and Dynamic Pressures Considering Surcharge Load

6.5.1. Check the First Wall's Design for Static Case According to TBDY Safety Factors

Table 6.11 below shows the values of the moments and the loads that will be used to estimate the safety factors regarding overturning, sliding, and bearing capacity.

Table 6.11. Obtaining ∑V and ∑MR for static safety checks for first design (including q).

Sections	Area (m^2)	Weight W (kN/m)	Distance from toe (m)	Moment (MR) (kN.m/m)
1	5.25	126.00	4.80	604.80
2	10.50	252.00	3.55	894.60
3	6.30	151.20	2.20	332.64
4	6.80	163.20	3.40	554.88
5	5.25	89.25	5.30	473.03
6	7.00	119.00	6.30	749.70
Sum	∑V	900.65	∑MR	3609.65

$$M_o = \left(F_s * \frac{H - z_c}{3}\right) + \left(Q_s * \frac{H}{2}\right)$$

$$= (65.15 * 1.44) + (32.8 * 4)$$

$$= 225.02 \text{ kN.m/m}$$

$$\text{FS}_{\text{overturning}} = \frac{\sum \text{MR}}{\text{M}_o} = \frac{3609.65}{225.02} = 16.04 > 1.5$$

$$\text{FS}_{(\text{sliding})} = \frac{(\Sigma V)\tan(k_1 \phi_2') + B k_2 c_2}{F_s + Q_s}$$

Assuming $K_1 = K_2 = \frac{2}{3}$,

$$\text{FS}_{(\text{sliding})} = \frac{(900.65)\tan(0.67 * 30) + (6.8)(0.67)(0)}{(65.15) + (32.8)}$$

$$= 3.36 > 1.5$$

For the stability regarding to bearing capacity, Table 6.12 shows the factors N_c, N_q, N_γ that are used to calculate q_u for $\phi_2 = 30^o$

Table 6.12. Factors of bearing capacity (Das and Sivakugan, 2018).

ϕ^o	N_c	N_q	N_γ
25	20.72	10.66	10.88
26	22.25	11.85	12.54
27	23.94	13.20	14.47
28	25.80	14.72	16.72
29	27.86	16.44	19.34
30	30.14	18.40	22.40

Now, by applying equations (3.39) through (3.52) the following value could be obtained:

$$\bar{X} = \frac{3609.65 - 225.02}{900.65} = 3.76\ m$$

e = $\frac{6.8}{2} - 3.76 = -0.36$ m, < B/6 (negative sign means it is in the heel side)

$$q_{heel} = \frac{900.65}{6.8}\left(1 - \frac{6*(-0.36)}{6.8}\right) = 174.52\ kN/m^2$$

$$q_{toe} = \frac{900.65}{6.8}\left(1 + \frac{6*(-0.41)}{6.8}\right) = 90.38\ kN/m^2$$

$$q = 18 * 2 = 36\ kN/m^2$$

$$B' = 6.8 - (2)(0.36) = 6.08\ m$$

$$F_{cd} = 1.10$$

$$F_{qd} = 1.10$$

$$F_{\gamma d} = 1$$

$$F_{ci} = F_{qi} = 0.87$$

$$F_{\gamma i} = 0.63$$

$$\psi^{\circ} = \tan^{-1}\left(\frac{P_a}{\Sigma V}\right) = 6.20^{o}$$

$$q_u = 1401.43\ kN/m^2$$

$$\text{FS}_{(\text{bearing capacity})} = \frac{1406.130}{174.52} = 8.06 > 3$$

6.5.2. Check the Second Wall Design for Static Case According to AASHTO Safety Factors

By following the same approach, the values obtained for the stability of the second design, which were compared with the safety factors provided by the AASHTO standard, are as following:

Table 6.13 below shows the values of the moments and the loads that will be used to estimate the safety factors regarding overturning, sliding, and bearing capacity.

Table 6.13. Obtaining ∑V and ∑MR for static safety checks for second design (including q).

Sections	Area (m^2)	Weight W (kN/m)	Distance from toe (m)	Moment (MR) (kN.m/m)
1	3.85	92.40	4.47	412.72
2	7.70	184.80	3.55	656.04
3	7.00	168.00	2.33	392.00
4	5.70	136.80	2.85	389.88
5	3.85	65.45	4.83	316.34
6	3.50	59.50	5.45	324.28
Sum	∑V	706.95	∑MR	2491.26

$$M_o = 221.73$$

$$\text{FS}_{\text{overturning}} = 11.24 > 2$$

$$\text{FS}_{(\text{sliding})} = 2.67 > 1.5$$

$$\bar{X} = 3.21\ m$$

e = -0.36 m, < B/6 (negative sign means it is in the heel side)

$$q_{heel} = 171.07\ kN/m^2$$

$$q_{toe} = 77\ kN/m^2$$

$$q = 36\ kN/m^2$$

$$B' = 4.98\ m$$

$$F_{cd} = 1.12$$

$$F_{qd} = 1.12$$

$$F_{\gamma d} = 1$$

$$F_{ci} = F_{qi} = 0.83$$

$$F_{\gamma i} = 0.55$$

$$\psi^\circ = 7.77$$

$$q_u = 1168.33\ kN/m^2$$

$$\text{FS}_{(\text{bearing capacity})} = \frac{1168.33}{171.07} = 6.83 > 3$$

6.5.3. Check the First Wall Design for Dynamic Case According to TBDY Safety Factors

Table 6.14 below shows the values of the moments and the loads that will be used to estimate the safety factors regarding overturning, sliding, and bearing capacity.

Table 6.14. Obtaining ∑V and ∑MR for dynamic safety checks for first design (including q).

		Area (m^2)	Weight W (kN/m)	Distance from toe (m)	Moment (MR) (kN.m/m)
Sections	1	5.25	126.00	4.80	604.80
	2	10.50	252.00	3.55	894.60
	3	6.30	151.20	2.20	332.64
	4	6.80	163.20	3.40	554.88
Forces	F_{ae}(v)	-	67.82	5.27	357.66
Sum		∑V	760.22	∑MR	2744.58

$$M_o = \left(F_{ae(h)} * h\right) + (Q_d * 4)$$

$$= (148.16 * 3.45) + (53.21 * 4)$$

$$= 724.69 \text{ kN.m/m}$$

$$\text{FS}_{\text{overturning}} = \frac{\sum \text{MR}}{\text{M}_\text{o}} = \frac{2744.58}{724.69} = 3.8 > 1.3$$

$$\text{FS}_{(\text{sliding})} = \frac{(\Sigma V)\tan(k_1\phi_2') + Bk_2c_2'}{F_{ae(h)} + Q_d}$$

Assuming $K_1 = K_2 = \frac{2}{3}$,

$$\text{FS}_{(\text{sliding})} = \frac{(760.22)\tan(0.67 * 30) + (6.8)(0.67)(0)}{(148.16) + (53.21)}$$

$$= 1.37 > 1.3$$

For the stability regarding to bearing capacity, Table 6.12 shows the factors N_c, N_q, N_γ that are used to calculate q_u for $\phi_2 = 30^o$. Now, by applying equations (3.39) through (3.52) the following value could be obtained:

$$\bar{X} = \frac{2751.15-744.51}{761.51} = 2.66\,m$$

$$e = \frac{6.8}{2} - 2.66 = 0.74 \text{ m}, < B/6$$

$$q_{heel} = \frac{760.22}{6.8}\left(1 - \frac{6*0.74}{6.8}\right) = 38.50\ kN/m^2$$

$$q_{toe} = \frac{760.22}{6.8}\left(1 + \frac{6*0.76}{6.8}\right) = 185.1\ kN/m^2$$

$$q = 18 * 2 = 36$$

$$B' = 6.8 - (2)(0.76) = 5.28\,m$$

$$F_{cd} = 1.11$$

$$F_{qd} = 1.11\ ,\ F_{\gamma d} = 1$$

$$F_{ci} = F_{qi} = 0.70$$

$$F_{\gamma i} = 0.26$$

$$\psi^\circ = \tan^{-1}\left(\frac{P_{ae(h)}+Q_d}{\Sigma V}\right) = 14.84$$

$$q_u = 785.93\ kN/m^2$$

$$FS_{(\text{bearing capacity})} = \frac{785.93}{185.1} = 4.25 > 1.4$$

6.5.4. Check the Second Wall Design for Dynamic Case According to AASHTO Safety Factors

Table 6.15 below shows the values of the moments and the loads that will be used to estimate the safety factors regarding overturning, sliding, and bearing capacity.

Table 6.15. Obtaining ∑V and ∑MR for dynamic safety checks for second design (including q).

		Area (m^2)	Weight W (kN/m)	Distance from toe (m)	Moment (MR) (kN.m/m
Sections	1	3.85	92.40	4.47	412.72
	2	7.70	184.80	3.55	656.04
	3	7.00	168.00	2.33	392.00
	4	5.70	136.80	2.85	389.88
Forces	F_{ae}(v)	-	50.36	4.85	244.37
Sum		∑V	632.36	∑MR	2095.01

$$M_o = 601.66 \text{ kN. m/m}$$

$$\text{FS}_{\text{overturning}} = \frac{\sum \text{MR}}{\text{M}_\text{o}} = 3.48 > 1.50$$

$$\text{FS}_{(\text{sliding})} = 1.31 > 1.1$$

$$\bar{\text{X}} = 2.36\ m$$

e = 0.49 m, < B/6

$$q_{heel} = 53.90\ kN/m^2$$

$$q_{toe} = 168\ kN/m^2$$

$$q = 18 * 2 = 36$$

$$B' = 4.72\ m$$

$$F_{cd} = 1.13$$

$$F_{qd} = 1.12$$

$$F_{\gamma d} = 1$$

$$F_{ci} = F_{qi} = 0.68$$

$$F_{\gamma i} = 0.23$$

$$\psi^{\circ} = \tan^{-1}\left(\frac{P_{ae(h)}+Q_d}{\Sigma V}\right) = 15.53^{o}$$

$$q_u = 730.33\ KN/m^2$$

$$\mathrm{FS}_{(\text{bearing capacity})} = \frac{730.33}{168} = 4.35 > 1.5$$

6.6. Stability Checks for Static and Dynamic Pressures Neglecting the Effect of Surcharge Load

The obtained safety factors against overturning, sliding, and bearing capacity for the first and second designs, without considering the surcharge load (q=0) in the static and dynamic conditions, are summarized in Table 6.16 below:

Table 6.16. Safety factor results for the first ans second designs (without q).

	First Design		Second Design	
	Static	Dynamic	Static	Dynamic
FoS Overturning	27.35 >1.50	3.86 >1.30	18.16 >2.00	3.34 >1.50
FoS Sliding	4.13 >1.50	1.55 >1.30	3.30 >1.50	1.46 >1.10
FoS Bearing capacity	7.29 >3.00	4.85 >1.40	6.26 >3.00	4.30 >1.50

7. STATIC AND DYNAMIC ANALYSIS USING PLAXIS 2D SOFTWARE

7.1. Plaxis 2D and Finite Element Method

Plaxis 2D is a geotechnical software developed by Delft University in the Netherlands, and released in 1987 as one of the advanced programs in its field. It employs the Finite Element Method (FEM). This popular numerical modeling technique that has gained widespread use in various engineering software today due to its ease of application and suitability for computer programming, thus saving time and effort for users. This method stands out from other numerical modeling techniques because it allows users to input specific parameters to solve numerous challenging and complex problems, such as nonlinear behavior, non-homogeneous materials, and complex boundary situations (Berilgen, 1996).

The principle behind this method involves dividing the model to be designed into several geometrically defined with limited-size elements. Plaxis applies this method by segmenting the geometry into triangular-shaped elements interconnected to form what is known as a mesh, which is a network consisting of triangular elements meeting at points called nodes. Moreover, Plaxis offers the flexibility to choose the calculation method based on the presence of either 15 or 6 points, meaning that each triangular element contains either 6 or 15 points, depending on the user's choice. The more points an element has, the greater the detail can be captured. As illustrated in Figure 7.1, a 15-point triangle includes 12 stress points, while a 6-point triangle has three stress points. Notably, the first type is considered a precise element that delivers high-quality results for complex problems, such as collapse calculations. In contrast, the second type is fairly precise and yields good results, making it suitable for deformation analyses (Can, 2024).

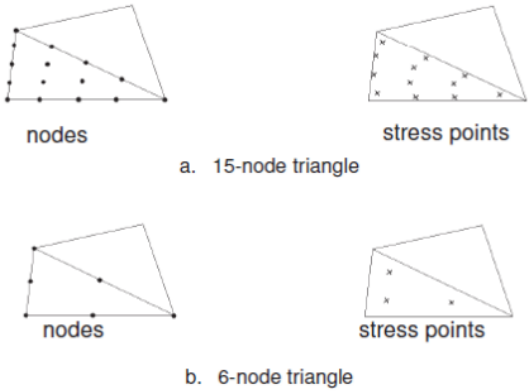

Figure 7.1. Stress points and nodes in each element (Plaxis 2D, 2024).

7.2. Analyzing the Model Using Plaxis 2D Software

Plaxis has five modules to help the designer model geotechnical projects: Soil, Structure, Mesh, Flow conditions, and Staged Construction modules. The term geometry modules is given for the first two modules, and the last three are the calculation modules. Now, to model the design to be worked on in the Plaxis program, one of the first steps the designer must take is to draw the outline boundaries of the design and divide the soil layers based on the type of design and its purpose, in addition, to specify the water level in the soil. These steps are carried out in the Soil module. Figure 7.2 illustrates the division of soil layers and their boundaries in the horizontal and vertical directions of the design created in this research.

After determining the boundaries of the design and the soil layers, the material for each element in the design is defined, starting with the soil layers and then the structural elements, so that each element is assigned a material that suits its imposed properties (Figure 7.3). Table 7.1 shows the material properties used in this study for the backfill soil, sub-soil, and wall. Regarding the addition of structural elements, this is simply done by moving to the Structure module, which enables the designer to insert various structural elements according to the type and purpose of the design, such as walls, tunnels, anchors, loads, and other structural elements. Figure 7.4 shows the design with structural elements like the wall and the surcharge load; now and after the model's geometry is done, we may proceed to the calculation steps.

Table 7.1. Inputs for backfill, sub-soil, and wall in Plaxis 2D.

Parameter	Notation	Backfill (clay)	Sub-soil (sand)	Wall
Model Type	-	Hardening soil	Hardening soil	Linear elastic
Drainage type	-	Undrained	Drained	Non-porous
Secant stiffness	$E_{50}^{\prime ref}$ (kN/m^2)	5000	30000	-
Tangent oedometer stiffness	$E_{oed}^{\prime ref}$ (kN/m^2)	5000	30000	-
Unloading/reloading stiffness	$E_{ur}^{\prime ref}$ (kN/m^2)	15000	90000	-
Interface reduction factor	R_{int}	0.9	1.0	1.0
Over consolidation ratio	OCR	1.0	1.0	-
Unsaturated unit weight	γ_{unsat} (kN/m^3)	17	18	24
Wall Stiffness	E_{ref} (kN/m^2)	-	-	28*10^6
Poisson's ratio	ν_{ur}	0.2	0.2	0.2
Cohesion	c (kN/m^2)	20	0	-
Friction angle	ϕ (^{o})	25	30	-

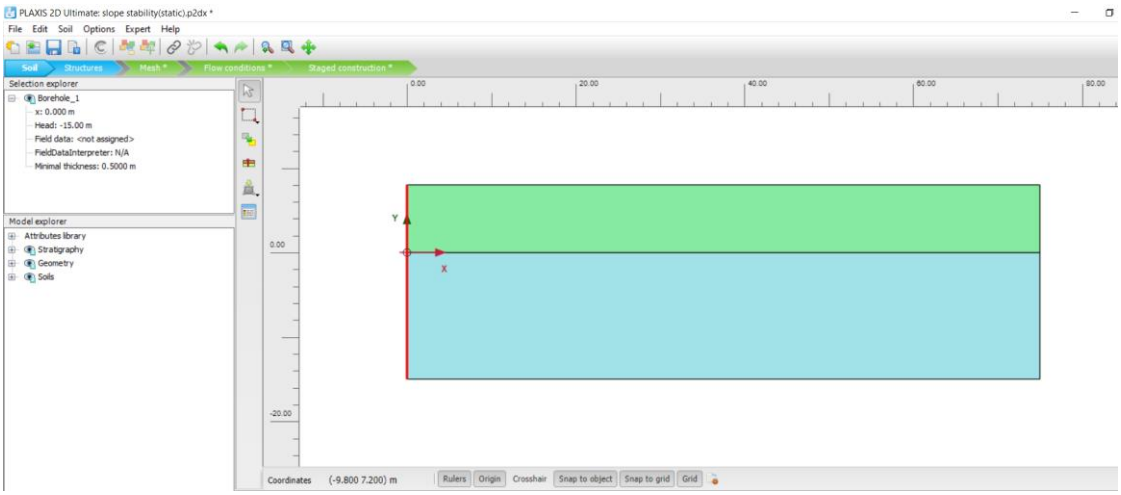

Figure 7.2. Creating the geometry including the soil layers and their boundaries using Plaxis 2D.

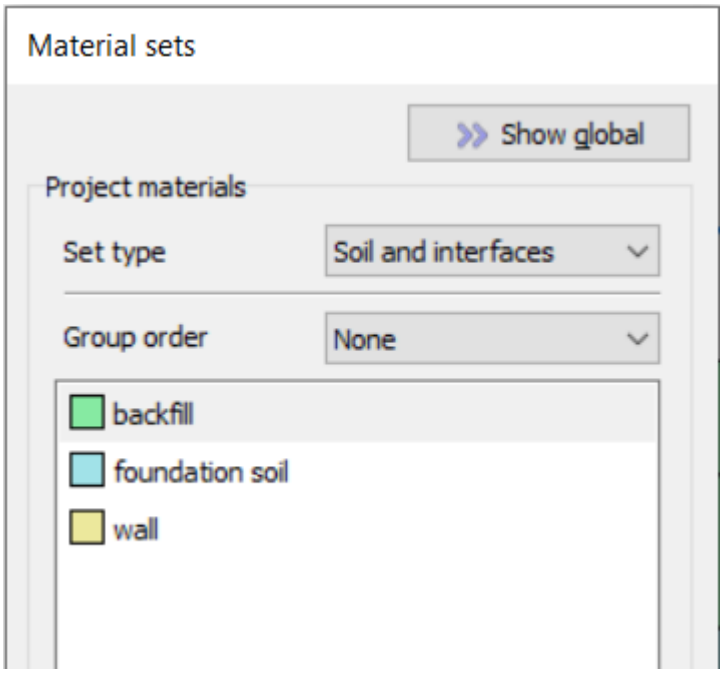

Figure 7.3. Material selection screen in Plaxis 2D.

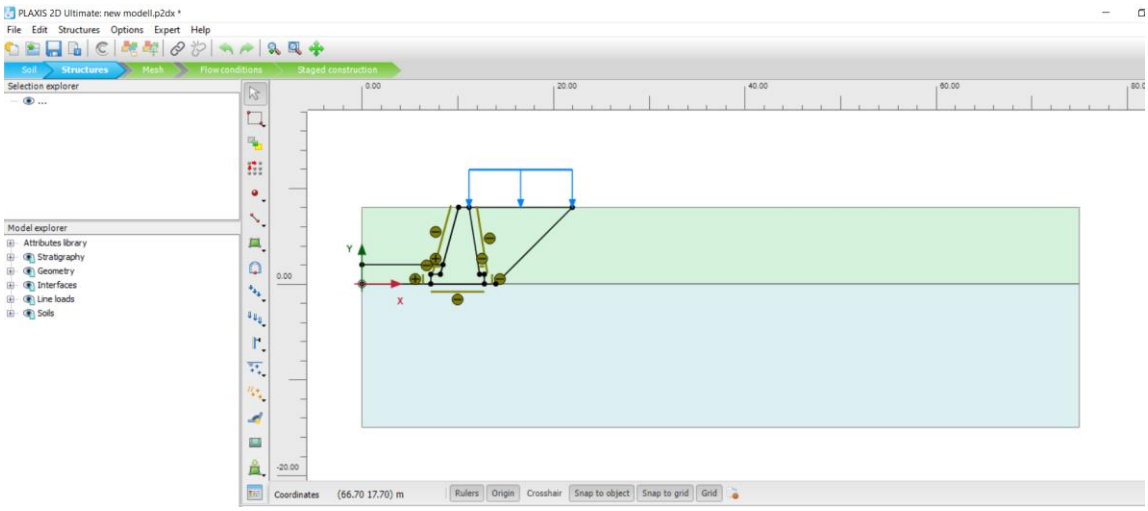

Figure 7.4. Structure elements (surcharge load, interfaces and the wall) using Plaxis 2D.

The first step of the calculation process begins from the third module (Mesh), which allows the designer to create a network for the design elements to find outputs, and control the density of this network according to the desired design. Figure 7.5, shows the design mesh.

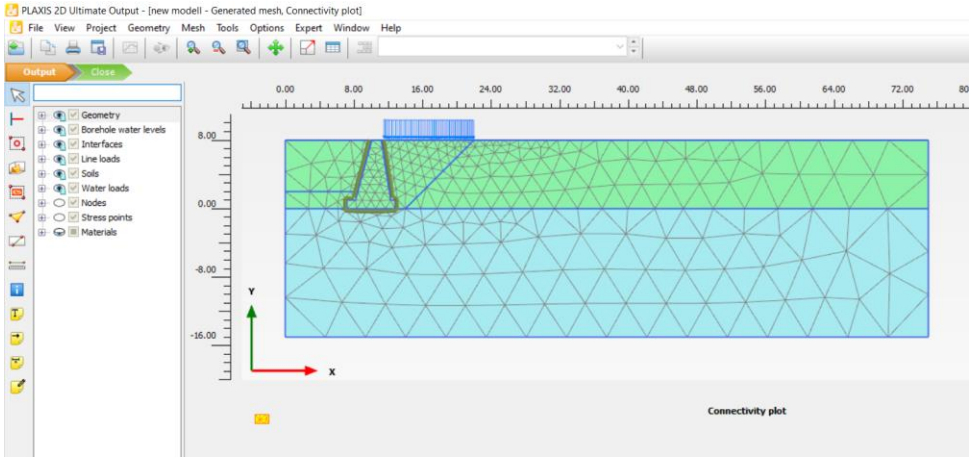

Figure 7.5. The design mesh from Plaxis 2D.

After completing the network, the process moves to the fourth module (Flow conditions), where more specialized control over the groundwater level, which was previously specified, is possible within the soil layers, such as adjusting the water level when excavating behind the wall in designs that require it, in addition to several other features that are performed based on the type of design. It should be noted that this study did not

consider the presence of groundwater within the design. Then, the process moves to the final step of the calculations (Staged construction). In this section, the design is executed by creating several phases, in which the activation or deactivation of the material for each element is possible, as shown in Figure 7.6, in addition to the structural elements according to the objective of each phase. After preparing all the stages, the Plaxis program can analyze the design created with all the phases defined in the last stage by clicking on a calculate command. Finally, we can display the values we want to review and the figures through the “view calculation results” button. (Plaxis 2D, 2024).

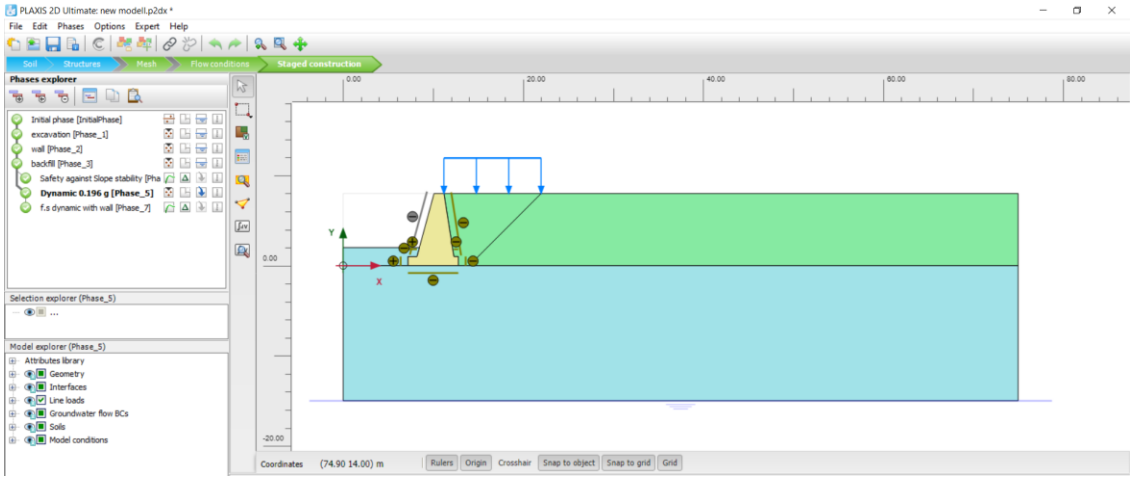

Figure 7.6. Staged construction module including the phases using Plaxis 2D.

7.2.1. Preparing the Model’s Geometry

Before creating the wall, knowing the suitable excavation angle for the available soil is essential. To do this, Plaxis 2D software was used to excavate the soil and level it at different angles. In each instance, a point above the slope was taken to examine the displacement value there, in addition to finding the safety factor for the stability of the slope in both cases (the static case and the dynamic case), as shown in Figure 7.7. The results determined the appropriate excavation angle that combines safety and enables the best utilization of the available land space.

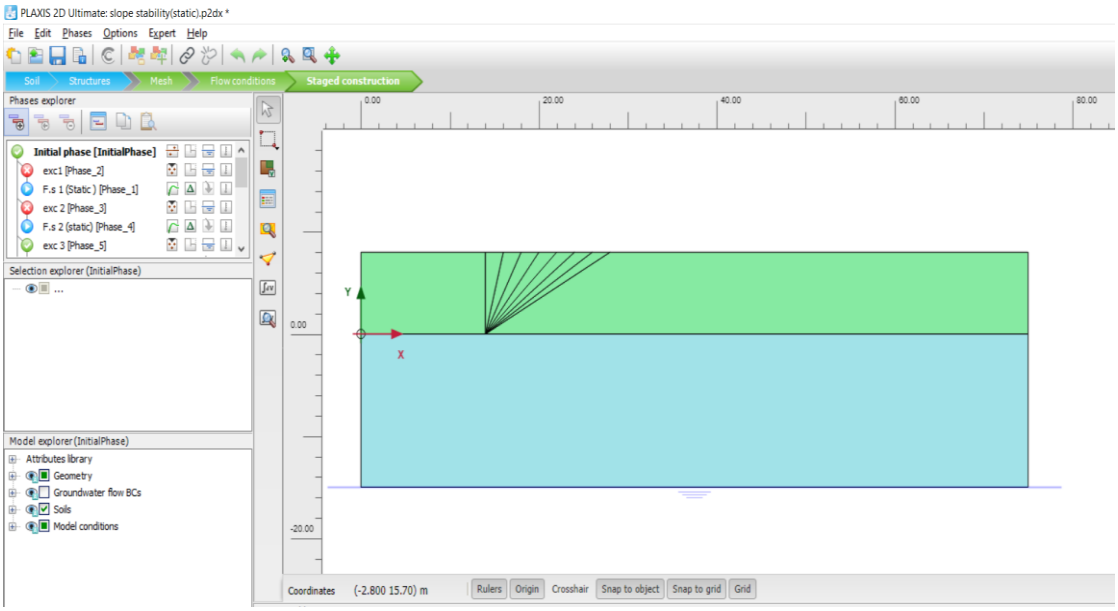

Figure 7.7. Excavating the desired soil in different angles using Plaxis 2D.

Based on the results obtained from the Plaxis 2D software for the static case, as Table 7.2 illustrates, we can observe that the design failed when using the angles (90, 76) with a safety factor of less than 1; with attention to the fact that the completion percentage of each of the first two stages has not yet been completed, but since it is close to 1 and with the noticeable difference in the decline between the first two stages and the rest of the stages, the results were compared with each another.

While the design did not fail at a slope angle of 63, the safety factor is still less than 1.5. As for the slope angles ranging from 53 to 30, the design yielded safety factor results above 1.5. As expected, the results prove that the smaller the slope angle, the closer it gets to the horizontal, the higher the safety factor. We can also observe from the design results for the total displacement at different slope angles, where the angle from 90 to 76 showed a significant displacement, leading to failure. In contrast, the displacement began to decrease until we reached the angle of 30, and the rate of displacement reduction gradually lessened after the angle of 45. Therefore, based on the results shown in the table above, an angle of 45 was chosen for the upcoming design regarding the retaining wall. This angle gives us the maximum possibility to utilize the land while keeping the safety factor above 1.5.

Table 7.2. Plaxis 2D results for static case regarding different slope angles.

Phase	Angle	Safety Factor	Total Displacement (cm)	Mstage
1	90.00	Fail	27.90	0.946
2	76.00	Fail	8.70	0.953
3	63.43	1.47	4.90	1
4	53.13	1.60	2.60	1
5	45.00	1.73	1.50	1
6	38.66	1.82	0.99	1
7	33.70	1.93	0.82	1
8	30.00	2.10	0.80	1

When adding a dynamic load to each excavation stage, as we can see in Table 7.3 and Table 7.4 above, the stages with slope angles (63.43 to 38.66) have failed, and the last two stages gave a safety factor of less than 1.5, due to the significant effect of the dynamic load.

Moreover, we also noticed that the first two stages were not included in the calculations because they failed in the static phase, and therefore, there is no point in adding a dynamic load to them. As stages with slope angles (38.66 to 63.43) for Table 7.3 and (45.00 to 63.43) for Table 7.4, their calculations have not been completed, as shown in the last column. If it had been possible for these stages to be completed, the displacement amount would have been more significant for them. Accordingly, to make the comparison realistic, only the results from the completed stages will be compared with the static case and the rest of the subsequent conditions.

Table 7.3. Plaxis 2D results for dynamic loads (TBDY) regarding different slope angles.

Phase	Angle	Safety Factor	Total Displacement (cm)	Mstage
1	90.00	Fail	-	-
2	76.00	Fail	-	-
3	63.43	Fail	7.90	0.120
4	53.13	Fail	5.50	0.161
5	45.00	Fail	6.10	0.315
6	38.66	Fail	6.70	0.419
7	33.70	1.09	42.1	1
8	30.00	1.13	33.8	1

Table 7.4. Plaxis 2D results for dynamic loads (AASHTO) regarding different slope angles.

Phase	Angle	Safety Factor	Total displacement (cm)	Mstage
1	90.00	Fail	-	-
2	76.00	Fail	-	-
3	63.43	Fail	8.10	0.275
4	53.13	Fail	5.30	0.260
5	45.00	Fail	6.10	0.520
6	38.66	1.27	13.50	1
7	33.70	1.33	11.00	1
8	30.00	1.38	9.30	1

Let's compare the displacement results of the static case with those in the tables above for the last two stages gained by applying TBDY regulation for the dynamic forces and the previous three stages of the results gained using AASHTO. We will notice an increase in the displacement value accompanied by a decrease in the safety factor due to the dynamic

load's effect. Therefore, it is essential to consider the design for dynamic forces when designing.

In addition, when comparing the results from Table 7.4, which were obtained by applying the AASHTO standard, it is noted that even though the safety factor was less than 1.5 during the sixth excavation phase, the phase was completed. No failure occurred compared with the same phase in Table 7.3. This is attributed to the horizontal seismic coefficient, whose value was lower when applying the AASHTO standard than the Turkish one. This suggests that the Turkish standard is more conservative in calculating the dynamic forces of retaining walls.

7.3. Results Obtained from Plaxis 2D.

In this section, horizontal displacement results obtained from Plaxis 2D software and the safety factors regarding slope stability for the static and dynamic conditions are presented to be compared with the related values. To obtain the horizontal displacement, a point was chosen at the top of the wall to see the displacement on it as illustrated in Figure 7.8, and regarding the factor of safety, it is given directly from the software as long as the calculation is finished for all phases.

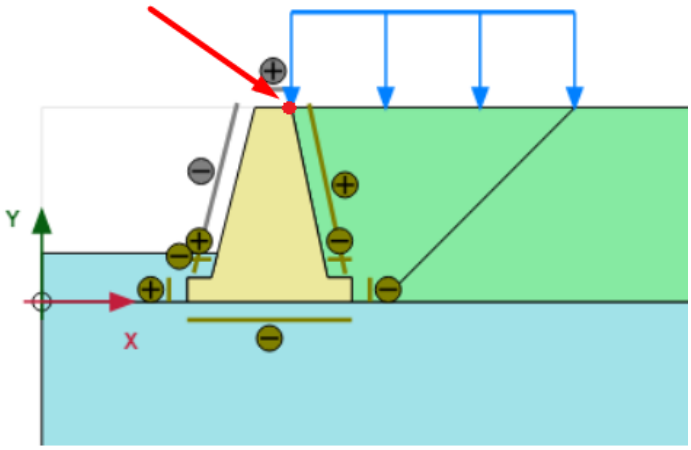

Figure 7.8. The chosen point to evaluate the horizontal displacement at.

This study included four models designed using the method presented in Section 5 to calculate the lateral pressure in the dynamic case, and the difference between the designs was in the seismic horizontal coefficient k_h, where this coefficient was calculated once

following the Turkish standard for the first two and following the AASHTO standard for the last two designs. However, the Rankine equation was used for the calculations regarding the static case, as previously explained. Additionally, a scenario involving a surcharge load on the soil and another scenario not involving a surcharge load was considered. Therefore, in the following sections, the displacement results for both models in the static and dynamic cases will be presented, considering the presence of surcharge load in one scenario and its absence in another.

In terms of the allowable displacement values, which will be compared with the results, many sources have talked about the allowable horizontal displacement for retaining walls, which, as mentioned before, is a sufficient wall displacement allowed to reduce the lateral pressure on it. According to Das, this displacement ranges between 0.01H and 0.04H, where h is the wall height. According to the AASHTO, the permissible lateral displacement equals 250 a_{max} (mm), and for the Eurocode (1994), this displacement equals 300 a_{max} (mm). Furthermore, Wu and Prakash have provided a limit for the allowable horizontal displacement based on the wall's height as 0.02H and added that collapse will occur if the displacement exceeds 0.1H. In this context, the results of the horizontal displacement obtained from the Plaxis 2D will be compared with the values assumed for each design, which are (120 SDS) for the design based on the Turkish standard and 250 a_{max} (mm) for the design based on the AASHTO standard. Also, the results shall be compared with the limit provided by Wu and Prakash, which is (0.02H).

In terms of the safety factors for the slope stability to be compared with the results, 1.54 for the static condition and 1.10 for the dynamic condition were chosen regarding AASHTO regulation, corresponding to the reduction factors 0.65 and 0.9, respectively, noting that the reduction factor equals to one over the safety factor obtained from Plaxis 2D software. However, regarding the TBDY standard, the safety factor for the slope stability in the static case is 1.5, and for the dynamic case, 1.1, considering the use of the horizontal seismic coefficient k_h equals to 0.2 SDS.

7.3.1. Results for the 1st Design with k_h = 0.267, k_v = 0.138 and Considering Surcharge Load Existence.

Table 7.5 shows the slope stability factors of safety for the first model under static and dynamic conditions, along with the horizontal displacement values for the wall. Vertical displacement values for the wall are provided in Figure 7.8.

The deformed mesh for the same model is shown in Figure 7.9, and the total horizontal and vertical displacements for the whole model are illustrated in Figures 7.10 and 7.11, respectively.

Table 7.5. Horizontal displacement values and slope stability factors of safety for the first model.

	Static	Dynamic	
Slope Stability FoS	2.16	1.64 (for 0.2SDS)	1.30 (for 0.4SDS)
Horizontal Displacement for (0.4 SDS)(cm)	0.80	11.00	

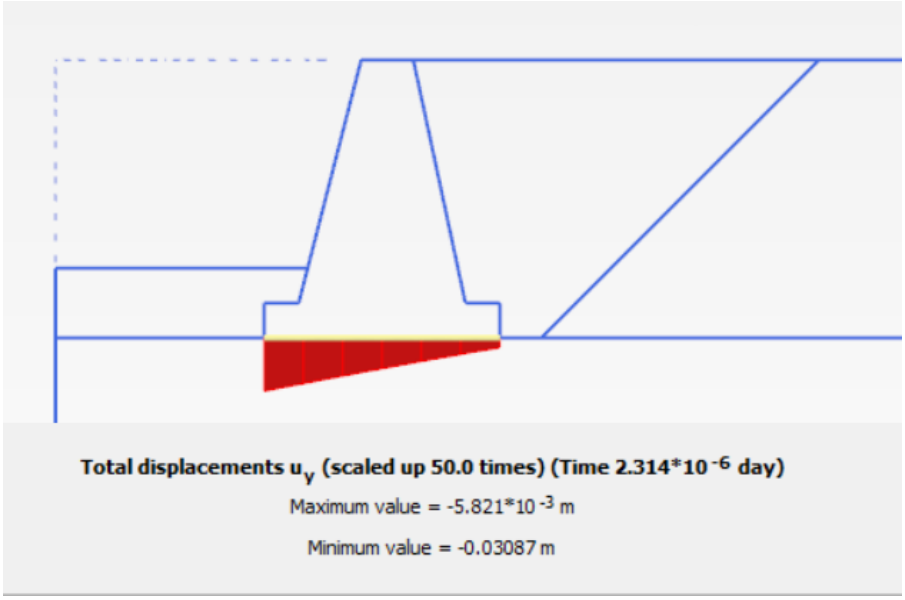

Figure 7.9. Total vertical displacement of the first wall design under dynamic condition.

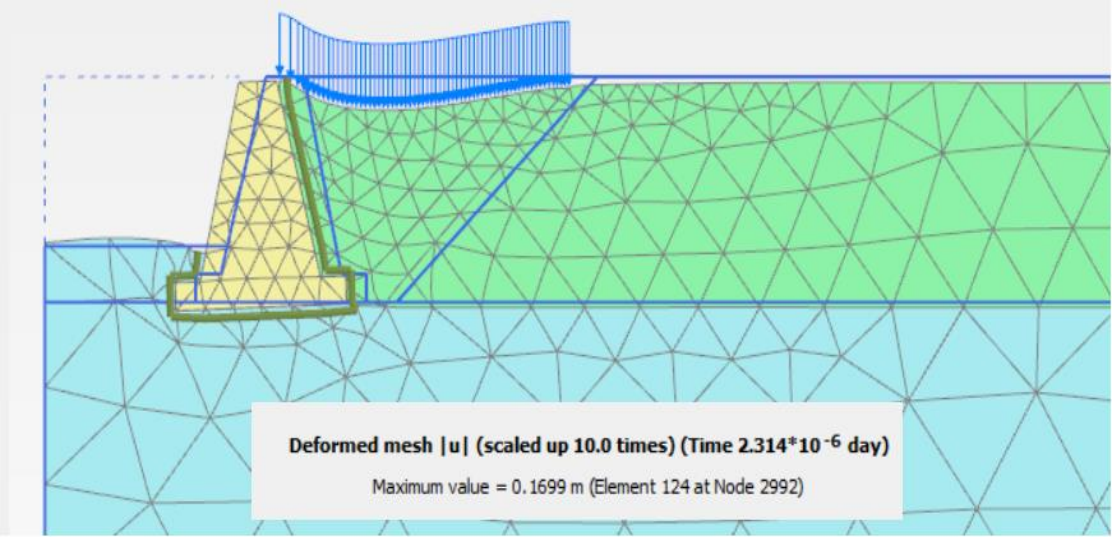

Figure 7.10. Deformed mesh for the first model under dynamic load from Plaxis 2D

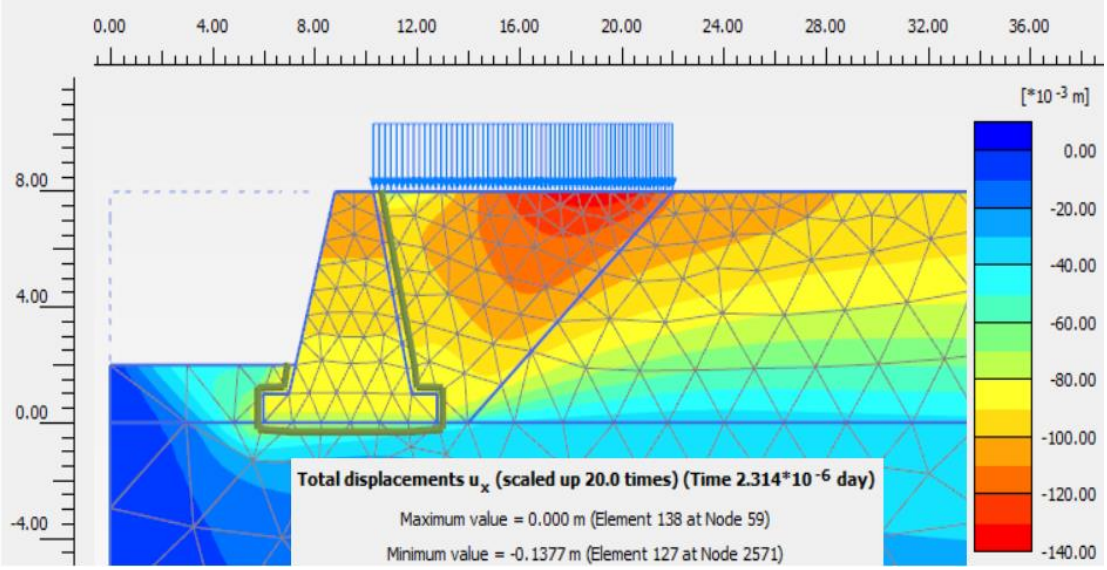

Figure 7.11. Total horizontal displacement for the first model under dynamic load.

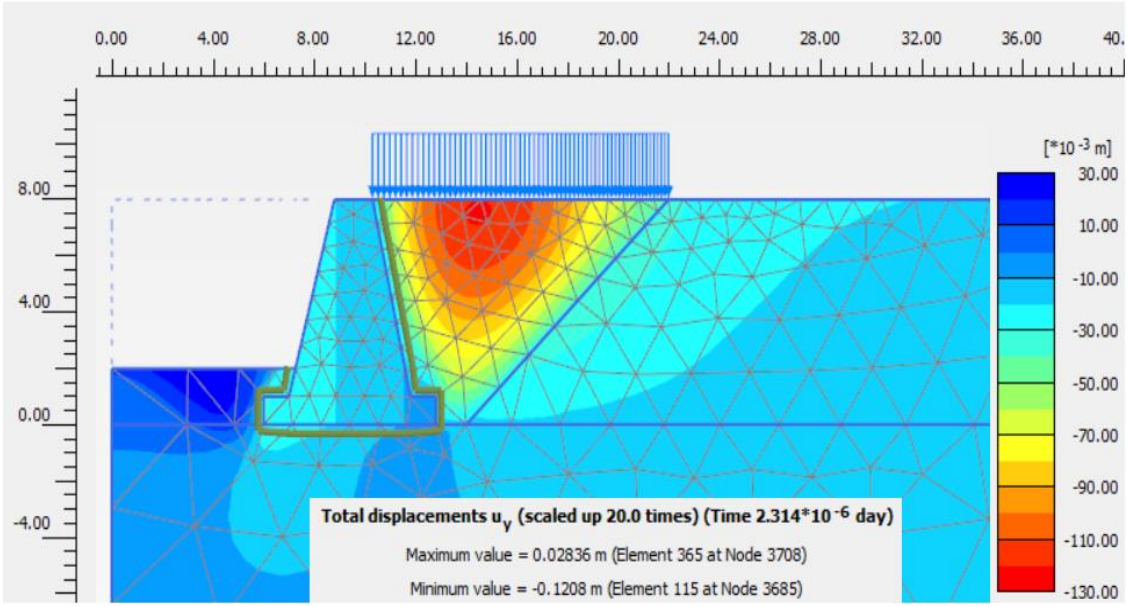

Figure 7.12. Total vertical displacement for the first model under dynamic load.

7.3.2. Results for the 2nd Design with k_h = 0.267, k_v = 0.138 and Without Considering Surcharge Load Existence.

Table 7.6 shows the slope stability factors of safety for the second model under static and dynamic conditions, along with the horizontal displacement values for the wall. Vertical displacement values for the wall are provided in Figure 7.12.

The deformed mesh for the same model is shown in Figure 7.13, and the total horizontal and vertical displacements for the hole model are illustrated in Figures 7.14 and 7.15, respectively.

Table 7.6. Horizontal displacements values and slope stability factors of safety for the second model using Plaxis 2D.

	Static	Dynamic	
Slope Stability FoS	2.26	1.68 (for 0.2SDS)	1.22 (for 0.4SDS)
Horizontal Displacement for (0.4 SDS)(cm) (cm)	1.00	13.30	

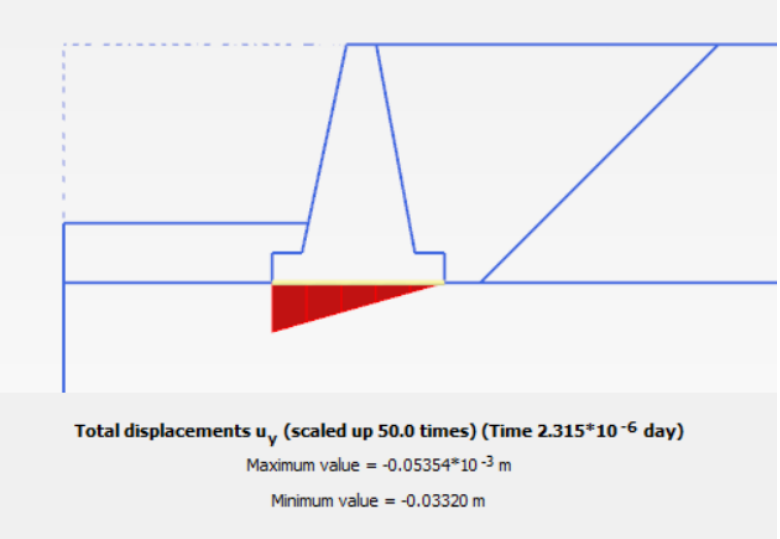

Figure 7.13. Total vertical displacement of the second wall design under dynamic condition.

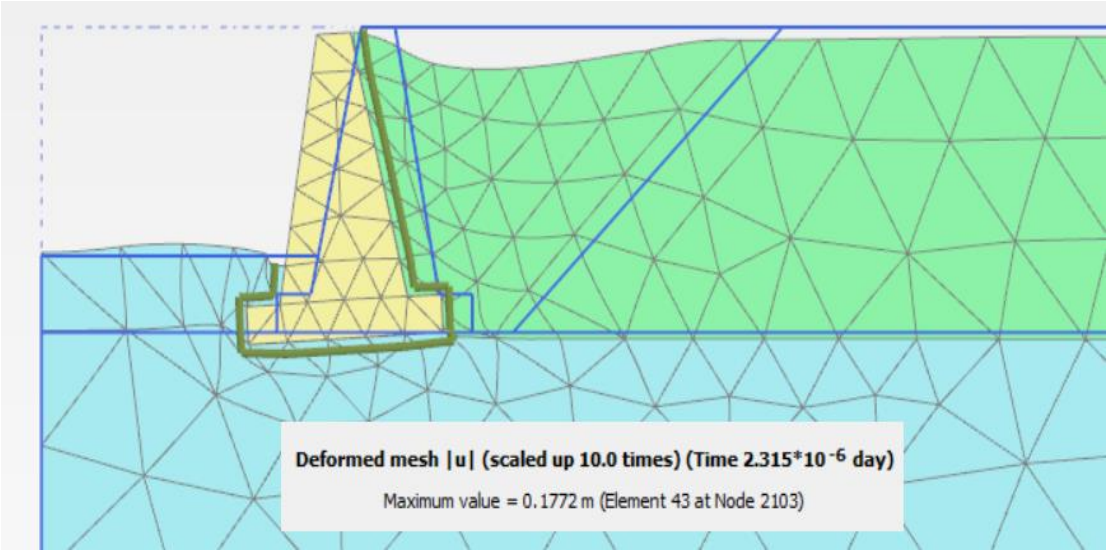

Figure 7.14. Deformed mesh for the second model under dynamic load from Plaxis 2D.

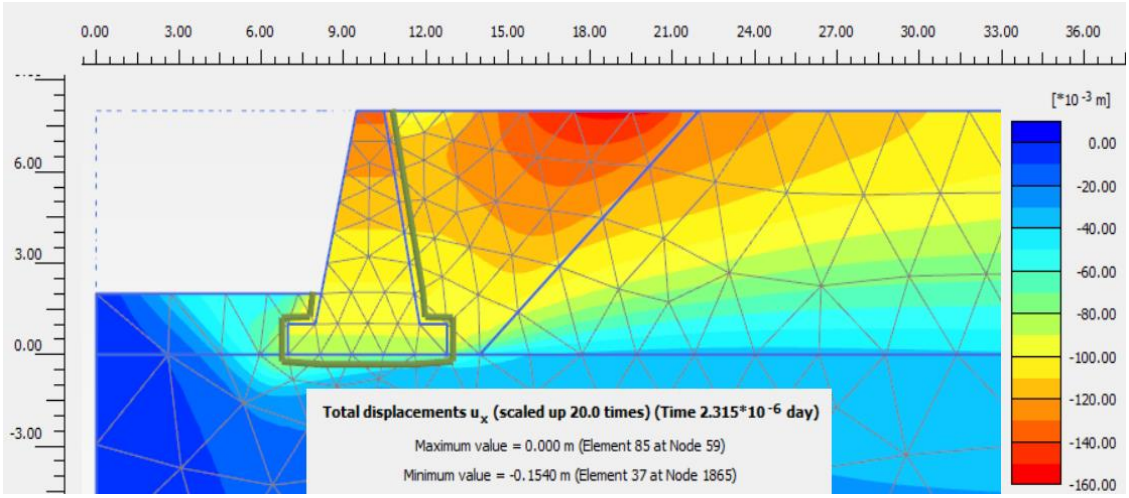

Figure 7.15. Total horizontal displacement for the second model under dynamic load.

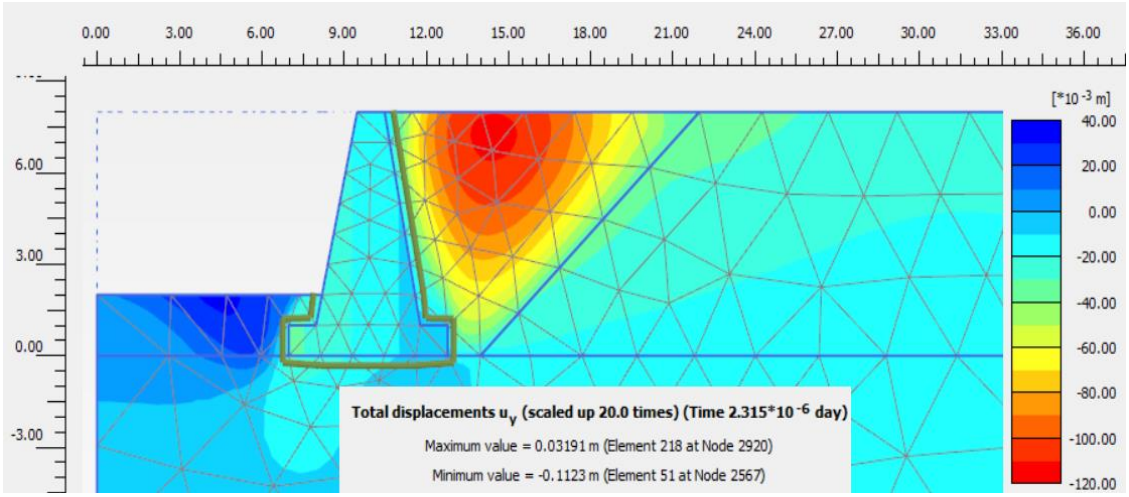

Figure 7.16. Total vertical displacement for the second model under dynamic load.

7.3.3. Results for the 3rd Design with k_h = 0.196, k_v = 0.00 and Considering Surcharge Load Existence.

Table 7.7 shows the slope stability factors of safety for the third model under static and dynamic conditions along with the horizontal displacement values for the wall. Vertical displacement values for the wall are provided in Figure 7.16.

The deformed mesh for the same model is shown in Figure 7.17, and the total horizontal and vertical displacements for the hole model are illustrated in Figures 7.18 and 7.19, respectively.

Table 7.7. Horizontal displacement values and slope stability factors of safety for the third model using Plaxis 2D.

	Static	Dynamic
Slope Stability FoS	2.00	1.37
Horizontal Displacement (cm)	0.70	6.00

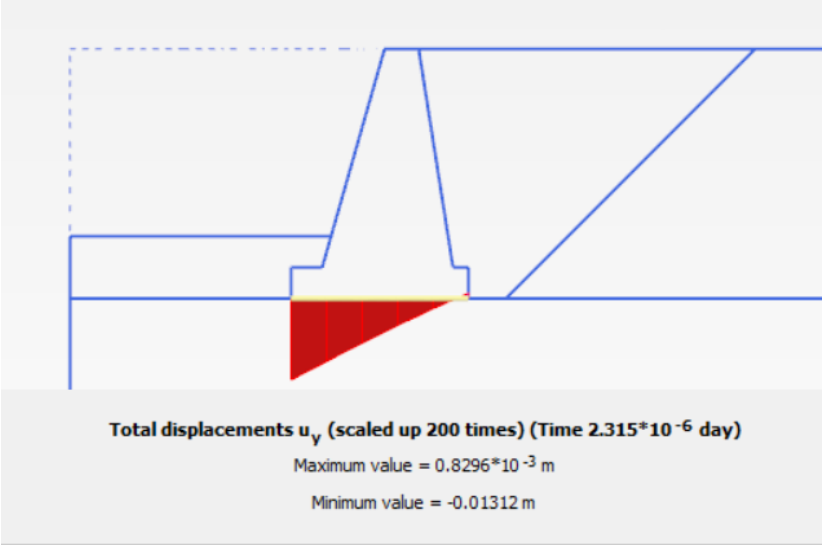

Figure 7.17. Total vertical displacement of the third wall design under dynamic condition.

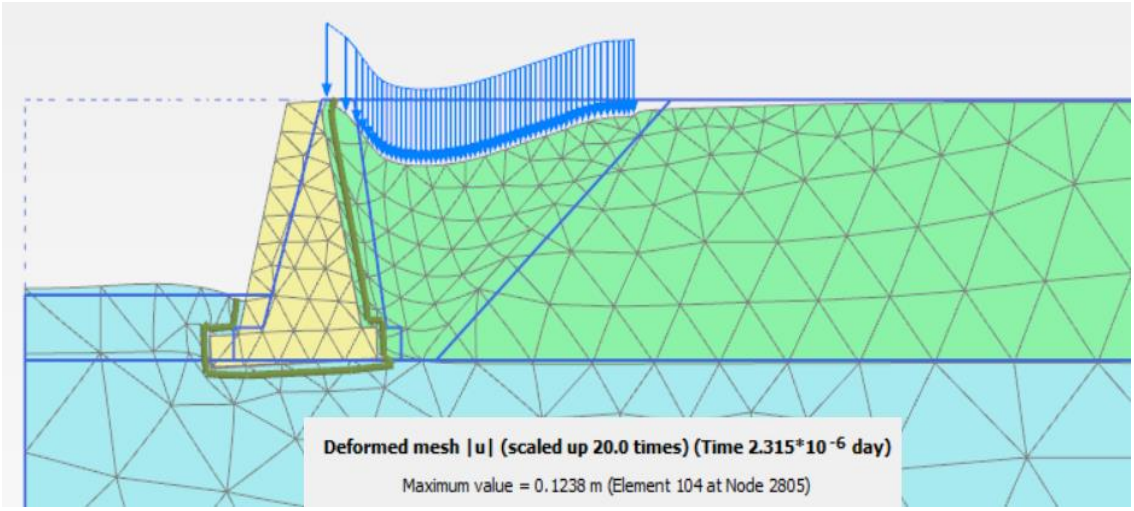

Figure 7.18. Deformed mesh for the third model under dynamic load from Plaxis 2D.

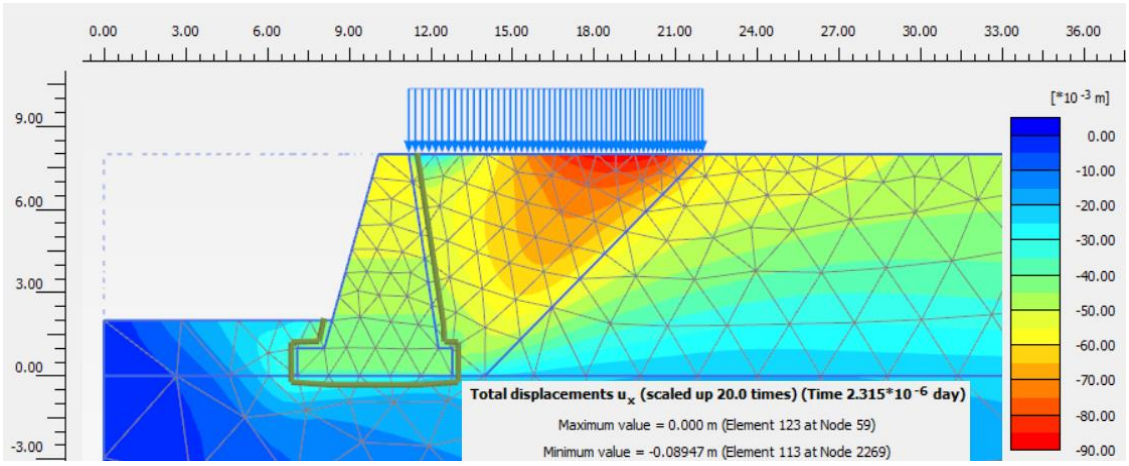

Figure 7.19. Total horizontal displacement for the third model under dynamic load.

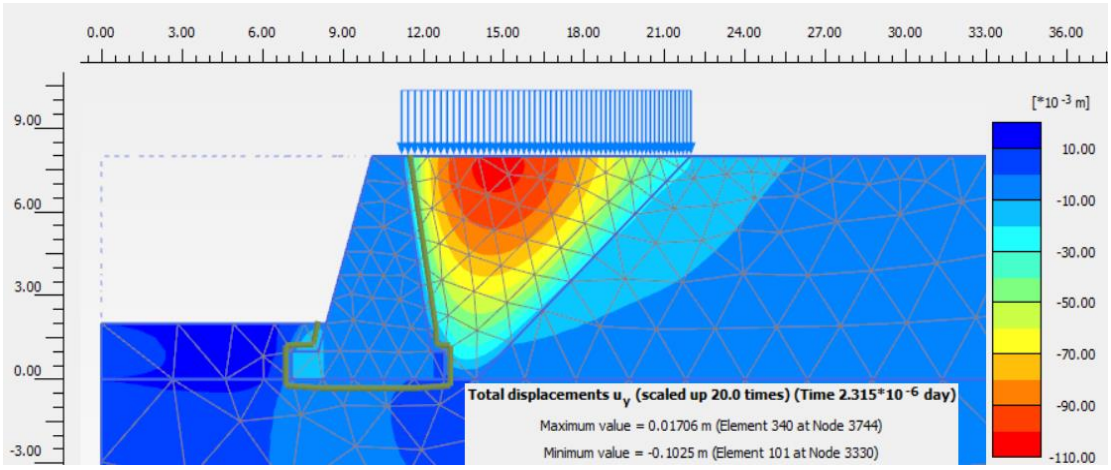

Figure 7.20. Total vertical displacement for the third model under dynamic load.

7.3.4. Results for the 4th Design with k_h = 0.196, k_v = 0.00 and Without Considering Surcharge Load Existence.

Table 7.8 shows the slope stability factors of safety for the third model under static and dynamic conditions along with the horizontal displacement values for the wall. Vertical displacement values for the wall are provided in Figure 7.20.

The deformed mesh for the same model is shown in Figure 7.21, and the total horizontal and vertical displacements for the hole model are illustrated in Figures 7.22 and 7.23, respectively.

Table 7.8. Horizontal displacements values and slope stability factors of safety for the fourth model using Plaxis 2D.

	Static	Dynamic
Slope Stability FoS	2.10	1.44
Horizontal Displacement (cm)	1.50	8.00

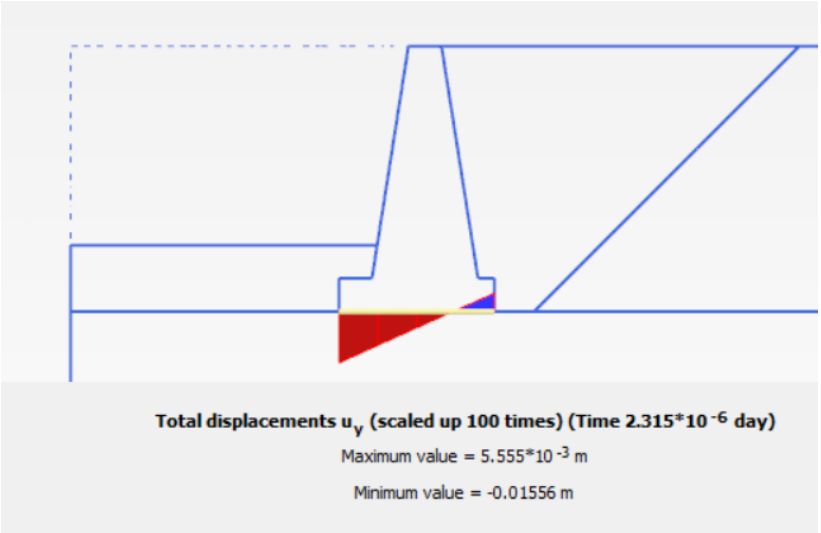

Figure 7.21. Total vertical displacement of the fourth wall design under dynamic condition.

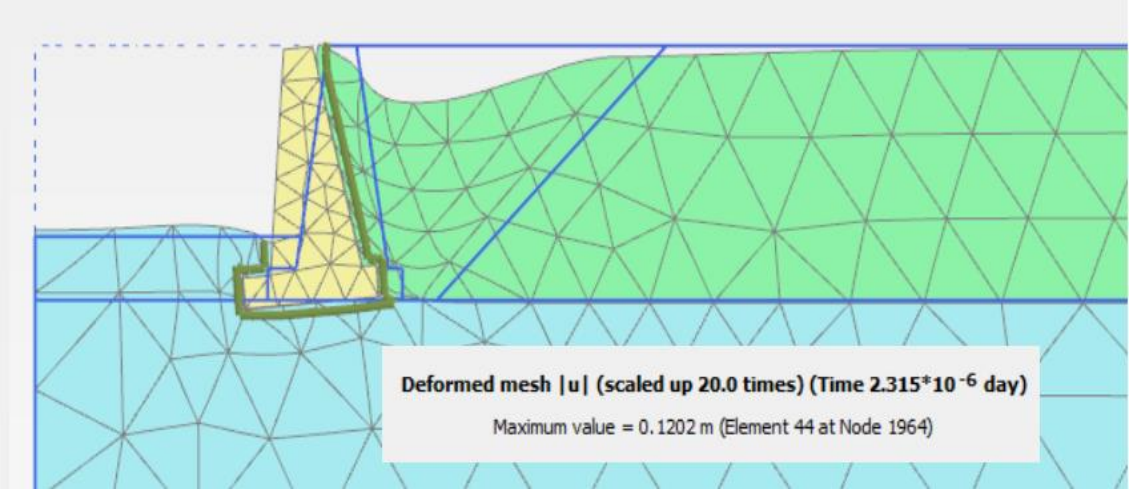

Figure 7.22. Deformed mesh for the fourth model under dynamic load from Plaxis 2D.

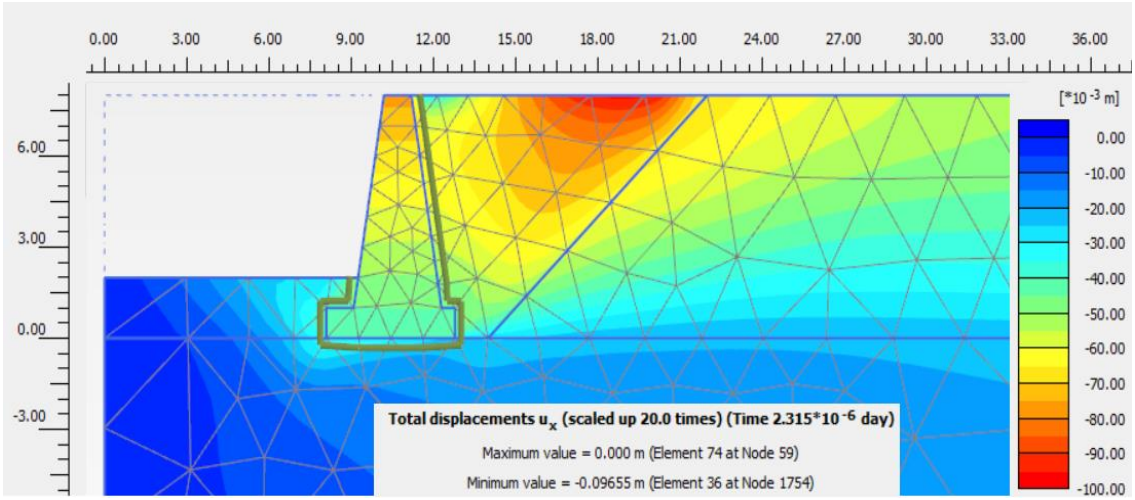

Figure 7.23. Total horizontal displacement for the fourth model under dynamic load.

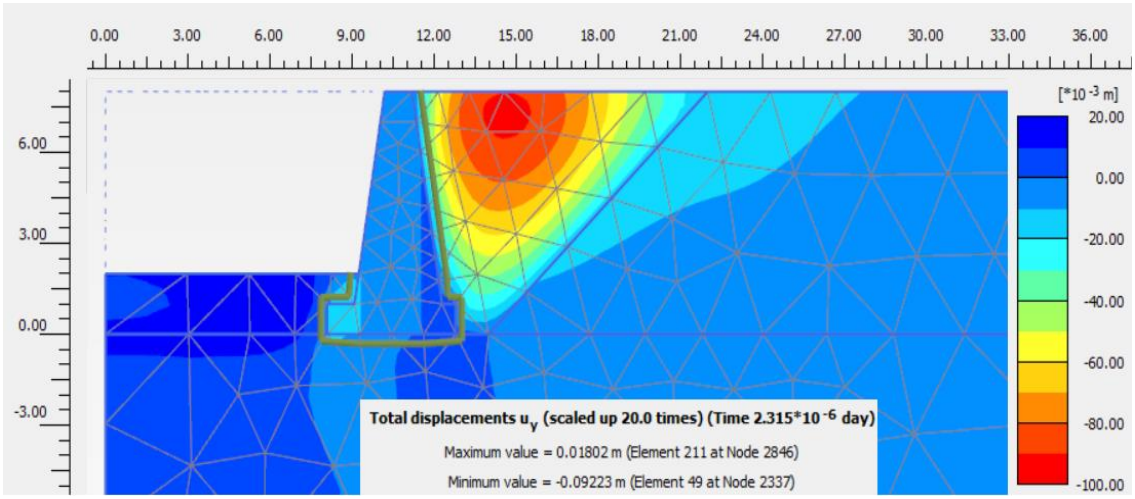

Figure 7.24. Total vertical displacement for the fourth model under dynamic load.

7.4. Water Effect

To recognize the water effect on the wall's safety, the water level was set at 8 m level (at the surface). Two models were made using Plaxis 2D software; one of them used granular soil as backfill, which allowed the water level to decrease to the bottom of the wall and the other model considered clay soil as backfill which is known with their low permeability.

Figure 7.24 shows the first design, which used a water-permeable material (granular soil) as a backfill. This led to a reduction in the water level, as illustrated in Figure 7.25. This

material acted as an effective drainage system, keeping the water's impact away from the wall, and the results showed no wall failure in this case.

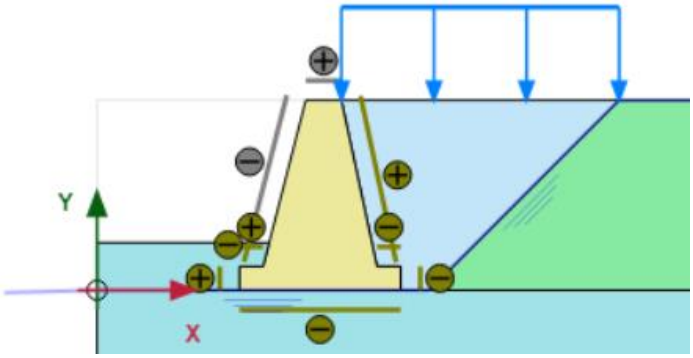

Figure 7.25. The model when the water effect is omitted.

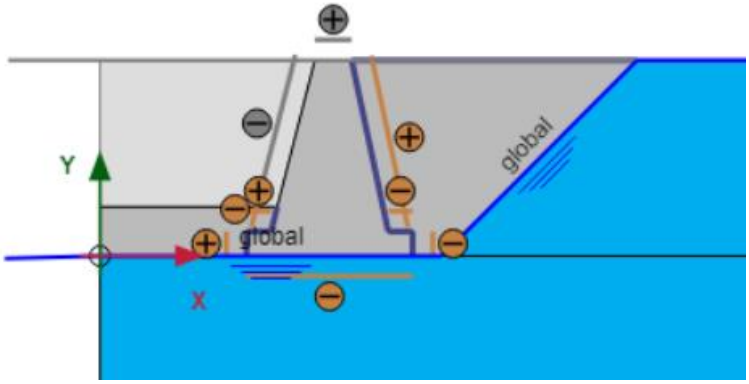

Figure 7.26. Water level after using granular backfill.

In the other case, clay soil was used as backfill, as shown in Figure 7.26, where the water level stayed at 8 m height, and the water's impact on the wall became present. When the design was implemented using the Plaxis 2D program, as the error message illustrated in Figure 7.27, the system failed. This indicates the significant impact of water on the stability of retaining walls. Additionally, having an appropriate drainage system in the backfill soil behind the retaining walls is crucial. It must be considered in the design to ensure the entire design is successful.

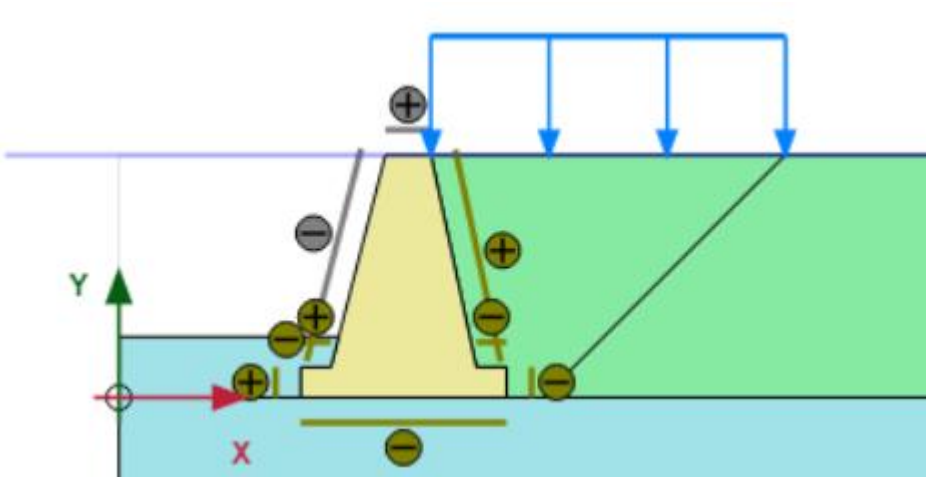

Figure 7.27. The model when the water effect is considered.

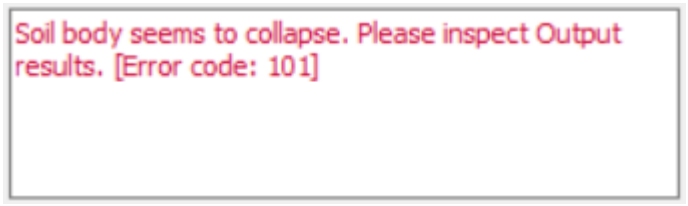

Figure 7.28. Error message from Plaxis 2D indicating the soil failure.

Therefore, in this research, all four designs were made under the assumption of having an appropriate drainage system that ensures no additional water pressure on the walls, which could lead to their failure.

8. CONCLUSIONS AND RECOMMENDATIONS.

Within the scope of this thesis, four models of rigid retaining walls, specifically gravity walls with horizontal surfaces, were designed using clay soil as backfill, assuming an effective and suitable drainage system behind the wall to prevent additional lateral water pressure. The lateral earth pressures for these walls were calculated in both static and dynamic conditions. Based on these pressures, the dimensions of the walls were designed. Rankine's method was used for the static condition, which considers the soil cohesion behind the wall when calculating lateral pressure. Susumu et al. method, newly published in 2022, was employed regarding the dynamic condition. This method incorporates soil cohesion into the calculation of seismic active earth pressures, and it has been combined with the modified Mononobe-Okabe method, which can be applied in cases of high seismic loading and considers the impact of the post-peak reduction in soil shear strength in addition to the strain localization of that backfill.For the four retaining wall models, the first two were designed under dynamic conditions using the horizontal seismic coefficient k_h defined by the Turkish standard TBDY (2018). In the first model, the surcharge load on the backfill soil was included, whereas it was not included in the second model. The remaining two models were designed using the horizontal seismic coefficient k_h from the AASHTO (2014), including the surcharge load on the soil behind the wall in the third model and omitting it in the fourth. This was done to assess the impact of the surcharge load on the lateral pressure exerted on the wall and its dimensions and to examine the differences in design based on whether the seismic coefficients were taken from the Turkish or AASHTO standards. Additionally, stability analyses were performed for all four designs in both static and dynamic states. These were compared with safety factors related to overturning, sliding, and bearing capacity as specified by the Turkish standard for the first two designs and the AASHTO standard for the last two. The equation used for

These checks was obtained from Das and Sivakugan, 2018). Furthermore, Plaxis 2D software version 2024 was utilized to calculate static and dynamic displacements, which were then evaluated against the permissible limits according to the design standards.

As shown in Tables 8.1 and 8.2, and resulting from the calculations that were conducted, it was revealed that the horizontal seismic coefficient calculated based on the Turkish standard was 40% greater than the coefficient calculated using the AASHTO standard, considering the displacement allowance assumed for each standard separately. This difference impacted the value of the lateral earth pressure, which in turn influenced the dimensions of the wall. The dimensions were larger when the Turkish standard's horizontal seismic coefficient was used. Consequently, we can state that the Turkish standard is more conservative when calculating this coefficient for the design of retaining walls in dynamic situations. However, the dimensions for the designs were significant in height, which could be due to the soil's characteristics, which is considered weak soil and makes it not recommended to be used as backfill. Additionally, referring back to Tables 8.1 and 8.2, we can observe a relatively significant difference between the values of lateral earth pressure in static and dynamic cases, indicating the importance of considering not only the static condition but also the dynamic situation in the design of retaining walls, especially in regions classified as seismic zones.

On the other hand, in preparing the model, an analysis was conducted on the effect of changing the excavation angle or cutting on the stability of the soil. Consequently, a suitable excavation angle was selected for constructing the retaining wall, which combined a secure safety factor regarding slope stability and efficient utilization of the space behind the wall. The analysis also extended to examining the excavation angle under different slope angles exposed to seismic loads without soil support. The results showed a reduced stability coefficient for the soil under these conditions and significant soil displacement resulting from the seismic load. This confirms the importance of including dynamic calculations, especially in areas exposed to seismic activities, as neglecting the dynamic impact could lead to unexpected lateral pressures for which the design was not intended and, therefore, potential design failure.

Furthermore, referring to Tables 8.1 and 8.2, we could observe the difference in values of lateral active earth pressure when accounting for the presence of a surcharge load on the soil versus when it is not considered. Initially, two designs were created with this surcharge load, and the safety factors concerning overturning, sliding, and the stability of the foundation soil were secure. Following the same approach, it became possible to reduce the design dimensions when the surcharge load was removed, and the wall was redesigned with different sizes because the lateral earth pressure values decreased. The safety factors also successfully met the stability requirements under these new conditions.

Regarding the displacement results obtained from the Plaxis 2D program concerning the horizontal displacement of the wall, they were compared with the allowable limits set by both the Turkish standard and AASHTO, which the wall was designed to assume (120 SDS for the Turkish standard and 250 a_{max} for the AASHTO standard), along with comparison to the limits allowed according to by Wu and Prakash (0.02H). As shown in Table 8.2, the values indicated successful compliance with these standards despite variations in displacement between the designs due to differences in the horizontal seismic coefficient k_h values. The designs based on the Turkish standard's horizontal seismic coefficient showed higher displacement values than those based on the AASHTO standard, confirming that the Turkish standard is more conservative and assigns higher values to seismic loads in the design of retaining walls. Additionally, the results regarding the safety factor for slope stability were secure compared with the Turkish standard for the first two designs and with the AASHTO for the last two designs.

Referring to Tables 8.1 through 8.4, concerning the designs that did not consider the presence of a surcharge load but were secure in terms of stability for overturning, sliding, and the bearing capacity, it is feasible that the dimensions of these walls could be reduced while still maintaining successful stability. However, attention must be paid to the horizontal displacement values when making such adjustments to ensure they stay within the allowed limits.

Consequently, it is important not just to focus on safety regarding the recently mentioned stability factors but also to pay close attention to the horizontal displacement values of the

design, which could potentially exceed the permissible displacement limit and thus create a risk of design failure.

Figures 7.10, 14, 18, and 20 illustrate the vertical displacement of the soil behind the wall for the four models, where these values were relatively high even without the addition of surcharge load on the soil due to the weak nature of the soil. Consequently, it is essential to consider the possibility of improving and strengthening this soil and taking the necessary measures to do so, especially if there is an intention to build on it or place additional loads on it, to avoid the risk of structural collapse resulting from the vertical displacement of this soil.

Despite the success of the designs under secondary seismic influence as categorized by AFAD, using clay as the backfill material behind the wall, the dimensions of the walls were relatively large even though lateral water pressure has not been accounted, for because the designs were made under the assumption of an existing effective and appropriate drainage system, confirming the inadequacy of clay soil for use behind retaining walls. The following is a summary of the conclusions that summarize the results of this research:

a) An effective water drainage system behind the wall is crucial to prevent any additional lateral pressure that could lead to wall failure.

b) It is essential to consider dynamic calculations due to their significant impact on the stability of retaining walls and that the Turkish standard is more conservative compared to the AASHTO standard in determining the value of the horizontal seismic coefficient k_h, where it was 40% higher in Turkish standards than AASHTO's, and that leads to 20% increase in the dimensions (base width).

c) Attention must be given to the soil’s bearing capacity if there is an intention to build on it, and efforts should be made to develop and improve the soil by the type of construction planned.

d) Even the cohesion of the soil has a positive effect in increasing the shear resistance of the backfill on the failure plane, but when it comes to cohesive soil like clay, for example, the negative impact of the decrease in the friction angle is more significant than the positive impact of soil cohesion.

Table 8.1. Computational results for the designs made according to TBDY.

Parameter	TBDY 2018			
	Including surcharge load		Without surcharge load	
	Static	Dynamic	Static	Dynamic
FoS Overturning	16.04 >1.50	3.80 > 1.30	27.35 > 1.50	3.86 >1.30
FoS Sliding	3.36 > 1.50	1.37 > 1.30	4.13 > 1.50	1.55 >1.30
FoS Bearing capacity	8.06 > 3.00	4.25 > 1.40	7.29 > 3.00	4.85 >1.40
FoS Slope stability	2.16 >1.50	1.30 > 1.10	2.26 > 1.50	1.22 >1.10
P_a (kN/m)	97.95	216.15	65.15	154.19
k_h	0.276			
k_v	0.138			

Table 8.2. Computational results for the designs made according to AASHTO

Parameter	AASHTO 2014			
	Including surcharge load		Without surcharge load	
	Static	Dynamic	Static	Dynamic
FoS Overturning	11.24 >2.00	3.48 > 1.50	18.16 > 2.00	3.34 > 1.50
FoS Sliding	2.67 > 1.50	1.31 > 1.10	3.30 > 1.50	1.46 > 1.10
FoS Bearing capacity	6.83 > 3.00	4.35 > 1.50	6.26 > 3.00	4.3 > 1.50
FoS Slope stability	2.00 >1.54	1.37 > 1.10	2.10 > 1.54	1.44> 1.10
P_a (kN/m)	97.95	185.30	65.15	137.94
k_h	0.196			
k_v	0.000			

Table 8.3. Plaxis 2D results for the designs made according to TBDY.

	TBDY 2018			
Parameter	Including surcharge load		Without surcharge load	
	Static	Dynamic	Static	Dynamic
Displacement u_x (cm)	0.80	11.00	1.00	13.30
Displacement u_y (cm)	0.07	3.10	0.26	3.30
Limit values for 120SDS (cm)	-	16.60	-	16.60
Limit values for 0.02H (cm)	-	16.00	-	16.00
Comparison result	-	Safe	-	Safe

Table 8.4. Plaxis 2D results for the designs made according to AASHTO.

	AASHTO 2014			
Parameter	Including surcharge load		Without surcharge load	
	Static	Dynamic	Static	Dynamic
Displacement u_x (cm)	0.70	6.00	1.50	8.00
Displacement u_y (cm)	0.12	1.30	0.23	1.60
Limit values for 250 a_{max} (cm)	-	11.80	-	11.80
Limit values for 0.02H (cm)	-	16.00	-	16.00
Comparison result	-	Safe	-	Safe

REFERENCES

AASHTO (American Association of State Highway and Transportation Officials). 2014. AASHTO LRFD Bridge Design Specifications. 7th ed., customary U.S. units. Washington, DC: AASHTO.

AFAD. (2024, 25 January). Türkiye Deprem Tehlike Haritaları. https://www.tdth.afad.gov.tr. Retrieved from the URL on January 25th, 2024 (url-4).

American Association of State Highway and Transportation Officials, Standard Specifications for Highway Bridges, (AASHTO), 2002.

Anderson, D. G., Martin, G. R., Lam, I. P., & Wang, J. N. (2008). Proposed AASHTO Specifications for the Seismic Design of Retaining Walls, Slopes and Embankments, and Buried Structures. In Sixth National Seismic Conference on Bridges and HighwaysMultidisciplinary Center for Earthquake Engineering ResearchSouth Carolina Department of TransportationFederal Highway AdministrationTransportation Research Board.

Berilgen, M. M. (1996). Examination of Soil Structure Interaction in Anchored Walls, [PhD thesis]. Yıldız Teknik University (in Turkish).

Bınıcı, H., Temız, H., Kayadelen, C., Kaplan, H., & Durgun, M. Y. (2010). Retaining Wall failure due to poor construction and design aspects a case study. Yapı Teknolojileri Elektronik Dergisi, 6(1), 46-61.

Bowles, J. E., & Guo, Y. (1996). Foundation analysis and design (Vol. 5, p. 127). New York: McGraw-hill.

Bray, J. D., & Travasarou, T. (2009). Pseudostatic coefficient for use in simplified seismic slope stability evaluation. Journal of geotechnical and geoenvironmental engineering, 135(9), 1336-1340. https://doi.org/10.1061/(ASCE)GT.1943-5606.0000012.

Bray, J. D., Travasarou, T., & Zupan, J. (2010). Seismic displacement design of earth retaining structures. In Earth Retention Conference 3 (pp. 638-655). https://doi.org/10.1061/41128(384)65.

British Standards Institution (1994). Code of Practice for Earth Retaining Structures. London: BSI, BS 8002.

Brooks, H., & Nielsen, J. P. (2013). Basics of Retaining Wall Design, 10th Edition: A Design Guide for Earth Retaining Structuress. Hba Publications Incorporated.

Brown, M., Burland, J., Chapman, T., Higgins, K., Skinner, H., & Toll, D. (Eds.). (2023). ICE Manual of Geotechnical Engineering, Volume II: Geotechnical design, construction and verification. Emerald Publishing Limited.

Budhu, M. (2010). Soil mechanics and foundations. John Wiley and Sons.

Can, S. (2024). Comparison of earth pressure approaches in support structures with mitigation console [Master's thesis]. Kocaeli University (in Turkish).

Clayton, C. R., Woods, R. I., Bond, A. J., & Milititsky, J. (2014). Earth Pressure and Earth-Retaining Structures, third edition. CRC Press.

Coduto, D.P., Kitch, W.A. and Yeung, M.-C.R. (2016) Foundation design: Principles and Practices.

Das, B. M., & Ramana, G. V. (1993). Principles of soil dynamics (pp. xii+-570). Boston, MA: PWS-Kent Publishing Company.

Das, B. M., & Sivakugan, N. (2018). Principles of foundation engineering. Cengage Learning.

Das, B.M. and Puri, V.K. (1996) 'Static and dynamic active earth pressure. Geotechnical and Geological Engineering, 14(4), pp. 353–366. https://doi.org/10.1007/bf00421949.

Das, B.M. and Sobhan, K. (2018) Principles of geotechnical engineering. Nelson Education.

Eurocode 8, P. (2005) : Design of structures for earthquake resistance-part 1: general rules, seismic actions and rules for buildings. Brussels: European Committee for Standardization.

Jaky, J. (1944). The coefficient of earth pressure at rest. Journal of the Society of Hungarian Architects and engineers.

Janbu, N., Bjerrum, L., & Kjaernsli, B. (1956). Soil mechanics applied to some engineering problems. Norwegian Geotechnical Institute.

Kapila, J. P. (1962). "Earthquake Resistant Design of Retaining Walls," Proceedings, 2nd Earthquake Symposium, University of Roorkee, Roorkee, India.

Kavazanjian, E. (1997). Design guidance: geotechnical earthquake engineering for highways. US Department of Transportation, Federal Highway Administration, Office of Engineering.

Kavazanjian, E., Wang, J. N., Martin, G., Shamsabadi, A., Lam, I., Dickenson, S. E., ... & Brinckerhoff, P. (2011). LRFD Seismic Analysis and Design of Transportation Geotechnical Features and Structural Foundations-NHI Course No. 130094 Reference Manual Geotechnical Engineering Circular No. 3 (No. FHWA-NHI-11-032). United States. Federal Highway Administration.

Khan, A. J., & Sikder, M. (2004). Design basis and economic aspects of different types of retaining walls. Journal of Civil Engineering (IEB), 32(1), 17-34.

Kim, W. C., Park, D., & Kim, B. (2010). Development of a generalised formula for dynamic active earth pressure. Geotechnique, 60(9), 723-727.

Kramer, S. L. (1996). Geotechnical earthquake engineering. Pearson Education India.

Leblebici, T. (2021). Investigation of the behavior of retaining walls constructed on water-saturated sand soils under static and dynamic loads [Master's thesis]. Eskişehir University (in Turkish).

Lin, Y. L., Leng, W. M., Yang, G. L., Zhao, L. H., Li, L., & Yang, J. S. (2015). Seismic active earth pressure of cohesive-frictional soil on retaining wall based on a slice analysis method. Soil Dynamics and Earthquake Engineering, 70, 133-147.

McCarthy, D.F. (2013) Essentials of Soil Mechanics and Foundations: Pearson New International Edition: Basic Geotechnics.

Mesri, G., & Hayat, T. M. (1993). The coefficient of earth pressure at rest. Canadian Geotechnical Journal, 30(4), 647-666.https://doi.org/10.1139/t93-056.

Mikola, R. G., & Sitar, N. (2013). Seismic earth pressures on retaining structures in cohesionless soils. California Department of Transportation, 5-9.

Milliyet. (2021, 02 December). A Retaining wall collapsed: 4 cars turned into scrap. https://www.milliyet.com.tr/gundem/istinat-duvari-coktu-4-otomobil-hurdaya-dondu-6653647. Retrieved from the URL on December 2nd, 2021 (url-2).

Mononobe, N., Matsuo, H., (1929). On determination of earth pressure during earthquake. Proc. World Eng. Cong. 9, 177–185.

Murthy, V.N.S. (2002) Geotechnical engineering: Principles and Practices of Soil Mechanics and Foundation Engineering. CRC Press.

Nakajima, S., Ozaki, T., Hong, K., and Koseki, J. (2023) 'Generalized solution to Coulomb's seismic active earth pressure acting on rigid retaining wall with cohesive backfill and trial application for evaluation of seismic performance of retaining wall,' Soil and Foundation, 63(1), p. 101247. https://doi.org/10.1016/j.sandf.2022.101247.

Nakajima, S., Ozaki, T., and Sanagawa, T. (2021). 1 g Shaking table model tests on seismic active earth pressure acting on retaining wall with cohesive backfill soil. Soils and Foundations, 61(5), 1251-1272. https://doi.org/10.1016/j.sandf.2021.06.014.

Nazarian, H.N. and Hadjian, A.H. (1979). Earthquake-Induced lateral soil pressures on structures. Journal of the Geotechnical Engineering Division, 105(9), pp. 1049–1066. https://doi.org/10.1061/ajgeb6.0000852.

Okabe, S., 1926. General theory of earth pressure. Proc. Japan Soc. Civ. Engineers 12 (1), 123–134.

Özcan, B. (2007). Determination of dynamic earth pressure affecting retaining walls under the effect of distributed load [Master's thesis]. Istanbul Teknik University.

Punmia, B., & Jain, A. K. (2005). Soil mechanics and foundations. Firewall Media.

Sabah. (2022, 09 February). A retaining wall collapsed in Trabzon. https://www.sabah.com.tr/yasam/trabzonda-istinat-duvari-coktu-5863023. Retrieved from the URL on February 9th, 2022 (url-3).

Saran, S. (2021) Dynamics of soils and their engineering applications. CRC Press.

Saran, S., & Prakash, S. (1968). Dimensionless parameters for static and dynamic earth pressures behind retaining walls. Indian Geotechnical Journal, 7(3), 295-310.

Seed, H. B., and Whitman, R. V. 1970. "Design of Earth Retaining Structures for Dynamic Loads," ASCE Specialty Conference, Lateral Stresses in the Ground and Design of Earth Retaining Structures, pp 103-147.

Sönmez, A. S. (2023). Examination of Console Retaining Walls According to 2018 TBDY [Master thesis]. Sakarya University (in Turkish).

Sözcü. (2018, 28 July). The retaining wall of the school in Sancaktepe collapsed. https://www.sozcu.com.tr/2018/gundem/sancaktepede-okulun-istinat-duvari-coktu-2545612. Retrieved from the URL on July 28th, 2018 (url-1).

Steedman, R.S. and Zeng, X. (1990). The influence of phase on the calculation of pseudo-static earth pressure on a retaining wall. Géotechnique/Geotechnique, 40(1), pp. 103–112. https://doi.org/10.1680/geot.1990.40.1.103.

Szymanski, A., Drozdz, A., & Bajda, M. (2006). Assessment of stress history in glacial soils on the basis of cone penetration tests. IAEG papers, 1, 365.

Taha, A. F., & Prust, R. E. (2004). Earth Retaining Systems for Urban Railway Tunneling Projects. In Geotechnical Engineering for Transportation Projects (pp. 1555-1565).

Terzaghi, K., Peck, R. B., & Mesri, G. (1996). Soil mechanics in engineering practice. John wiley & sons.

Wilson, P., & Elgamal, A. (2015). Shake table lateral earth pressure testing with dense c-ϕ backfill. Soil Dynamics and Earthquake Engineering, 71, 13-26. https://doi.org/10.1016/j.soildyn.2014.12.009.

Wood, J. H. (1973). Earthquake-induced soil pressures on structures [PhD thesis]. California Institute of Technology).

Woodward, P. K., & Griffiths, D. V. (1970). Earthquake induced forces on retaining walls. WIT Transactions on The Built Environment, 3.

Xie, Y., & Yang, X. (2009). Characteristics of a New-Type Geocell Flexible Retaining Wall. Journal of Materials in Civil Engineering, 21(4), 171–175. https://doi.org/10.1061/(asce)0899-1561(2009)21:4(171)

Yavan, O., Tabak, T. and Tuncan, A. (2022) 'Behavior Of Retaining Walls Constructed In The Saturated Clay And Water-Saturated Sand Soils Under The Dynamic Loads,' Kırklareli University Journal of Engineering and Science, 8(2), pp. 253–272.https://doi.org/10.34186/klujes.1183631.

Yıldırım, I. Z. (2004) Examination of earthquake effects in the design of retaining walls [Master's thesis]. Istanbul Teknik university (in Turkish).

Yıldız, E. (2007). A numerical study on the dynamic behaviour of gravity and cantilever retaining walls with granular backfill [PhD thesis]. Middle East Technical University.

Yıldız, M. C. (2015). Dynamic earth pressure affecting the retaining wall [Master's thesis]. Istanbul Teknik University (in Turkish).

CURRICULUM VITAE

Name Surname : Ahmed Almassri

EDUCATION:

- **Undergraduate** : 2019, An-Najah National University, Engineering Faculty, civil Engineering